N73-15920

NASA CR-120834

CASE FILE COPY

SUBCRITICAL CRACK GROWTH OF SELECTED AEROSPACE PRESSURE VESSEL MATERIALS

By
L. R. Hall and W. D. Bixler

THE BOEING COMPANY

Prepared For
NATIONAL AERONAUTICS AND SPACE ADMINISTRATION

NASA Lewis Research Center
Contract NAS 3-12044
Gordon T. Smith, Project Manager

Requests for copies of this report should be referred to

National Aeronautics and Space Administration
Office of Scientific and Technical Information
Attention: AFSS-A
Washington, D.C. 20546

1. Report No.	2. Government Accession No.	3. Recipient's Catalog No.
NASA CR-120834		

4. Title and Subtitle	5. Report Date
Subcritical Crack Growth of Selected Aerospace Pressure Vessel Materials	December 1972
	6. Performing Organization Code

7. Author(s)	8. Performing Organization Report No.
L. R. Hall and W. D. Bixler	D180-14855-1
	10. Work Unit No.
9. Performing Organization Name and Address The Boeing Company - Aerospace Group Research and Engineering Division Seattle, Washington 98124	11. Contract or Grant No. NAS 3-12044

12. Sponsoring Agency Name and Address	13. Type of Report and Period Covered
National Aeronautics and Space Administration Lewis Research Center Cleveland, Ohio	Contractor Report
	14. Sponsoring Agency Code

15. Supplementary Notes

Project Manager, Gordon T. Smith, Materials and Structures Division
NASA Lewis Research Center, Cleveland, Ohio 44135

16. Abstract

This experimental program was undertaken to determine the effects of combined cyclic/sustained loads, stress level, and crack shape on the fatigue crack growth rate behavior of cracks subjected to plane strain conditions. Material/environment combinations tested included: 2219-T87 aluminum plate in gaseous helium, room air, and 3.5% NaCl solution at room temperature, liquid nitrogen, and liquid hydrogen; 5Al-2.5 Sn (ELI) titanium plate in liquid nitrogen and liquid hydrogen and 6AL-4V (ELI) STA titanium plate in gaseous helium and methanol at room temperature. Most testing was accomplished using surface flawed specimens instrumented with a clip gage to continuously monitor crack opening displacements at the specimen surface. Tapered double cantilever beam specimens were also tested. Static fracture and ten hour sustained load tests were conducted to determine fracture toughness and apparent threshold stress intensity values. Cyclic tests were performed using sinusoidal loading profiles at 333 MHz (20 cpm) and trapezoidal loading profiles at both 8.3 MHz (0.5 cpm) and 3.3 MHz (0.2 cpm). Data were evaluated using modified linear elastic fracture mechanics parameters.

17. Key Words (Suggested by Author(s))	18. Distribution Statement
Subcritical Crack Growth Fatigue Stress Corrosion Cracking Fracture Mechanics 2219 Aluminum 6AL-4V (ELI) STA Titanium 5Al-2.5 Sn (ELI) Titanium Surface Flaw Flaw Shape	Unclassified, Unlimited

19. Security Classif. (of this report)	20. Security Classif. (of this page)	21. No. of Pages	22. Price*
Unclassified	Unclassified	126	$3.00

* For sale by the National Technical Information Service, Springfield, Virginia 22151

PREFACE

This report describes an investigation of static, sustained, cyclic and combined cyclic/sustained flaw growth characteristics performed by The Boeing Company from August 1969 to November 1970 under Contract NAS 3-12044. The work was administered by Mr. Gordon T. Smith of NASA Lewis Research Center.

Boeing personnel who participated in the investigation include J. N. Masters, project supervisor; L. R. Hall, technical leader; and W. D. Bixler and R. W. Finger, research engineers. Program support was provided by A. A. Ottlyk and C. C. Mahnken, specimen testing; and D. G. Good, technical illustrations and art work.

The information contained in this report is also released as Boeing Document D180-14855-1.

TABLE OF CONTENTS

TABLE OF CONTENTS (Cont.)

SYMBOLS AND ACRONYMS

a	Crack depth of semi-elliptical surface flaw; crack length in double cantilever beam specimen
B	Compliance of double cantilever beam specimens (deflection between loading points measured along load line divided by applied load
b	Specimen width for double cantilever beam specimen
b_n	Crack width for double cantilever beam specimen
$2c$	Crack length at specimen face for semi-elliptical surface flaw
E	Young's modulus
h	One-half depth of double cantilever beam specimen
K_I	Opening mode stress intensity factor
K_{IE}	Fracture toughness obtained from tests of surface-flawed specimens
K_{max}	Peak stress intensity factor for a given loading cyclic
K_{min}	Minimum stress intensity factor for a given loading cycle
ΔK	$K_{max} - K_{min}$
K_{TH}	Threshold stress intensity factor
M_K	Stress intensity magnification factor for deep surface flaws
N	Number of loading cycles
P	Applied concentrated force
Q	$\Phi^2 - 0.212\ (\sigma/\sigma_{ys})^2$
R	Ratio of minimum to maximum applied loads during a loading cycle
T	Temperature
t	Specimen thickness
W	Specimen width

Φ	Complete elliptical integral of the second king corresponding to the modulus $k = [(c^2-a^2)/c^2]^{\frac{1}{2}}$
σ_{ys}	Uniaxial tensile yield stress
δ	Opening mode crack displacement
μ	Poisson's ration
ELI	Extra Low Interstitial
STA	Solution Treated and Aged
GHe	Gaseous Helium
LN_2	Liquid Nitrogen
LH_2	Liquid Hydrogen
SENB	Single Edge Notched Bend
TDCB	Tapered Double Cantilever Beam
WR, RW, WT, RT	Crack propagation directions defined in Figure 6
x,y,z	Cartesian coordinates

LIST OF FIGURES

LIST OF FIGURES (CONT'D)

LIST OF FIGURES (CONT'D)

LIST OF FIGURES (CONT'D)

LIST OF TABLES

LIST OF TABLES (CONT'D)

LIST OF TABLES (CONT'D)

SUMMARY

This experimental program is one of a series of programs undertaken to develop and refine methods for estimating minimum performance capabilities of metallic pressure vessels with emphasis being placed on aerospace applications. On the basis of results of previous programs, fracture control methods for high strength metallic pressure vessels have been developed and documented. These methods require knowledge of the fracture toughness and subcritical crack growth characteristics for the material/environment combination of interest. Previous programs were undertaken to evaluate the individual effects of cyclic and sustained loadings on subcritical crack growth for various material/environment combinations.

This program was directed to an evaluation of the effects of combined sustained and cyclic loadings on subcritical crack growth in both previously tested and new material/environment combinations. In addition, the effects of peak cyclic stress and crack shape on fatigue crack growth behavior of surface flaws were investigated. Material/environment couples tested include: 2219-T87 aluminum in gaseous helium, room air, and 3.5% NaCl solution at room temperature, liquid nitrogen, and liquid hydrogen; 5Al-2.5Sn(ELI) titanium in liquid nitrogen and liquid hydrogen; and 6Al-4V(ELI) STA titanium in gaseous helium and methanol at ambient temperature. Most testing was accomplished using surface flawed specimens instrumented with a clip gage to continuously monitor crack opening displacements at the specimen surface. Tapered double cantilever beam specimens were also tested. Static fracture and ten hour sustained load tests were conducted to determine fracture toughness and apparent threshold stress intensity values. Cyclic tests were performed using sinusoidal loading profiles at 333 mHz (20 cpm) and trapezoidal loading profiles at both 8.3 mHz (0.5 cpm) and 3.3 mHz (0.2 cpm). Data were evaluated using linear elastic fracture mechanics parameters.

No effect of cyclic frequency on fatigue crack propagation rates was observed for any material/environment combination tested except 6Al-4V(ELI) STA titanium in methanol. For the 6Al-4V(ELI) STA/methanol combination, fatigue

crack growth rates increased as cyclic frequency was decreased. This effect was observed at stress intensity factors both above and below an apparent threshold value determined from 10 hour duration sustained load tests.

Crack growth under invariant loadings was observed in all material/environment combinations tested except 5Al-2.5Sn(ELI) titanium in LN_2. Crack growth occurred both during the loading ramp and invariant load segments of the sustained load profiles. The value of crack tip stress intensity factor above which crack growth under invariant load could be expected to result in specimen failure was defined as the threshold stress intensity factor. Actual sustained load failures were observed only for 2219-T87 aluminum in liquid nitrogen and liquid hydrogen.

Fatigue crack depth growth rates for surface flaws were found to be independent of variations in peak cyclic stress level and crack shape as long as variations in stress intensity factor were held constant. On the other hand, there were indications that stress level did affect the value of apparent threshold stress intensity factor (K_{TH}) with K_{TH} varying inversely with stress level. This effect was not investigated in sufficient detail to establish any firm trends.

1.0 INTRODUCTION

Pressure vessels for booster and spacecraft applications may contain crack-like defects due to material processing or fabrication procedures. Experience has shown that such defects can provide origins for brittle fracture either during initial pressurization or after limited service use. Fracture control methods for high strength metallic pressure vessels (1)* have been developed to ensure that the largest crack-like defects will not grow during service use to a size sufficiently large to impair performance. These methods require knowledge of the fracture toughness and subcritical crack growth characteristics of the constituent materials. Data obtained from tests of surface flawed specimens have proven to be the most useful for fracture control of spacecraft and booster structure. Surface flaws are commonly found in aerospace hardware and are subjected to plane strain crack tip deformations. Since plane strain deformations result in minimum resistance to both brittle fracture and stress corrosion cracking, surface flawed specimens are a severe but realistic model of potential failure origins in aerospace hardware.

Several test programs (2-5) have been undertaken to evaluate the effects of cyclic and sustained loadings on subcritical crack growth in aerospace materials. Earlier investigations evaluated the individual effects of cyclic and invariant loads on subcritical crack growth characteristics of surface flaws for various material environment combinations. Similar effects of loadings influenced by weld induced residual stresses, weld land buildups, and circular holes were investigated in the latter program. The results of the referenced programs aided in the development of fracture control procedures for aerospace hardware. It was also noted that there appeared to be effects of peak cyclic stress level and surface flaw shape on subcritical crack growth that had not been systematically evaluated. Furthermore, effects of combined cyclic and sustained loadings were not evaluated.

This program was undertaken to investigate the combined effects of cyclic and sustained loadings on subcritical crack growth in material/environment

*Numbers in parenthesis refer to References at end of report.

combinations pertinent to aerospace pressure vessel applications, and evaluate the effects of peak cyclic stress and crack shape on fatigue crack growth rates for surface flaws. Material/environment combinations tested include: 2219-T87 aluminum in gaseous helium, room air, and 3.5% NaCl solution at ambient temperature, liquid nitrogen, and liquid hydrogen; 5Al-2.5Sn(ELI) titanium in liquid nitrogen and liquid hydrogen; and 6Al-4V (ELI) STA titanium in gaseous helium and methanol at ambient temperature. Most testing was accomplished using surface flawed specimens instrumented with a clip gage to continuously monitor crack opening displacements at the specimen surface. Tapered double cantilever beam specimens were also tested. Static fracture and ten hour sustained load tests were conducted to determine fracture toughness and threshold stress intensity values. Cyclic tests were performed using sinusoidal loading profiles at 333 mHz (20 cpm) and trapezoidal loading profiles at both 8.3 mHz (0.5 cpm) and 3.3 mHz (0.2 cpm). Data were evaluated using modified linear elastic fracture mechanics parameters.

2.0 BACKGROUND

The surface flaw is a realistic model of failure origins in aerospace pressure vessels. Hence, surface-flawed specimens are tested extensively to develop design data and fracture control design methods within the aerospace industry. Most surface-flawed specimen data have been evaluated and correlated in terms of opening mode stress intensity factors defined by linear elastic fracture mechanics theory. In the past, some difficulty in evaluating surface-flawed specimen fracture and fatigue data has resulted from the lack of a good stress analysis for flaws having depths that are large with respect to the specimen thickness. However, good approximate solutions are now available for deep surface flaws and the fracture and fatigue crack growth behavior of such flaws is the subject of continuing experimental work. Some background information relating to stress analyses and experimental results for surface flawed specimens are summarized in the following paragraphs.

2.1 Stress Analyses for Surface Flaws

Irwin was the first to recognize the practical importance of surface flaws and derived an approximate expression for stress intensity factor for such flaws (6). The maximum value of stress intensity factor occurs at the point of deepest penetration of a semi-elliptical flaw designated by Point A in Figure 1, and is given by

$$K_1 = 1.1\sigma \sqrt{\frac{\pi a}{Q}}$$

$$Q = [\ \Phi\ ]^2 - 0.212\ (\sigma/\sigma_{ys})^2 \qquad (1)$$

where

- Φ is the complete elliptical integral of the 2nd kind
- σ is uniform tensile stress acting perpendicular to the plane of the crack
- σ_{ys} is the yield strength of the material
- $x = c\cos\theta$ and $y = a \sin\theta$ are parametric equations of the semi-elliptical flaw periphery

Equation 1 is applicable for flaw depth-to-length (a/2c) and flaw depth-to-thickness (a/t) ratios less than 0.5.

A number of approximate solutions for stress intensity factor at the tips of surface flaws deeper than 50 percent of the parent plate thickness have been proposed. Some of the earliest approximations were reported in two unpublished Boeing memoranda (7,8). Theoretical solutions for surface flaw problems date back to Smith's solution for a semi-circular surface flaw in a semi-infinite solid (9) which was subsequently extented to full and part-circular cracks (10,11), and to part-circular cracks in a finite thickness solid (12). A series of publications by Shah and Kobayashi (13-16) have documented a series of solutions for elliptical cracks located near the surface of a semi-infinite solid and subjected to arbitraty normal loadings, and for semi-elliptical surface cracks in finite plates subjected to both bending and tension stresses.

The method used to calculate stress intensity factors in this report is the semi-empirical method proposed by Masters et al (17). Static fracture tests of 2219-T87 aluminum and 5Al-2.5Sn(ELI) titanium surface flawed specimens containing both shallow and deep flaws showed that fracture strength could be predicted using the equation

$$K_{IE} = 1.1\sigma \sqrt{\frac{\pi a}{Q}} M_K \qquad (2)$$

where K_{IE} is the fracture toughness of the parent material for the depthwise crack propagation direction, and M_K is a deep flaw stress intensity magnification factor that was found to be dependent on material, a/t, and a/2c as shown in Figures 3 and 4. A more recent investigation by Masters (18) has demonstrated that the M_K values for 2219-T87 aluminum in Figure 4 are applicable to 6Al-4V STA titanium and 7075-T651 aluminum alloys. All stress intensity factors for surface flawed specimens reported herein were calculated using Equation 2 and M_K values in Figures 3 and 4 (Figure 3 for 5Al-2.5Sn(ELI) specimens and Figure 4 for 2219-T87 aluminum, and 6Al-4V STA titanium specimens.

2.2 Fatigue Crack Growth Behavior of Surface Flaws

Fatigue tests of surface flawed specimens have shown that, when critical flaw size is less than one-half the specimen thickness, the number of uniform loading cycles required to grow a flaw fom some initial size to the critical size is dependent primarily on the maximum stress intensity factor applied to the tip of the flaw during the initial loading cycle (K_{Ii}). Consequently, fatigue data for surface flawed specimens are often plotted on graphs of K_{Ii} or K_{Ii}/K_{IE} versus cycles to failure where data for given loading profiles and test conditions can be reasonably represented by a single curve called a cyclic life curve. This approach requires knowledge of only initial and final conditions for each test and is called an "end-point" approach. Crack growth rates are calculated using slopes of the cyclic life curves and are expressed in terms of d(a/Q)/dN. For constant stress intensity factor, crack growth rates calculated using the end-point approach are found to be inversely proportional to the square of the stress level for which the calculations are made. In view of this result, the effect of peak cyclic stress level on surface crack growth rates was investigated in this experimental program.

A later analyses of surface crack growth rates (4) arrived at the conclusion that the practice of expressing surface crack growth rates in terms of d(a/Q)/dN was consistent with the widely accepted notion that crack growth can be considered as a continuous process, and that fatigue crack growth is primarily a function of the range in stress intensity factor applied to the crack tip during a loading cycle. The cited analyses yielded relationships between surface crack depth growth rate (da/dN) and d(a/Q)/dN; one such relationship is included in Figure 2. The implication of the curve in Figure 2 is that if crack depth growth rate (da/dN) is a function only of the variation in stress intensity factor, surface flaw growth rate (d(a/Q)/dN) should vary with flaw shape ratio (a/2c) for given stress intensity factor. This result is particularly true for $0<a/2c<0.25$. Accordingly, tests were included in the following experimental program to investigate the effect of flaw shape on surface flaw growth behavior.

2.3 Relationship of Crack Opening Measurements to Crack Growth Rates

An expression for the opening displacements of a completely embedded elliptical flaw was proved by Green and Sneddon (19). The flaw, embedded in an elastic solid, was subjected to a uniform load normal to the crack surface at infinity. The maximum opening displacement occurs at the diametral center of the crack and is expressed by the equation

$$\delta = \frac{4(1 - \mu^2)}{E} \quad \frac{\sigma a}{\Phi} \tag{3}$$

Although a rigorous solution is not available for flaw opening displacements for a semi-elliptical surface flaw, such displacements should also be proportional to σ and a/Φ for elastic materials. By following Irwin's procedure (6) to account for the effect of plastic yielding, the flaw opening displacement for a surface flaw can be approximated by

$$\delta = C \frac{\sigma a}{\sqrt{Q}} \tag{4}$$

where C is a constant. The value of C can be determined at test initiation and termination from knowledge of the stress level, initial and final flaw sizes, and the corresponding flaw opening displacements as indicated below:

$$\begin{aligned} C_i &= \frac{\delta_i}{\sigma} \left(\frac{\sqrt{Q}}{a}\right)_i \\ C_f &= \frac{\delta_f}{\sigma} \left(\frac{\sqrt{Q}}{a}\right)_f \end{aligned} \tag{5}$$

where the subscripts i and f refer to initial and final conditions, respectively.

Tests have shown that the value of C tends to increase with increasing crack size, rather than remain constant. For tests in which both initial and final crack depths are less than one-half the specimen thickness, variations in the value of C are moderate. Analyses in which the variation in C between initial and final values was assumed to be either linear or a fourth order polynominal have shown that computed crack growth rates are very insensitive to the manner in which C varies. Crack growth rate calculations in this report were based on an assumed linear variation in C between the known initial and final values.

In order to relate the flaw parameter $(a/\sqrt{Q})$ to δ for values of $a/\sqrt{Q})$ between the initial and final values an assumption must be made as to the manner in which the flaw shape changes from test initiation to termination. It was assumed that

$$\frac{a - a_i}{a_f - a_i} = \frac{2c - (2c)_i}{(2c)_f - (2c)_i} \tag{6}$$

i.e., both flaw depth and width growth simultaneously reach the same percentage of their respective total growth from initial to final values. The flaw shape parameter (Q) can now be determined as a function of flaw depth and, in turn, δ can be related to crack depth using Equation 4. The number of cycles (N) or time corresponding to each selected flaw depth value can be determined from the test record and, consequently, the change in N or time for each increment of flaw depth is known. The crack growth rate da/dN or da/dt can then be calculated.

2.4 Stress Intensity Factors for Double Cantilever Beam Specimens

Stress intensity factors for double cantilever beam (DCB) specimens (Figure 5) can be evaluated using semi-empirical methods based on beam theory and compliance measurements. Stress intensity factors are related to specimen compliance (ratio of deflection of loading points to load) by the relationship (20).

$$K_I = \frac{P}{\sqrt{2b_n}} \left(\alpha \frac{\partial B}{\partial a}\right)^{1/2} \tag{7}$$

where

- P is applied load
- b_n is crack width
- B is specimen compliance
- a is crack length
- α = Young's modulus (E) for plane stress or $E/(1 - \mu^2)$ for plane strain where μ is Poisson's ratio.

An approximate expression for $\partial B/\partial a$ for DCB specimens has been derived (21) using simple beam theory and takes the form

$$\frac{\partial B}{\partial a} = \frac{8}{Eb} \left[3 \frac{a^2}{h^3} + \frac{1}{h} \right]$$

where h is beam height at the distance 'a' from the load line, and b is specimen width.

Tapered double cantilever beam specimens can be designed so that stress intensity factor is independent of crack length for constant load. This can be accomplished by contouring the specimen so that $(3\ a^2/h^3 + 1/h) = q =$ constant, resulting in specimens having the configuration shown in Figure 5. Experiments have shown (21) that specimens contoured as in Figure 5 yield compliance values that are linearly related to crack length. However, actual values of compliance are considerably greater than approximate values calculated using Equation 8.

Crack propagation in DCB specimens has a strong tendency to rotate from the original crack plane and sever one of the specimen arms. This problem can generally be alleviated by side grooving the specimens as shown in Figure 5. Stress intensity factors for side grooved specimens can be calculated using Equation 7 by setting b_n equal to the crack width.

Stress intensity factors for DCB specimens in this program were calculated using $\alpha = E/(1-\mu^2)$ in Equation 7. In retrospect, it is now believed that the value of $\alpha = E$ may have been more appropriate since the state of stress in the arms of DCB specimens is probably closer to plane stress than plane strain. However, the maximum possible error in the calculated values of stress intensity factor is less than five percent regardless of which value of α is used in the calculations.

3.0 TEST PROGRAM

The test program conducted during this investigation is presented in Table 1 along with the pertinent test parameters. For each material/temperature condition, mechanical property and static fracture tests were conducted with surface flawed specimens having a flaw shape ratio (a/2c) of about 0.25. In addition, flaw shape ratios of about 0.10 were evaluated for 2219-T87 aluminum at 295°K (72°F) and 78°K (-320°F), and 5Al-2.5Sn(ELI) titanium at 78°K (-320°F).

In general, ten hour sustained load tests were conducted as presented in Table 1. Originally the program plan called for testing of 6Al-4V(ELI) STA titanium in Freon TF, but after several sustained load tests in this environment it was concluded that the particular titanium plate/flaw orientation selected was not very susceptible to stress corrosion cracking (SCC) in the Freon TF since the threshold stress intensity factor was about 80% of the critical value. It was the original intent in selecting this material/environment combination to have a pronounced stress corrosion cracking situation so that cyclic flaw growth rates could be evaluated both above and below the threshold stress intensity factor. This objective could not be met with the Freon TF environment so methanol was substituted for the Freon TF.

The majority of the sustained load tests were run at stress levels approaching the yield strength of the material, namely, $\sigma_{ys}/1.10$ for the aluminum and $\sigma_{ys}/1.15$ for the titanium. The purpose of these tests was to define the threshold stress intensity at high stress levels and to compare the results with previously generated thresholds obtained at moderate stress levels. Where moderate stress level thresholds were not readily available, an attempt was made to establish them.

All sustained load specimens were instrumented with crack opening displacement (COD) measurement devices with the exception of the 5Al-2.5Sn(ELI) titanium tested at 20°K (-423°F). The program plan did not call for any of the 20°K (-423°F) tests to be instrumented but during the course of this program a clip gage measurement device was developed to work at 20°K (-423°F). Previously, the clip gages used at room temperature and 78°K (-320°F) would not work at

20°K (-423°F) due to excessive noise in the COD output. This new COD device was significantly smaller than previously used devices and was not coated. The purpose of instrumenting these specimens was to obtain sustained load crack growth rates.

In conjunction with the sustained load tests conducted, it became necessary to perform load/unload tests so that crack growth during loading could be separated from the time dependent crack growth under invariant loads. A previous investigation (3) reported the same phenomena. The load/unload tests were conducted at the same stress levels and with the same flaw shapes (a/2c = 0.25) as the sustained load tests.

Baseline cyclic tests were conducted at 333 mHz (20 cpm) as specified in Table 1 using surface flawed specimens. All specimens were instrumented with a COD measurement device (except the 5Al-2.5Sn(ELI) titanium at 20°K (423°F). The variables involved included stress level and flaw shape. Tests were conducted to evaluate the effect of stress level on the crack growth rates. The high stress levels selected were generally $\sigma_{ys}/1.15$ for the titanium while the low stress levels were one-half of the high stress levels. In general, the flaw shape ratios investigated were 0.10 and 0.25.

The effect of combined cyclic/sustained loading on the subcritical crack growth characteristics were evaluated by conducting the tests specified in Table 1 at 8.3 mHz (0.5 cpm) and 3.3 mHz (0.2 cpm). Surface flawed specimens with flaw shape ratios of about 0.25 were subjected to a trapezoidal cyclic loading profile having a very short rise and fall time. During each loading cycle, the maximum stress was maintained for some period of time, thus introducing a sustained loading in conjunction with the cyclic loading. All specimens were instrumented with a COD measurement device (except the 5Al-2.5Sn(ELI) titanium at 20°K (-423°F)). Test stresses were maintained at the high levels established for the baseline cyclic tests. The tests were run so that the effects of combined cyclic/sustained loading on the subcritical crack growth rates could be assessed at stress intensities above, just below, and significantly below the threshold value.

Cyclic load and combined cyclic/sustained load tests were conducted as indicated om Table 1 using tapered double cantilevered beam (TDCB) specimens. The objective of these tests was to evaluate the effect of combined sustained and cyclic loads on the subcritical crack growth characteristics at a constant stress intensity. The tests were conducted at stress intensity levels significantly below, just below, and significantly above the threshold value. Test frequencies and loading profiles used were the same as used for the surface flawed specimen tests.

4.0 MATERIALS AND PROCEDURES

4.1 Materials

The 2219-T87 aluminum specimens were machined from one plate 2.5 (1.0) x 122 (48) x 366 (144) cm (inches) purchased per BMS 7-105C. This material was obtained from a previously completed NASA Contract NAS 3-12003. The surface flawed specimens were machined so that the flaw would propagate in the WT direction whereas the tapered double cantilever beam (TDCB) specimens were machined so that the flaw would propagate in the WR direction. Nomenclature used to denote crack propagation direction is included in Figure 6.

The 5Al-2.5Sn(ELI) titanium specimens were machined from 2 different batches of material. The majority of the specimens were machined from plates, 0.48 (0.188) x 61 (24) x 183 (72) cm (inches), purchased in the annealed condition per MIL-T-9046E, Type II, Composition B. The remaining specimens were taken from surplus material from NASA Contract NAS 3-12003; this material was found to be in a inhomogeneous and layered state, and required an eight hour thermal cycle at 1122°K (1550°F) to produce a homogeneous microstructure; the final grain size was greater than normally encountered. Since these plates were thought to be atypical examples of this type material, it was decided to use them only when required flaw dimensions were such that the extra thickness, 0.95 cm (0.375 inches) compared to 0.48 cm (0.188 inches), was needed to curcumvent deep flaw problems. Therefore, the 0.95 cm (0.375 inches) thick material was used only for the specimens designed to investigate the effects of stress level. All of the surface flaw specimens were machined so that the flaw would propagate in the RT direction.

The 6Al-4V(ELI) titanium plates were obtained from previously completed NASA contract, NAS 3-7993. The plate material, 0.95 (0.375) x 61 (24) x 183 (72) cm (inches), was purchased in the annealed condition per AMS 4911A, except that the interstitial content was specified not to exceed the following percentage limits: C = 0.08 max; O_2 = 0.13 max; N_2 = 0.05 (500 ppm) max; H_2 = 0.0125 (125 ppm) max; and Fe = 0.25 max. The plates were ordered from the same heat and rolling batch. Prior to machining of specimens, the plates were solution treated and aged at The Boeing Company per BAC 5613; the solution treatment of 1327°K (1730°F) for 10 minutes was followed by a water quench and a 811°K (1000°F) aging temperature for four hours. The surface flaw specimens were machined so that the flaw would propagate in the RT direction whereas the TDCB specimens were machined so that the flaw would propagate in the RW direction.

4.2 Specimen Fabrication Procedures

Three different types of test specimens were fabricated on this program. Smooth tensile specimens used for determining mechanical properties are shown in Figure 7. Surface flawed specimens used to evaluate static, sustained and cyclic flaw growth characteristics for surface flaws are shown in Figures 8 through 12. TDCB specimens used to evaluate cyclic flaw growth characteristics are shown in Figures 13 and 14.

Tapered double cantilever beam specimens were fabricated with a linearly tapered section as shown in Figures 13 and 14. The linear taper was an approximation of the contour defined by the equation

$$3\ a^2/h^3 + 1/h = 4.0 \qquad (8)$$

which is the approximate contour required to make stress intensity factor independent of crack length for constant load. Since Equation 8 is approximate and deviates only slightly from a straight line, it was decided to use a linearly tapered contour rather than a contour conforming to Equation 8.

All initial flaws were prepared by using an electric discharge machine (EDM) to introduce a starter notch with a terminating radius of less than 0.008 cm (0.003 inches). The EDM starter notch was then extended using low stress/ high cycle fatigue; periodic examinations were conducted, using a microscope, to determine when a fatigue crack had been initiated around the entire periphery of the EDM notch. The precracking operation was done in air at room temperature.

4.3 Experimental Procedures

Mechanical property tests were conducted per ASTM standards for tensile testing. Yield strength (at 0.2% offset), ultimate strength, elongation and reduction in area were determined. A strain rate of 0.005 cm/cm/minute was used during the tensile tests until the yield strain was exceeded, then the strain rate was increased to 0.02 cm/cm/minute failure. Static fracture tests, using surface flawed specimens, utilized a loading rate to percipitate fracture within about 2 minutes after initial application of load.

Specimens that were to be sustained loaded were first exposed to the test environment and then were loaded to the maximum desired stress level in about 2 minutes. The load/unload tests conducted were also loaded to the maximum desired stress level and then immediately unloaded. Basic cyclic tests were conducted using a sinusoidal loading profile with a $\sigma_{min}/\sigma_{max}$ ratio of zero while the combined cyclic/sustained loading tests utilized the trapezoidal loading profile shown in Figure 15. All specimens that were subjected to sustain load, load/unload, cyclic load, and combined cyclic/sustain load profiles (except for those that failed during test) were marked by low stress/high cycle fatigue so that the flaw growth that occurred during the test could be easily distinguished. The marking operation was done in room temperature air, except for some 2219-T87 aluminum specimens that were marked at 78°K (-320°F) in liquid nitrogen.

All specimens, except for the static fracture, load/unload and 20°K (-423°F) titanium, were instrumented using a crack opening displacement (COD) clip gage to provide a continuous record of crack opening displacement. When flaws were of sufficient size, the clip gage was mounted in the flaw as shown in Figure 16. For the smaller flaws, COD brackets were micro-spot welded on the surface of the specimen as shown in Figure 17. COD recordings were used both to calculate crack growth rates and as a basis for terminating tests just prior to failure. Normally, a cyclic or sustained load test could be terminated within a few cycles or minutes of specimen failure by observing the COD output.

4.4 Stress Intensity Factor Calculations

Stress intensity factors for surface flaws were calculated using Equation 2 and M_K value in Figures 3 and 4. Values of M_K were taken from Figure 3 for the 5Al-2.5Sn(ELI) titanium specimens, and from Figure 4 for the 2219-T87 aluminum and 6Al-4V STA titanium surface flaw specimens.

Stress intensity factors for aluminum alloy tapered double centilever beam specimens were calculated using Equation 3 with $\alpha = E/1-\mu 2$ and $\partial B/\partial a = 1.19 \times 10^{-6} (N)^{-1}$ ($5.30 \times 10^{-6} (lbs)^{-1}$); values of $E = 68.95 \times 10^3$ MN/m2 (10×10^3 ksi) and $\mu = 0.30$ were used in the calculations. The value of $\partial B/\partial a$ was determined experimentally through compliance measurements as described in Appendix B.

5.0 PRESENTATION AND ANALYSIS OF RESULTS

Data from all tests are included in Tables 4 through 41. Tables 4 through 9 contain the mechanical property and static fracture test data while the following data tables are grouped by material and include data for: load/unload tests, sustained load tests, cyclic load tests, combined cyclic/sustained load tests, and TDCB cyclic tests. Data for each load/unload, sustained load, cyclic and combined cyclic/sustained load test are, in general, given on three sequential lines in a given table. The first line gives values of test parameters at the outset of the test. The second line gives similar values at the end of the test. The third line includes test parameters at the time the specimen was pulled to failure for specimens that did not fail during the initial test.

5.1 Mechanical Property Test Results

The results of the mechanical property tests are presented graphically in Figures 18 and 19 for the aluminum and titanium alloys, respectively. The 2219-T87 aluminum (transverse grain) demonstrated yield strengths (0.2% offset) of 383 (55.5), 453 (65.7) and 492 (71.3) MN/m^2 (ksi) at temperatures of 295 (72), 78 (-320) and 20 (-423)°K (°F), respectively. The baseline (0.48 cm or 0.188 inch thick) 5Al-2.5 Sn(ELI) titanium (longitudinal grain) had a yield strength of 1252 MN/m^2 (181.7 ksi) at 78°K (-320°F) and 1446 MN/m^2 (209.7 ksi) at 20°K (-423°F). The tough titanium plate (0.95 cm or 0.375 inch thick) tested had a somewhat lower yield strength of 1226 MN/m^2 (177.6 ksi) at 78°K (-320°F). The yield strength of the 6Al-4V (ELI) STA titanium (longitudinal grain) was determined to be 975 MN/m^2 (141.3 ksi) at 295°K (72°K).

5.2 Static Fracture Test Results

The results of the static fracture tests are presented graphically in Figures 20 and 21 for the aluminum and titanium, respectively. Only those results for specimens that failed at less than 90% of the yield strength were considered valid surface flaw plane strain fracture toughness (K_{IE}) values. The K_{IE} values for the 2219-T87 aluminum (WT direction) were determined to be 46.8 (42.6), 50.9 (46.4) and 54.0 (49.1) $MN/m^{3/2}$ (ksi $\sqrt{in}$), at temperatures of 295 (72), 78 (-320) and 20 (-423)°K (°F), respectively. The aluminum tests were conducted with specimens containing flaw shapes of 0.11 and 0.27 but no significant differences were observed in the static results. The baseline 5Al-2.5 Sn(ELI) titanium (RT direction) demonstrated K_{IE} values of 89.4 (81.3) and 69.2 (63.0) $MN/m^{3/2}$ (ksi $\sqrt{in}$) at temperatures of 78 (-320) and 20 (-423)°K (°F), respectively. The fracture toughness of the tough 5Al-2.5 Sn(ELI) titanium plate was determined to be 92.8 $MN/m^{3/2}$ (84.4 ksi $\sqrt{in}$) at 78°K (-320°F). A K_{IE} value of 80.3 $MN/m^{3/2}$ (73.1 ksi $\sqrt{in}$) was obtained for the 6Al-4V (ELI) STA titanium at 295°K (72°F).

5.3 Sustained Load Test Results

5.3.1 2219-T87 Aluminum

Results for both load/unload and sustained load 2219-T87 aluminum surface flawed specimens are included in Tables 10 through 13. Crack depth growth observed after each test is related to the corresponding stress intensity factors in Figure 22.

The data in Figure 22 indicates that, for stress intensity factors above some minimum value, crack depth growth during sustained load tests was greater than crack depth growth during load/unload tests. For the purposes of this program, the maximum stress intensity factors for which crack growth observed during both load/unload and sustrained load tests were equal were defined as the threshold stress intensity factors. Values of the threshold stress intensity factor were found to be 33 $MN/m^{3/2}$ (30 ksi $\sqrt{in}$) in the ambient 3.5 percent NaCl solution, greater than 44 $MN/m^{3/2}$ (40 ksi $\sqrt{in}$) in LN_2, and 39.6 $MN/m^{3/2}$ (36 ksi $\sqrt{in}$) in LH_2.

Previously conducted surface flawed specimen tests (3) for 2.5 cm (1.0 inch) thick 2219-T87 plate in the environments of air, LN_2, and LH_2 showed that crack growth under sustained loads could occur in four stages including: (a) crack growth during rising loads; (b) initial transient crack growth; (c) crack acceleration; and (d) unstable crack propagation resulting in failure. The number of stages that occurred in a given test was dependent on the magnitude of the crack tip stress intensity factor (K) at peak load.

For low K values, no growth was observed; for intermediate K values, crack growth during loading and transient crack growth followed by crack growth arrest were observed; for high K values, all stages of crack growth were observed resulting in specimen failure.

In the sustained load tests conducted in this program, both crack growth during rising load and crack growth to failure were observed. However, there was no evidence of a stage of transient crack growth followed by crack growth arrest. At 295°K (72°F), the test records of crack opening displacement versus time for all sustained load tests continued to increase at an ever accelerating rate throughout the duration of each test. No evidence of any tendency for the COD to stabilize could be detected. At 78°K (-320°F) and 20°K (-423°F), specimens failed when loaded to generate crack tip stress intensity factors slightly above the level at which crack depth growth during load/unload tests was equal to crack depth growth during sustained load tests. This observation is indicative of a three stage crack growth behavior, i.e., crack growth during rising load followed by crack acceleration and unstable crack propagation.

The data obtained in this investigation were compared with other reported (3, 22) sustained load test data for 2219-T87 aluminum surface flawed specimens. The Reference 3 investigation included tests of 1.68 cm (0.66 inch) thick specimens in room air, LN_2 and LH_2. Test durations were up to 100 hours in air and LN_2, and 10 hours in LH_2. Test stress levels were less than $\sigma_{ys}/1.4$. The results of the comparison are summarized in Table 2. In addition, sustained load results from Reference 22 for a 3.5 percent salt solution are presented in Table 2. This result was based on tests of 1.52 cm (0.60 inch) thick specimens loaded for 16 hours and at a stress level of $\sigma_{ys}/1.25$. Two threshold stress intensities are generally included for each environment in Table 2; the lower value is that below which flaw depth growth did not occur during the loading ramp of the sustained load profile; the higher value is that above which flaw depth growth was observed during the sustained load part of the loading profile. The lower stress intensity values for the present investigations were taken as the stress intensity at which extrapolated "growth during initial loading" curves in Figure 22 intersected the stress intensity ordinate at a Δa less than 0.003 cm (0.001 inches). Results for the air and 3.5% NaCl solutions were not directly comparable. In LN_2 and LH_2, the "no growth" threshold stress intensity factors (values below which growth during loading is not observed) are in very good agreement. The "growth-to-failure" threshold stress intensity factors obtained in this investigation did not agree with the Reference 3 results. Furthermore, there was no consistent relationship between results since values obtained in this program were higher at 78°K (-320°F) and lower at 20°K (-423°F) than previously reported results. It was anticipated that the high stress levels used in this program could affect the "growth-to-failure" threshold stress intensity factors. However, no conclusions regarding the effect of test stress level can be drawn in view of the inconsistent relationships to previous results.

5.3.2 5Al-2.5 Sn(ELI) Titanium

Results of sustained load and load/unload tests of 5Al-2.5 Sn(ELI) titanium surface flawed specimens in LN_2 and LH_2 are included in Tables 26, 27, and 28, and Figure 23. Ten hour sustained load tests were conducted with stress levels of $\sigma_{ys}/1.15$ and $\sigma_{ult}/1.4$ in LN_2, and $\sigma_{ult}/1.4$ in LH_2. Each specimen was then fatigue marked and loaded to failure.

The LN_2 data shows that the K_{TH} is > 69.3 $MN/m^{3/2}$ (63.0 ksi $\sqrt{in}$). There is an indication that for a given applied stress intensity, the 5Al-2.5 Sn(ELI) titanium is more susceptible to sustained load crack growth at 1090 MN/m^2 (158 ksi) than at 951 MN/m^2 (137.9 ksi). However, such a conclusion could not be drawn from the small amount of data generated in this investigation. However, a previous investigation (3) of sustained load crack growth behavior in 5Al-2.5 Sn(ELI) titanium surface flawed specimens in LN_2 did establish that threshold stress intensity does vary with applied stress level. For stress levels less than 1034 MN/m^2 (150 ksi) no sustained load crack growth was observed in 30 tests at stress intensity levels between 80 and 98 percent of the fracture toughness. When stress level was increased to between 1034 and 1172 MN/m^2 (150 and 170 ksi), considerable crack growth was observed at stress intensity levels as low as 83 percent of the fracture toughness. The threshold data of Reference 3 is presented in Table 3 along with that generated in the present program and results from the two investigations are in good agreement.

The LH_2 data (Figure 23) shows that sustained stress crack growth does not occur at stress intensity levels approaching the fracture toughness of the material when tested at $\sigma_{ult}/1.4$ or 1131 MN/m^2 (164.0 ksi). At this stress level, the threshold stress intensity is > 92 percent of K_{IE} or higher than that reported in Reference 3 (see Table 3).

5.3.3 6Al-4V (ELI) STA Titanium

Results of sustained load and load/unload tests of 6Al-4V (ELI) STA titanium surface flawed specimens in gaseous helium and methanol are included in Tables 33 through 35. Sustained load tests were conducted with stress levels of $\sigma_{ys}/1.15$ and $\sigma_{ult}/1.40$ in gaseous helium, and $\sigma_{ys}/1.15$ and $\sigma_{ult}/1.50$ in methanol applied for a maximum of 10 hours. Each specimen was then fatigue marked and loaded to failure.

Figure 24 contains plots of flaw depth growth (Δa) as a function of stress intensity applied to the flaw tip at the outset of each test. In the gaseous helium environment, flaw depth growth was uniformly small in all but one specimen. That specimen failed after only one minute after an initial stress intensity of 69.8 $MN/m^{3/2}$ (63.5 ksi $\sqrt{in}$) was applied. The flaw depth growth that occurred in the failed specimen could not be determined from visual observation of the fracture surface.

In the methanol environment, flaw depth growth was more pronounced than for any other material/environment combination tested. For an applied stress of 648 MN/m^2 (94 ksi), a well ordered relationship between flaw depth growth and stress intensity was obtained and the threshold stress intensity equaled 67 percent of the fracture toughness. For an applied stress of 848 MN/m^2 (123 ksi), a single test yielded significantly more flaw depth growth than did the 648 MN/m^2 (94 ksi) tests indicating that the threshold stress intensity may be sensitive to stress level for the methanol environment.

5.4 Cyclic and Combined Cyclic/Sustained Test Results

Cyclic and combined cyclic/sustained data for each of the alloys tested is presented and discussed separately. The effects of environment, combined cyclic/sustained loadings, stress level, and flaw shape on crack growth rates are described and assessed.

5.4.1 Results for 2219-T87 Aluminum Alloy

Environmental Effects

Crack depth growth rates (da/dN) obtained at a cyclic frequency of 333 mHz (20 cpm) and in the room temperature environments of helium gas, air, and a 3.5% NaCl solution are included in Figures 25, 26 and 27, respectively. For constant peak cyclic stress intensity factor, crack growth rates were slower in air and 3.5% NaCl solution than in helium gas. The areas of fatigue crack growth on the fracture surfaces of specimens tested in air and 3.5% NaCl solution were much rougher to the naked eye than for specimens tested in helium gas. Apparently, the growth mechanisms leading to surface roughness also contributed to retarding the overall average growth rate. Furthermore, calculated critical stress intensity factors for cyclic specimens increased with increased roughness of the fatigue crack growth area. As a result, fatigue crack growth rates were obtained for stress intensity factor values in excess of the K_{IE} value of 46.8 $MN/m^{3/2}$ (42.6 ksi $\sqrt{in}$) determined from room temperature static tests.

Combined Cyclic/Sustained Loading Effects

The effects of combined cyclic/sustained loadings on fatigue crack growth rates were investigated in the environments of 3.5% NaCl solution at 295°K (72°F), LN_2 at 78°K (-320°F) and LH_2 at 20°K (-423°F). The 8.3 and 3.3 mHz (0.5 and 0.2 cpm) data were obtained using a trapezoidal loading profile having a very short rise and fall time and varying time at peak load as shown in Figure 15. The 333 mHz (20 cpm) data were obtained using sinusoidal loading profiles. Results are included in Figures 27 through 32. Tests at the two slower frequencies were conducted either above or below the apparent threshold stress intensity value obtained from the corresponding

10 hour duration sustained load tests. In salt water, fatigue crack growth rates obtained from the 8.3 and 3.3 mHz tests were slower than those obtained from the 333 mHz (20 cpm) tests over the entire range of stress intensity factor values tested. In LN_2 and LH_2, the fatigue crack growth rates obtained at the two slower frequencies generally fall within the scatter band for the 333 mHz (20 cpm) data. At stress intensity factors above the apparent threshold value, there was a slight increase in fatigue crack growth rates with decreasing cyclic frequency.

The areas of fatigue crack growth in specimens tested at cryogenic temperatures were less rough than in specimens tested at room temperature. The critical stress intensity factors resulting from cryogenic tests were equal to or slightly greater than the corresponding K_{IE} values determined from static fracture toughness tests, contrary to the room temperature behavior where critical stress intensity factors for cyclically tested specimens were significantly greater than for statically tested specimens.

Cyclic life data for specimens listed in Figures 25 through 32 are plotted as a function of K_{1i} in Figues 33, 34 and 35 for 295°K (72°F), 78°K (-320°F), and 20°K (-423°F) data, respectively. A single data point with coordinates (K_{1i}, N) is plotted for specimens that were cycled to failure where K_{1i} is the peak cyclic stress intensity factor applied to the crack tip during the initial loading cycle, and N is cycles to failure. Two data points are plotted for specimens that were cycled, but not to failure; the coordinates of the two points are (K_{1i}, N_1) and (K_{1f}, N_2) where K_{1f} is the peak cyclic stress intensity factor applied to the crack tip during the final loading cycle, and $(N_1 - N_2)$ is equal to the number of applied loading cycles; each set of two data points for a single specimen is connected by a short curved line. The data agree with previous observations (2, 4) that cyclic lives of surface flawed specimens are primarily a function of K_{1i} when all test variables other than stress level and flaw dimensions are held constant, and critical crack depth is less than one-half the specimen thickness.

Stress Level Effects

For constant test conditions and loading profile, fatigue crack depth growth rates were found to depend only on variations in stress intensity factor at the crack tip. This result is evident in Figures 25, 26, 27, 29 and 31 where crack growth rates developed using two different peak cyclic stress levels are plotted as a function of peak stress intensity factor. The data show that doubling the peak cyclic stress level had no effect on crack growth rate as long as peak cyclic stress intensity factor was held constant.

Previously reported (2, 4) crack growth rates for surface flaws (d(a/Q)/dN) appeared to be dependent on both variations in stress intensity factor and peak cyclic stress level. Values of d(a/Q)/dN were calculated using cycle-to-failure data and no direct measurements of crack growth rate were made. It appears that the previously reported apparent stress level effects were at least partially due to the omission of deep flaw magnification factors in stress intensity factor calculations. For constant specimen thickness, critical crack depth in specimens subjected to high stresses are a smaller percentage of the specimen thickness than in specimens subjected to lower stresses. Hence, stress intensity factors in high stress specimens are not elevated by deep flaw effects as much as in low stress specimens. As a result, cyclic lives in low stress specimens are reduced by deep flaw effects more than for high stress specimens and, if deep flaw effects are not accounted for in the analyses of results, it would appear that crack growth rates are faster in the low stress than in the high stress specimens. As an example of this effect, Figure 36 shows flaw growth rates for 2219-T87 aluminum alloy surface flawed specimens tested in 3.5 percent NaCl solution analyzed both with and without the use of deep flaw magnification factors (M_K). An apparent stress level effect is evident in the rates analyzed without considering deep flaw effects. When deep flaw effects were accounted for, no stress level effect is observed. This observation was also made for the 5Al-2.5 Sn (ELI) titanium and 6Al-4V(ELI) STA titanium crack growth rate results.

Flaw Shape Effects

No effect of surface flaw shape on either crack depth growth rate (da/dN) or flaw growth rate (d(a/Q)/dN) was observed in any of the aluminum alloy data. This result is evident in Figures 25, 26, 27, 29 and 31 where crack growth rates developed using two different initial flaw shapes are plotted as a function of peak stress intensity factor. Any differences in crack growth rate behavior between flaws having different shapes were small and inconsistent and it is believed that the observed differences were due to data scatter.

Tapered Double Cantilever Beam Specimen Results

Crack growth rate data obtained from tests of tapered double cantilever beam specimens in a 3.5% NaCl solution are listed in Table 25 and plotted as a function of stress intensity factor in Figure 37. Crack growth rates obtained under 333, 8.3, and 3.3 mHz (20, 0.5 and 0.2 cpm) loading profiles identical to those used to test surface flawed specimens were in good agreement. The rates were significantly higher than crack depth growth rates obtained from tests of surface-flawed specimens shown by the scatter band which was taken from Figure 27. This discrepancy was due to the differences in crack propagation direction and fracture toughness between the two specimen types. Crack growth rates for the surface flawed specimens were obtained for the WT direction as compared to the WR direction in TDCB specimens (see Figure 6 for direction nomenclature). Fracture toughness values were not measured for the WR direction but the rapid increase in crack growth rates with increase in stress intensity factor for the TDCB specimen data indicates that the fracture toughness was probably less than 33 $MN/m^{3/2}$ (30 ksi $\sqrt{in}$). Fatigue crack growth rates for the RW direction in 2219-T87 aluminum alloy plate (23) are also plotted in Figure 37 for comparison. The RW crack growth rates lie between the WR and WT rates and exhibit trends that are similar to those observed for the WR data obtained in this investigation.

It is evident that the fatigue crack propagation rates and fracture toughness values for the WT and WR directions of 2219-T87 aluminum alloy plate differ greatly and data obtained from tests of TDCB specimens is not applicable to prediction of surface flaw behavior. The effects of combined cyclic/sustained loadings on crack growth behavior as measured using TDCB and surface flawed specimens were qualitatively similar.

5.4.2 Results for 5Al-2.5 Sn(ELI) Titanium

Surface flawed specimen tests were conducted in LN_2 to evaluate flaw shape and peak cyclic stress level effects, and in LH_2 to investigate combined cyclic/sustained load effects on fatigue crack growth behavior. The LN_2 data are included in Table 29 and Figures 38 and 39. The LH_2 data are presented in Table 30 through 32, and Figure 40.

Stress Level Effects

Fatigue crack depth growth rates for the 5Al-2.5 Sn(ELI) titanium alloy were found to be insensitive to peak cyclic stress level as long as cyclic variations in stress intensity factor were held constant. This result is illustrated in Figure 38 where crack growth rates for two widely different peak cyclic stresses are plotted as a function of peak cyclic stress intensity factor. No consistent effect of peak cyclic stress on crack growth rates at constant stress intensity factor are evident in the figure.

Flaw Shape Effects

There was some evidence that flaw shape affected crack growth rates in the 5Al-2.5 Sn(ELI) titanium alloy. Only two specimens were tested with results shown in Figure 39 where both crack depth growth rates (da/dN) and flaw growth rates (d(a/Q)/dN) are plotted as a function of peak cyclic stress intensity factor. The da/dN plot shows that crack depth growth rates were slower for the specimen with the higher initial value of a/2c (the difference could be due to data scatter). The d(a/Q)/dN plot shows that, at the lower stress intensity factors, the flaw growth rate curve for the specimen having the lower initial a/2c value is displaced to the right of that for the specimen with the higher initial a/2c value; as stress intensity factor increases, the two curves gradually merge. The behavior of the d(a/Q)/dN curves in Figure 39 is in agreement with results of a previously conducted analyses (4) showing, that, for constant strees intensity factor, flaw growth rates should increase with decreasing a/2c for $0 < a/2c < 0.5$. As the specimen with the lower initial a/2c was cycled, the flaw shape ratio increased from the initial value of 0.24 to a final value of 0.46, i.e., to a value at which the referenced analyses predicts little or no effect of crack shape on d(a/Q)/dN. Since an effect of crack shape or d(a/Q)/dN for surface flaws was noted in only one of five material/environment combinations in which the effect was investigated, it is not a general occurrence. Since the magnitude of shape effects on crack growth rates are less than normal scatter in fatigue crack growth rate data, the effect cannot be thoroughly investigated without testing large numbers of specimens.

Combined Cyclic/Sustained Loading Effects

Tests in LH_2 revealed no effect on crack growth rate of superimposing sustained loadings on cyclic loadings. The supporting data are plotted in Figure 40 where cyclic life data for specimens cycled at 333, 8.3 and 3.3 mHz (20, 0.5 and 0.2 cpm) are plotted. A single data point with coordinates (K_{1i}, N) is plotted for specimens that were cycled to failure where K_{1i} is the peak cyclic stress intensity factor applied to the crack tip during the initial loading cycle, and N is cycles to failure. Two data points are plotted for specimens that were cycled, but not to failure; the coordinates of the two points are (K_{1i}, N_1) and (K_{1f}, N_2) where K_{1f} is the peak cyclic stress intensity factor applied to the crack tip during the final loading cycle, and (N_1 - N_2) is equal to the number of applied loading cycles. It is evident that all data fall close to a single curve and that the addition of sustained loadings to cyclic loadings had no effect on crack growth rates for 5Al-2.5 Sn(ELI) titanium alloy tested in LH_2.

5.4.3 Results for 6Al-4V(ELI) STA Titanium

The effects of combined cyclic/sustained loadings on crack growth rates for 6Al-4V(ELI) STA titanium was investigated in the room temperature envinronments of gaseous helium and methanol. Results for gaseous helium are listed in Tables 36 through 38 and are plotted in Figures 41 through 43. Results for methanol are listed in Tables 39 through 41 and are plotted in Figures 44 through 46.

Combined Cyclic/Sustained Loading Effects

Tests in gaseous helium, with one exception, showed that cyclic crack growth rates for the three cyclic frequencies of 333, 8.3, and 3.3 mHz (20, 0.5 and 0.2 cpm) can all be represented by a single scatter band except for specimen

6T-8A-26 in Figure 42. Crack growth rates obtained during the early stages of growth in 6T-8A-26 were significantly greater than rates within the scatter band for all other specimens. The reasons for the discrepancy are not known since no errors could be determined in test parameters. It is believed that results obtained from specimen 6T-8A-26 are probably spurious and that the duration of peak cyclic load has no effect on cyclic crack propagation rate for peak stress intensity factors below K_{TH}.

Tests in methanol showed that crack growth rate is affected by duration of peak cyclic load. This is evident in Figures 44 through 46 where there is a trend of increasing crack growth rates with decreasing cyclic frequency (increasing duration of peak cyclic load). The acceleration in crack growth rates appeared to be most pronounced at stress intensity factors below the apparent threshold stress intensity. This result is probably primarily due to phenomenological differences in crack propagation behavior under cyclic and sustained loadings. Whereas cyclic crack growth rates continually increase with increasing stress intensity factors, sustained load or stress corrosion cracking rates usually reach a plateau region where rates remain constant over a wide range of stress intensity factors. Hence, a direct summation of cyclic and sustained load rates in the plateau region yields a decreasing percentage difference between total and cyclic crack growth rates with increasing stress intensity factor as was observed in the tests under discussion. This type of behavior is most evident whe results are plotted on either log-log or semi-log graphs of stress intensity versus crack growth rate.

The existence of increasing crack growth rates with increasing duration of peak cyclic load at stress intensity factors below the apparent threshold value (K_{TH}) may have been due to dynamic effects and/or the manner in which K_{TH} was obtained. Due to the dynamic effects of load cycling on conditions at the crack tip, it is conceivable that environments could influence crack growth rates at stress intensity factor levels below the apparent threshold values obtained from static tests. In addition, there are many material/ environment couples (including titanium/methanol) for which a true threshold stress intensity factor has yet to be determined. As test duration is increased, crack propagation continues at ever decreasing rates and the value of apparent threshold stress intensity is dependent on test duration. The values of K_{TH} in this program were determined from ten hour duration tests and so the value of true threshold stress intensity factor is probably somewhat less than the value of K_{TH} reported herein for 6Al-4 V(ELI) STA titanium in methanol.

Stress Level Effects

There was some evidence that crack growth rates at constant stress intensity factor may have been influenced by peak cyclic stress level. The evidence is included in Figures 41 and 44 where crack growth rates for difference peak cyclic stress levels are plotted as a function of peak cyclic stress intensity factor. Doubling the peak cyclic stress level resulted in slower crack growth rates in both gaseous helium and methanol. However, this result could have been due to data scatter rather than peak stress level effects. Since no stress level effects were noted in any other material/environment combination tested, it is difficult to conclude that such effects exist on the basis of the 6Al-4V(ELI) STA titanium data.

6.0 OBSERVATIONS AND CONCLUSIONS

Tests undertaken to evaluate the effects of sustained, cyclic, and combined cyclic/sustained loadings on the subcritical crack growth characteristics of sharp cracks under plane strain conditions led to the following observations:

2219-T87 Aluminum Alloy

1. Crack growth in 2219-T87 aluminum alloy surface flawed specimens (WT direction) subjected to sustained loadings seemed to occur in three stages including: crack growth during rising load; crack growth rate acceleration; and unstable crack propagation. The number of stages of crack growth that occurred in any given specimen was dependent on the stress intensity factor (K) applied to the crack tip. For low K values, it appeared that no growth would occur (a conclusion substantiated by results in Reference 3); for intermediate K values, growth during rising load (and possibly a small amount of transient crack growth followed by crack growth arrest) is observed; for high K values above a threshold stress intensity factor (K_{TH}), all three stages of crack growth are observed resulting in specimen failure. It was found that all three stages of crack growth occurred when specimens tested at 78°K (-320°F) and 20°K (-423°F) were subjected to crack tip stress intensity factors equal or greater than 85 and 70 percent of the corresponding critical stress intensity factors, respectively. Comparison of the results obtained in this program with previously reported results obtained using lower stress levels did not reveal any consistent effects of stress level on threshold stress intensity factors. The above ratios were higher at 78°K (-320°F) and lower at 20°K (-423°F), respectively, than previously reported (3) ratios.

2. For a cyclic frequency of 333 mHz (20 cpm), fatigue crack growth rates at 295°K (72°F) were the same in air, helium gas, and 3.5% NaCl solution. For cyclic frequencies of 8.3 and 3.3 mHz (0.5 and 0.2 cpm), crack growth rates in 3.5% NaCl solution were slower than those obtained at a cyclic frequency of 333 mHz (20 cpm) at stress intensity factors

both above and below the threshold stress intensity factor. This result was due to the ability of the salt water to induce a very irregular crack front at the lower test frequencies.

3. In liquid nitrogen and liquid hydrogen, fatigue crack growth rates for stress intensity factors both above and below the threshold values were independent of cyclic frequency for a frequency range of 333 to 3.3 mHz (20 cpm to 0.2 cpm).

4. Surface flawed specimens subjected to fatigue loadings in air, helium, and 3.5% NaCl solution failed at calculated crack tip stress intensity factors well above the critical value as determined from static fracture tests. Cyclically tested specimens had much rougher crack surfaces than did the static fracture specimens. The roughness was indicative of irregular crack peripheries which impart greater resistance to static fracture than do smooth regular peripheries (4).

5. Fatigue crack growth rates obtained from tests of tapered double cantilever beam (TDCB) specimens in a 3.5% NaCl solution were independent of cyclic frequency for frequencies between 333 and 3.3 mHz (20 and 0.2 cpm). For the range of stress intensity factors tested, fatigue crack growth rates obtained from the TDCB specimens (WR direction) were about an order of magnitude greater than crack depth growth rates obtained from surface flawed specimens (WT direction). The result was due to the different crack propagation directions and fracture toughness values for the two propagation directions. All stress intensity factors applied to the TDCB specimens were a high percentage of the critical stress intensity factor.

Titanium Alloys 5Al-2.5 Sn(ELI) and 6Al-4V(ELI) STA

1. Crack growth in titanium alloy specimens occurred both during rising and invariant loadings. Crack growth behavior in ambient helium, LN_2 and LH_2 appeared to parallel that observed for the 2219-T87 aluminum alloy tested in the same environments, i.e., three stages of crack growth were observed. It is believed that the crack growth observed

in helium, nitrogen, and hydrogen was not environmentally assisted. The 6Al-4V titanium alloy is known to be very susceptible to stress corrosion cracking (SCC) in methanol and pronounced SCC was observed during this program for the RT direction of 6Al-4V(ELI) STA titanium surface flawed specimens tested in methanol.

2. Indications of a stress level effect on the value of threshold stress intensity factor were observed in 5Al-2.5 Sn(ELI) titanium tested in LN_2 and 6Al-4V(ELI) STA titanium tested in methanol at 295°K (72°F). TQreshold stress intensity factors appeared to decrease with increasing stress. This effect was not investigated in sufficient detail to establish any firm trends.

3. There was no effect of cyclic frequency (333 to 3.3 mHz or 20 to 0.2 cpm) on fatigue crack growth rates at stress intensity factors (K) both above and below the threshold value (K_{TH}) in 5Al-2.5 Sn(ELI) titanium in LN_2 and LH_2 and 6Al-4V(ELI) STA titanium in ambient helium gas. For these material/environment combinations, the ratio of threshold to critical stress intensity factors was very high and there was only a limited range of K values over which to evaluate the effect of cyclic frequency on fatigue crack growth rates at K values above K_{TH}.

4. There was a marked effect of cyclic frequency (333 to 3.3 mHz or 20 to 0.2 cpm) on fatigue crack growth rates at stress intensity levels both above and below the threshold values in 6Al-4V(ELI) STA titanium tested in methanol. For constant stress intensity factor, fatigue crack growth rates increased with decreasing cyclic frequency. In these limited tests, the greatest acceleration in crack growth rates occurred at stress intensity factors below the threshold value.

General

1. No effect of stress level on either crack depth growth rate (da/dN) or flaw growth rate d(a/Q)/dN was observed for limited ranges of stress intensity factor. This result is in disagreement with previously reported (2-4) apparent stress level effects on flaw growth rates. The

disagreement is believed to be mainly due to differences in stress intensity factor calculation methods used in this program and previous programs (2-4). Deep flaw magnification factors that were not available during previous programs were used to calculate stress intensity factors in this program.

2. No effects of flaw depth-to-length (a/2c) ratio on crack depth growth rate (da/dN) was noted. Only one of five material/environment combinations in which the effect was investigated yielded flaw growth rates (d(a/Q)/dN) that were affected by the (a/2c) ratio; for 5Al-2.5 Sn(ELI) titanium in LN_2, flaw growth rates were observed to increase with decreasing a/2c ratio for a/2c values less than 0.25. This behavior is in agreement with results of a previously reported (4) analysis of surface flaw fatigue growth behavior.

Conclusions

1. There is a threshold stress intensity factor for metallic alloy/inert environment combinations above which crack growth can occur under invariant loadings resulting in unstable crack propagation and failure. The resultant crack growth is believed to be due to mechanical processes occurring in the plastically deformed material at the crack tip and does not involve chemical or electrochemical processes. The value of threshold stress intensity factor appears to be dependent on stress level at least for stresses appraoching the uniaxial yield stress.

2. It is very likely that, for inert environments in which sustained load crack growth is due to mechanical processes, fatigue crack growth rates at stress intensity factors below the threshold stress intensity factor will be independent of cyclic frequency.

3. For environments which promote stress corrosion or hydrogen cracking, fatigue crack growth rate may be dependent on cyclic frequency at stress intensity factors below the threshold value.

4. Fracture control methods (1) developed on the basis of previous programs adequately handle the situation of metallic pressure vessels subjected to combined cyclic and sustained loadings for material/environment combinations that are immune to stress corrosion or hydrogen cracking. For combinations prone to environmentally induced cracking, Reference 1 states: "If it is necessary to use materials having low-threshold, stress intensity values (less than 70 to 80 percent K_{1c}) in the expected operating environment, it appears that the effect of environment and cyclic frequency on cyclic growth rates of flaws should be determined and the appropriate rates used to estimate the life of the pressure vessel. As previously mentioned, the minmum allowable cyclic life is limited to the number of cycles required to increase the value of the initial stress intensity K_{1i} to the K_{TH} value."

The foregoing statement is still a necessary requirement.

REFERENCES

1. C. F. Tiffany, *"Fracture Control of Metallic Pressure Vessels"*, NASA Space Vehicle Design Criteria (Structures) NASA SP-8040, May 1970.

2. C. F. Tiffany, P. M. Lorenz, and L. R. Hall, *"Investigation of Plane Strain Flaw Growth in Thick-Walled Tanks"*, NASA CR-54837, February 1966.

3. C. F. Tiffany, P. M. Lorenz, and R. C. Shah, *"Extended Loading of Cryogenic Tanks"*, NASA CR-72252, July, 1967.

4. L. R. Hall, *"Plane-Strain Cyclic Flaw Growth in 2014-T62 Aluminum and 6Al-4V (ELI) Titanium"*, NASA CR-72396, November 1968.

5. L. R. Hall and R. W. Finger, *"Investigation of Flaw Geometry and Loading Effects on Plane Strain Fracture in Metallic Structures"*, NASA CR-72659, August 1971.

6. G. R. Irwin, *"Crack Extension Force for a Part-Through Crack in a Plate"*, Journal of Applied Mechanics, Vol. 29, Trans. ASME, Vol. 84, Series E, December 1962.

7. A. S. Kobayashi, *"On the Magnification Factors of Deep Surface Flaws"*, Boeing Structural Research Memorandum, No. 16, Dec. 1965.

8. F. W. Smith, *"Stress Intensity Factors for a Semi-Elliptical Surface Flaw"*, Boeing Structural Development Research Memorandum, No. 17, Aug. 1966.

9. F. W. Smith, A. F. Emery, and A. S. Kobayashi, *"Stress Intensity Factors for Semi-Circular Cracks, Part 2 - Semi-Infinite Solid,"* Journal of Applied Mechanics, Vol. 34, Trans. ASME, Vol. 89, 1967, pp. 953-959.

10. F. W. Smith, and M. J. Alavi, *"Stress Intensity Factors for a Penny Shaped Crack in a Halfspace,"* Journal of Engineering Fracture Mechanics, Vol. 3, Oct. 1971, pp. 241-254.

11. F. W. Smith, and M. J. Alavi, *"Stress Intensity Factors for a Part-Circular Surface Flaw,"* Proceedings of the First International Conference on Pressure Vessel Technology, Delft, Holland 1969.

12. R. W. Thresher, and F. W. Smith, *"Stress Intensity Factors for a Surface Crack in a Finite Solid,"* Journal of Applied Mechanics, Vol. 39, Trans. of ASME, Vol. 95, March 1972, pp. 195-200.

13. R. C. Shah, and A. S. Kobayashi, *"Stress Intensity Factor for an Elliptical Crack Under Arbitrary Normal Loading,"* Journal of Engineering Fracture Mechanics, Vol. 3, No. 1, July 1971, pp. 71-96.

14. R. C. Shah, and A. S. Kobayashi, *"Stress Intensity Factors for an Elliptical Crack Approaching the Surface of a Semi-Infinite Solid,"* to be published in the International Journal of Fracture Mechanics.

15. R. C. Shah, and A. S. Kobayashi, *"Stress Intensity Factors for an Elliptical Crack Approaching the Surface of a Plate in Bending,"* to be published in Stress Analysis and Growth of Cracks, ASTM Special Technical Publication No. 513.

16. R. C. Shah, and A. S. Kobayashi, *"On the Surface Flaw Problem,"* to be published in the Proceedings of ConCam Symposium on the Surface Flaw, Applied Mechanics Division of ASME, Winter, 1972.

17. J. N. Masters, W. P. Haese and R. W. Finger, *"Investigation of Deep Flaws in Thin Walled Tanks"*, NASA CR-72606, December 1968.

REFERENCES (CONT.)

18. J. N. Masters and R. W. Finger, *"Fracture Characteristics of Structural Aerospace Alloys Containing Deep Surface Flaws"*, NASA Contract NAS 3-14341, The Boeing Company (to be published).

19. A. E. Green and I. N. Sneddon, *"The Distribution of Stress in the Neighborhood of a Flat Elliptical Crack in an Elastic Solid"*, Proc. Cambridge Phil. Soc., 46, 1959 (1950).

20. G. R. Irwin and A. A. Wells, *"A Continuum Mechanics View of Crack Propagation"*, Metallurgical Reviews, Vol. 10, No. 38, 1965.

21. S. Mostovoy, P. B. Crosley and E. J. Ripling, *"Use of Crack-Line-Loaded Specimens for Measuring Plane Strain Fracture Toughness"*, Journal of Materials, Vol. 2, No. 3, September 1967.

22. L. R. Hall and R. W. Finger, *"Stress Corrosion Cracking and Fatigue Crack Growth Studies Pertinent to Spacecraft, Boosters and Transportable Cryogenic Pressure Vessels"*, NASA CR-120823, September, 1972.

23. T. W. Crooker, *"Crack Propagation in Aluminum Alloys Under High-Amplitude Cyclic Load"*, NRL Report 7286, July 1971.

APPENDIX A

CALCULATION OF CRACK GROWTH RATES FROM SURFACE FLAW OPENING MEASUREMENTS

The method used for calculating crack growth rates using continuous measurements of opening mode crack displacements for surface flaws is illustrated in this appendix. The calculations made for a specific specimen, namely 2219-T87 aluminum alloy specimen A3A-23 listed in Table 16, are described.

The test record of flaw opening displacement versus cycles for specimen A3A-23 is included in Figure A-1. The displacement measured was the opening mode displacement at the intersection of the semi-minor and semi-major axes of the crack. Specimen A3A-23 was unloaded after the application of 397 zero-to-tension loading cycles at which time failure was imminent. The record in Figure A-1 shows that permanent set in flaw opening displacement occurred during the initial loading cycle and increased throughout the test. For each loading cycle, the permanent set was subtracted from the peak displacement to arrive at the displacement (δ_A) on which crack growth rate calculations were based. A plot of δ_A versus cycles for specimen A3A-23 is included in Figure A-2.

Flaw dimensions both at the beginning and end of the cycle test were measured from the fracture face and were found to be:

	Value at	
Dimension	Initiation	Termination
a cm(in)	0.231 (0.091)	0.564 (0.222)
2c cm(in)	2.070 (0.815)	2.337 (0.920

Equation 4 from the body of this report was used to relate flaw opening displacement (δ_A) to crack dimensions, i.e.,

$$\delta_A = C \frac{\sigma a}{Q} \qquad \text{(A1)}$$

and values of C were calculated using the known values of δ_A, a, and Q at the beginning and end of the test as follows:

$$C_i = \frac{\delta_{Ai}}{\sigma}\left(\frac{\sqrt{Q}}{a}\right)_i = \frac{6.15 \text{ X } 10^{-5}\text{m}}{345 \text{ MN/m}^2} \cdot \frac{0.956}{2.31 \text{ X } 10^{-3}\text{m}} = 75.3 \frac{\text{pm}^2}{\text{N}} \quad (0.519 \frac{\mu\text{in}^2}{\text{lb}})$$

$$C_f = \frac{\delta_{Af}}{\sigma}\left(\frac{\sqrt{Q}}{a}\right)_f = \frac{16.0 \text{ X } 10^{-5}\text{m}}{345 \text{ MN/m}^2} \cdot \frac{1.280}{5.64 \text{ X } 10^{-3}\text{m}} = 92.7 \frac{\text{pm}^2}{\text{N}} \quad (0.639 \frac{\mu\text{in}^2}{\text{lb}})$$

where subscripts i and f refer to initial and final conditions, respectively. Values of Q were obtained from Figure 1.

Average crack growth rates were calculated for arbitrary increments of crack depth. After initial and final values of crack depth for a given increment were selected, corresponding values of flaw width (2c) and coefficients (C) were calculated using the equations

$$\frac{a_n - a_i}{a_f - a_i} = \frac{2c_n - 2c_i}{2c_f - 2c_i}$$

$$\frac{a_n - a_i}{a_f - a_i} = \frac{C_n - C_i}{C_f - C_i} \qquad \text{(A3)}$$

where subscripts i and f refer to initial and final values at the beginning and end of the test, and both $2c_n$ and C_n are the values of 2c and C corresponding to a_n where $a_i < a_n < a_f$. Next, values of Q_n were determined from Figure 1 and values of $(\delta_A)_n$ determined using Equation A1. The number of loading cycles (N) corresponding to each δ_A value were read from the δ_A versus N plot in Figure A2. Average crack depth growth rates (da/dN) and flaw growth rates (d(a/Q)/dN) were then calculated for the selected crack depth growth increment using the equations

$$\frac{da}{dN} = \frac{a_{n+1} - a_n}{N_{n+1} - N_n}$$

$$\frac{d(a/Q)}{dN} = \frac{(a/Q)_{n+1} - (a/Q)_n}{N_{n+1} - N_n} \qquad \text{(A4)}$$

where the subscripts n and n+1 refer to values at the beginning and end of the crack growth increment. Results of the calculations for specimen A3A-23 are included in Table A1 and are plotted in Figure 27.

APPENDIX B

COMPLIANCE MEASUREMENTS FOR TAPERED DOUBLE CANTILEVER BEAM SPECIMENS

Tests undertaken to measure specimen compliance as a function of crack length for 2219-T87 aluminum alloy TDCB specimens are described in this appendix. Values of specimen compliance (the ratio of relative displacement of loading points along the load line to applied load) were used in stress intensity factor calculations for TDCB specimens described in the main body of this report. Tests were conducted for three TDCB specimens having the configuration shown in Figure 13. The taper angle of the specimen arms was chosen to yield compliance values that varied linearly with crack length.

PROCEDURES

Compliance values were determined using the slopes of load-displacement plots obtained when specimens were loaded in tensile test machines. Displacements were measured using clip gages spring loaded against integrally machined knife edges located as shown in Figure 13. Since the knife edges were not located on the load line, deflections at the load line were calculated by multiplying the measured deflections by the ratio of distance from crack tip to the knife edge location, i.e., $a/(a+1.27)$ where a is crack length in centimeters. Other tests (A1) of uniform height double cantilever beam specimens have shown that the above ratioing method is applicable. Both load cell and clip gage were connected to an X-Y recorder to obtain load-displacement graphs. The slopes of the graphs (deflection divided by load) were measured and multiplied by $a/(a+1.27)$ to calculate compliance.

RESULTS

Compliance measurements for three different specimens (TA-1, TA-2 and TA-3) are plotted against crack length in Figure B1. All data fall very close to a straight line which was the desired result. The slope of the line in Figure B1 was used as the average value of the rate of change of compliance with respect to crack length with which to calculate stress intensity factors for the 2219-T87 aluminum alloy TDCB specimens.

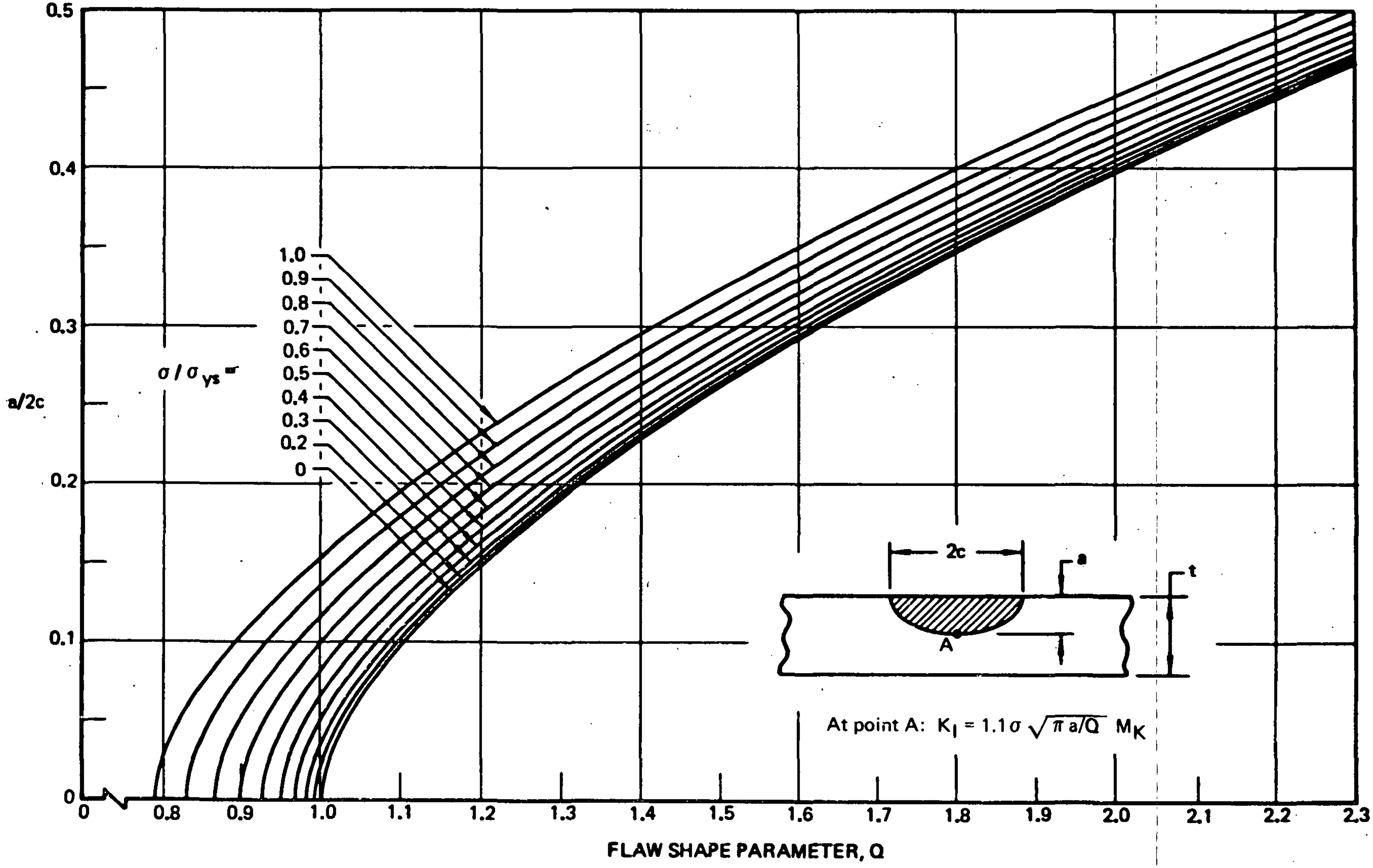

Figure 1: Shape Parameter Curves for Surface and Internal Flaws

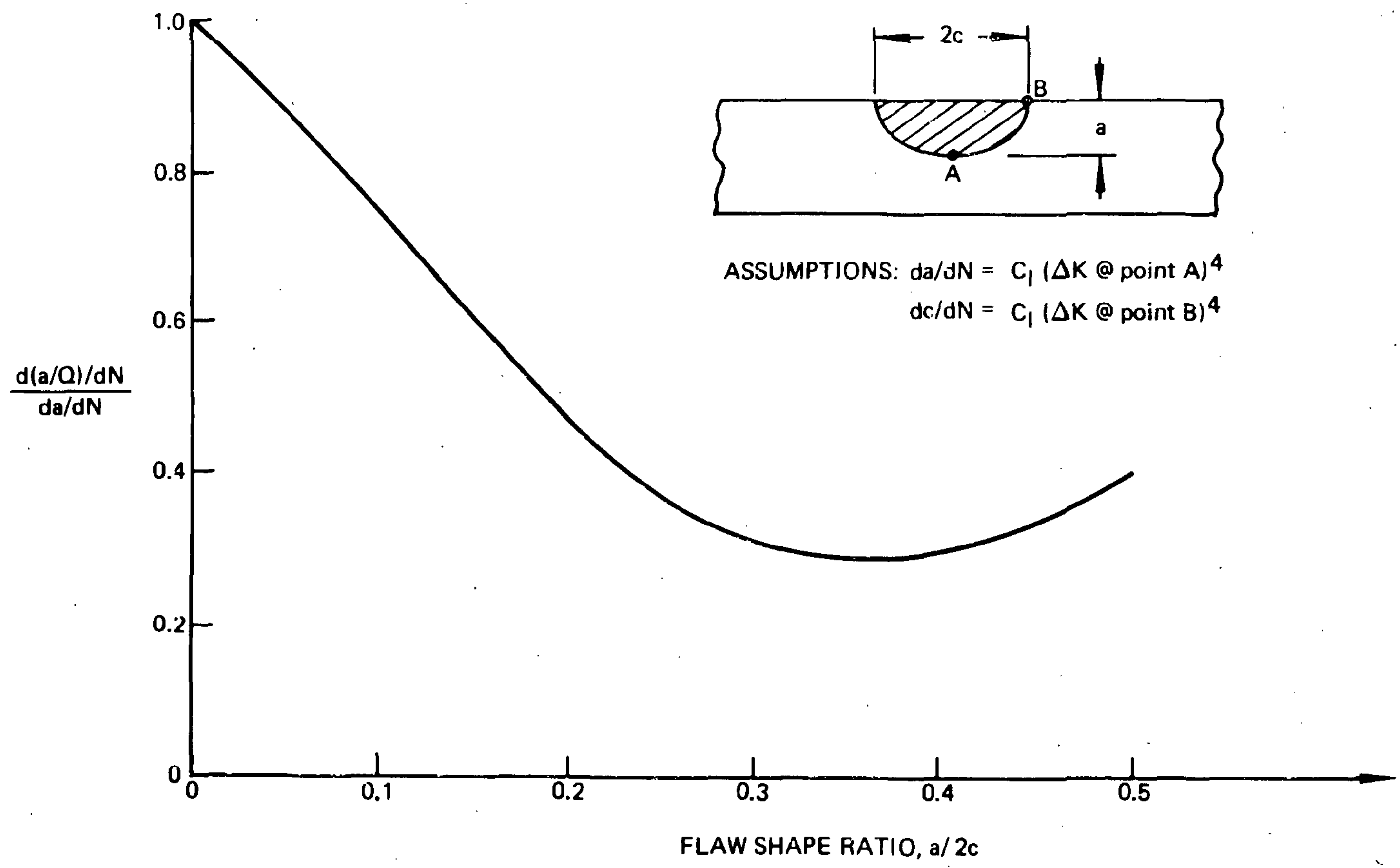

Figure 2: Analytically Derived Relationship Between d(a/Q)/dN and da/dN for Semi-Elliptical Surface Flaws

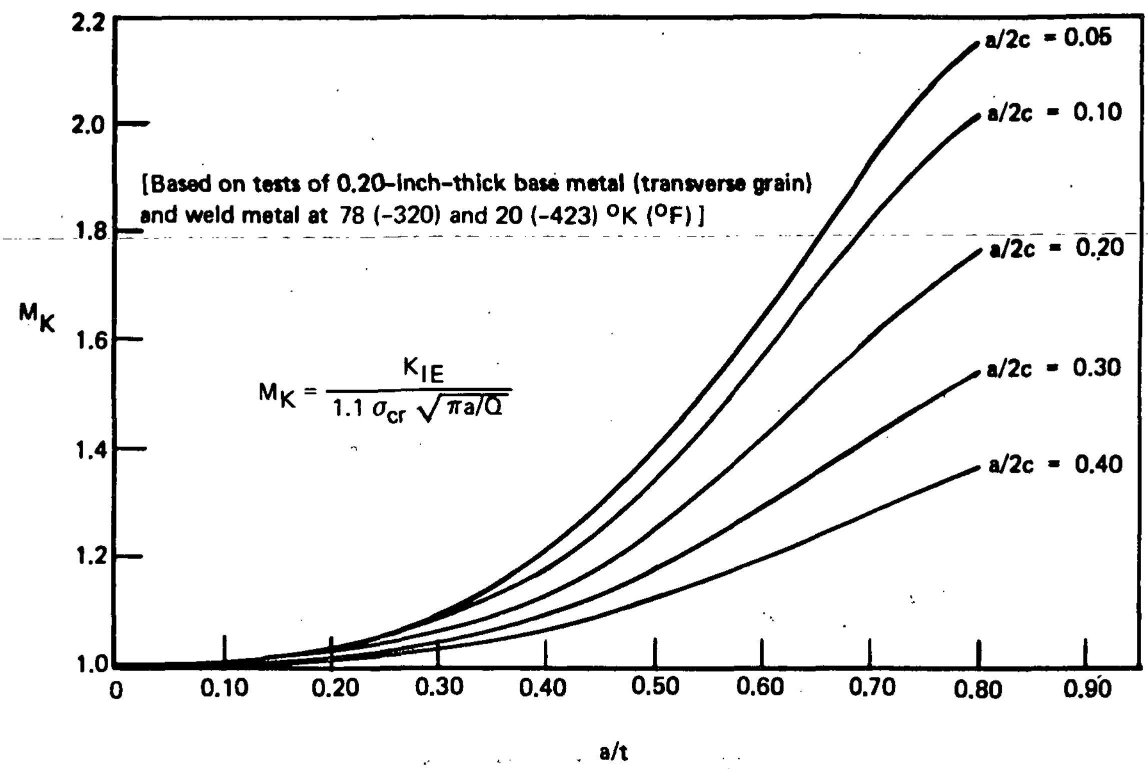

Figure 3: M_K Curves for 5Al-2.5Sn (ELI) Titanium Alloy

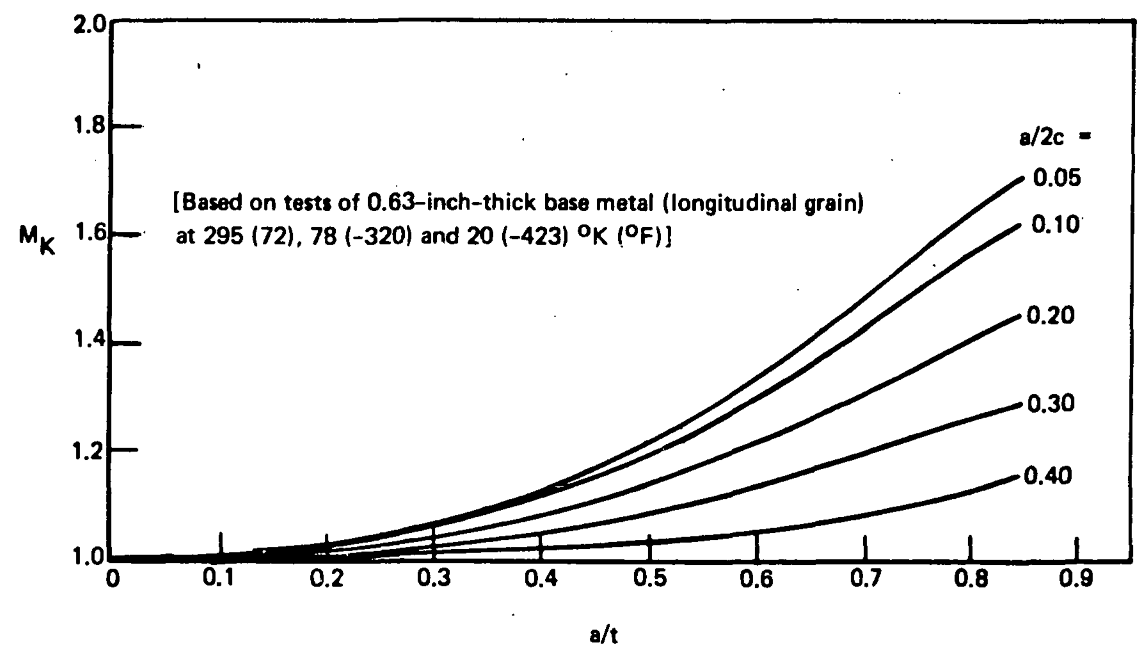

Figure 4: M_K Curves for 2219-T87 Aluminum Alloy

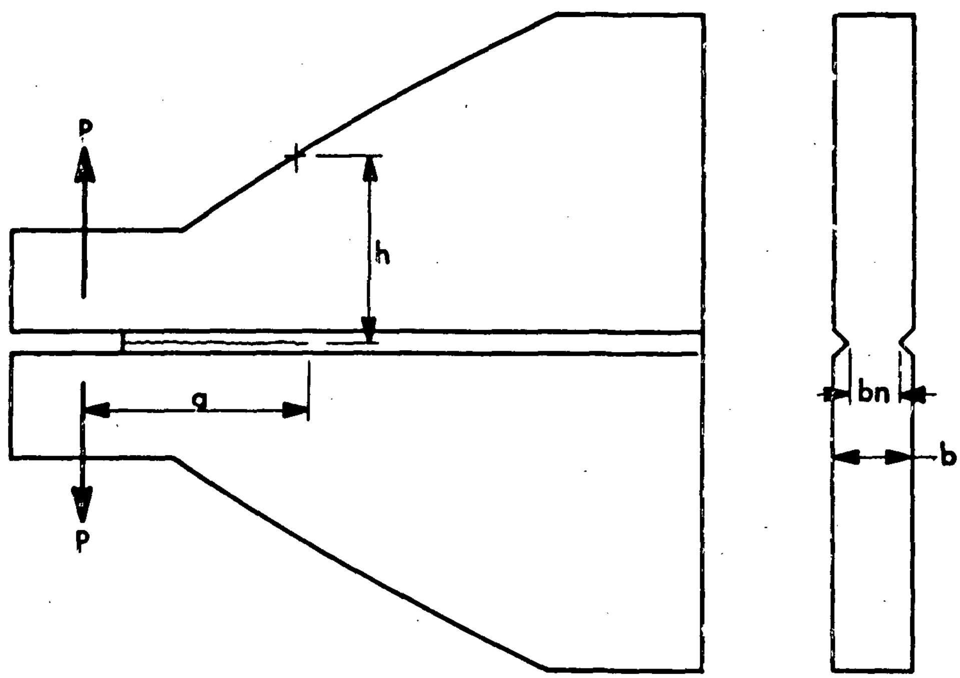

Figure 5: Tapered Double Cantilever Beam Specimen

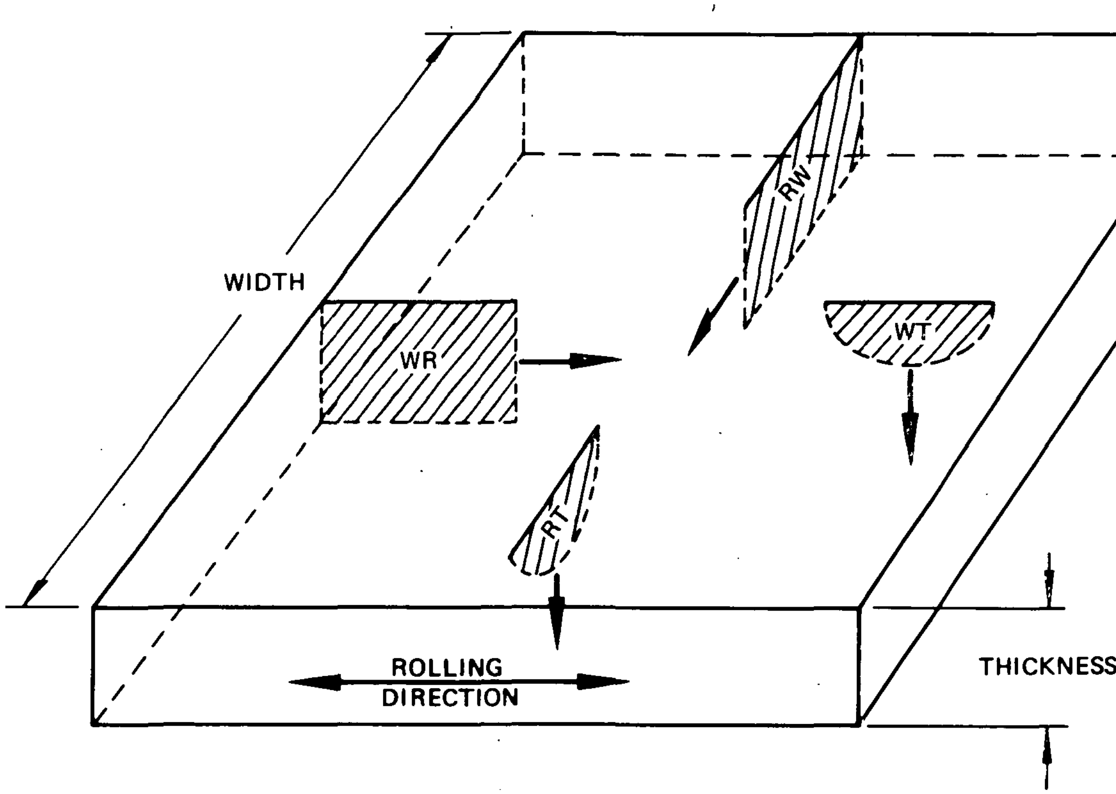

Figure 6: Nomenclature for Denoting Crack Propagation Directions

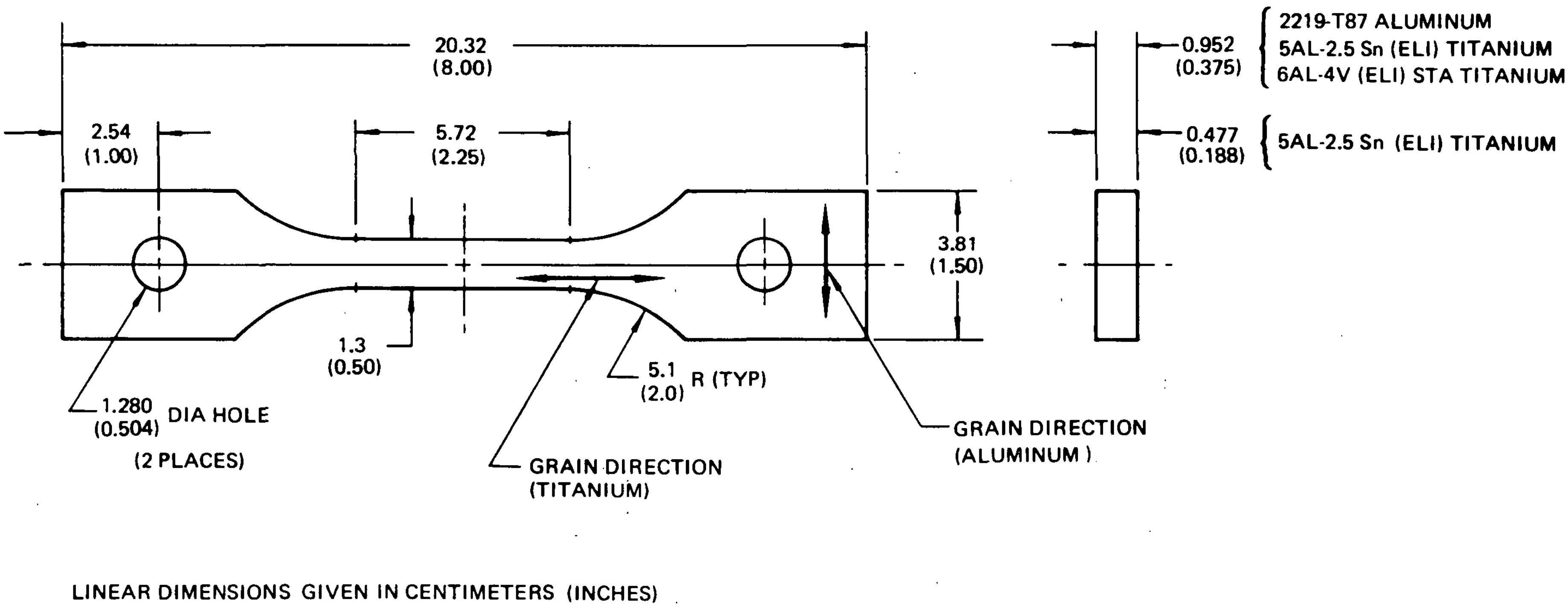

Figure 7: Aluminum and Titanium Tensile Specimen

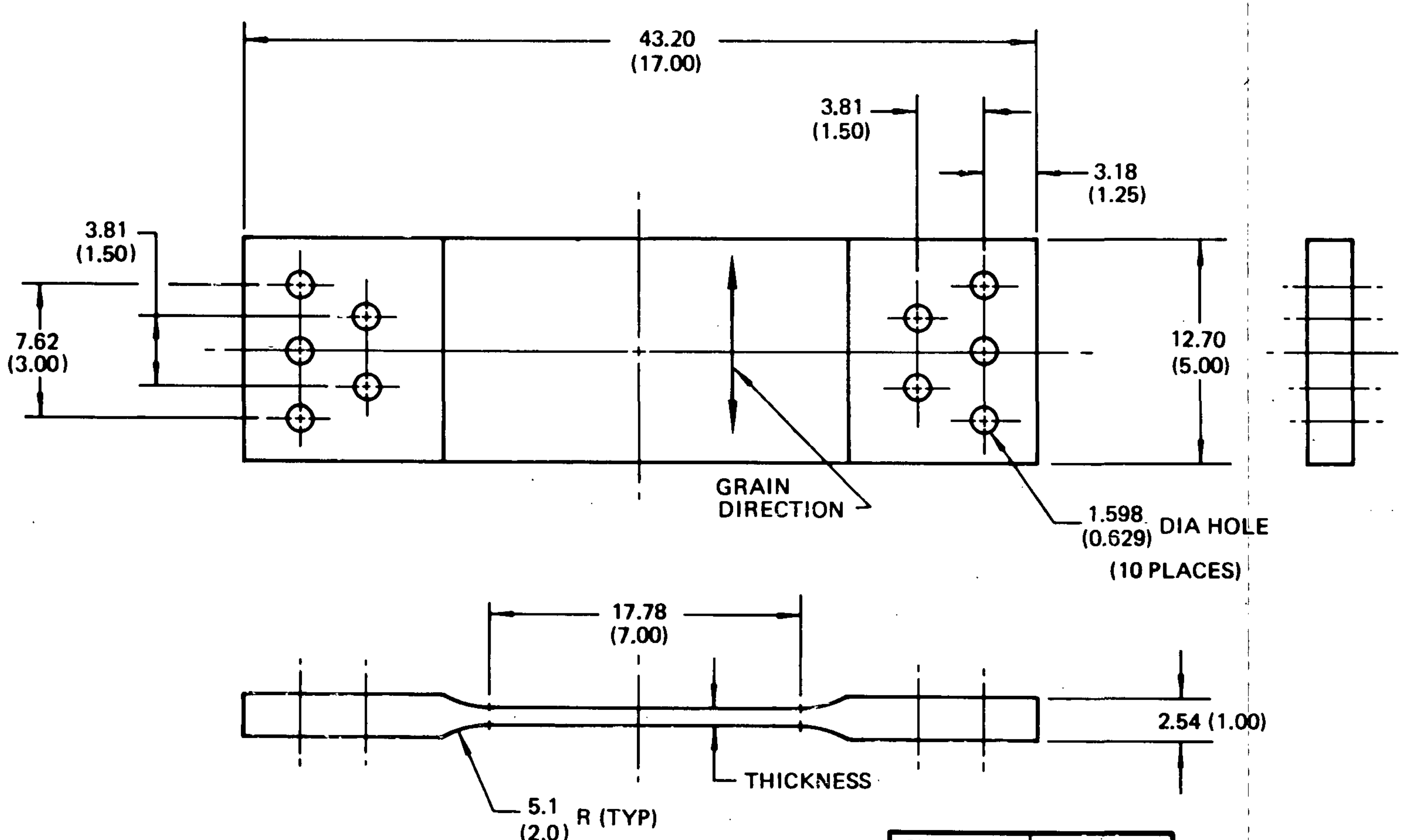

LINEAR DIMENSIONS GIVEN IN CENTIMETERS (INCHES)

SPECIMEN CONF.	THICKNESS
3A	1.016 (0.400)
3B	2.032 (0.800)

Figure 8: 2219-T87 Aluminum (295°K/72°F and 78°K/-320°F) Specimen Configuration

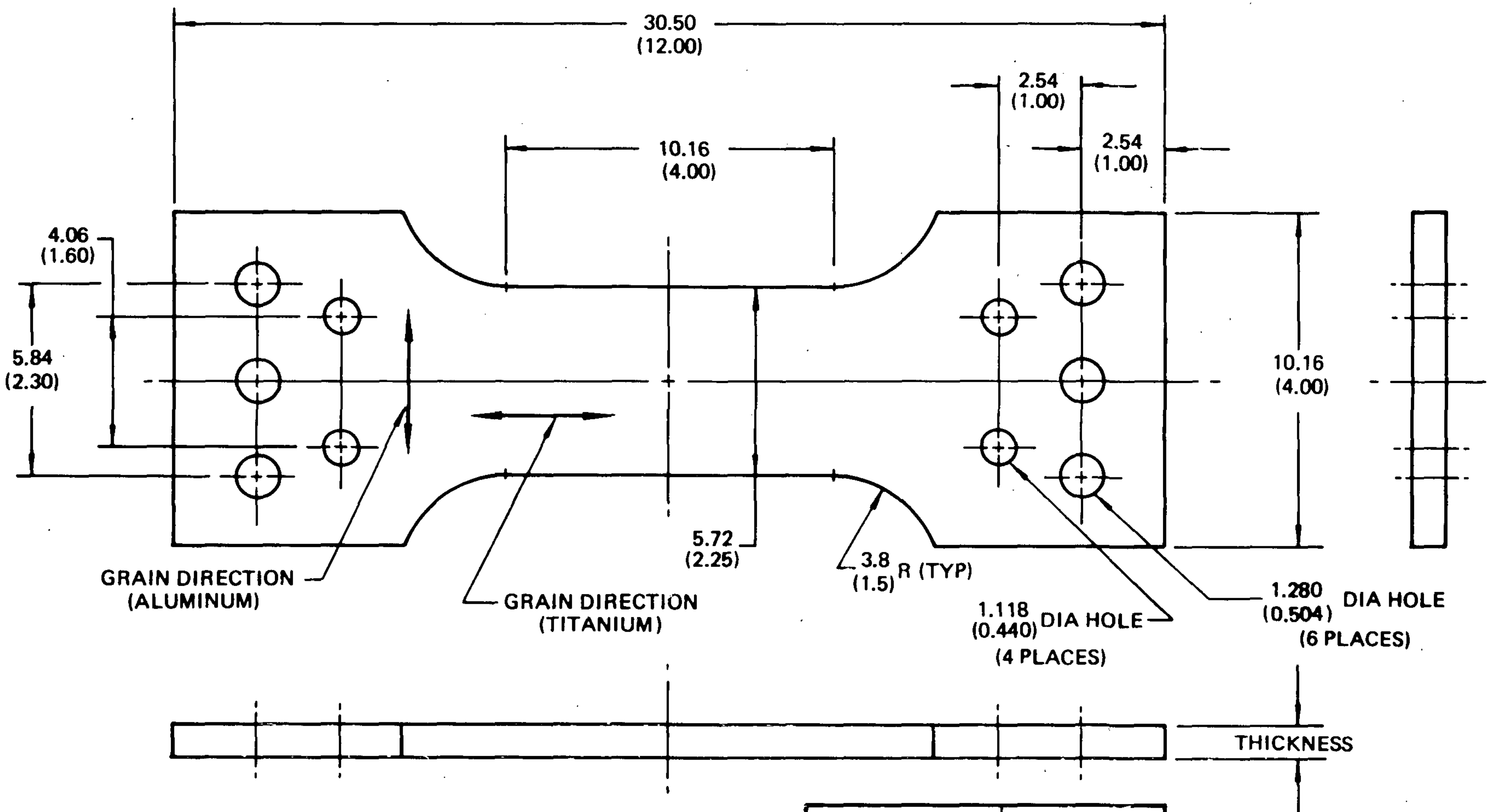

LINEAR DIMENSIONS GIVEN IN CENTIMETERS (INCHES)

SPECIMEN CONF.	THICKNESS
2A	0.381 (0.150)
2B	0.952 (0.375)
2C	1.016 (0.400)
2D	0.477 (0.188)

***Figure 9:** 5Al-2.5 Sn (ELI) Titanium (78°K/-320°F), 6Al-4V (ELI) STA Titanium (295°K/72°F), and 2219-T87 Aluminum (20°K/-423°F) Specimen Configurations*

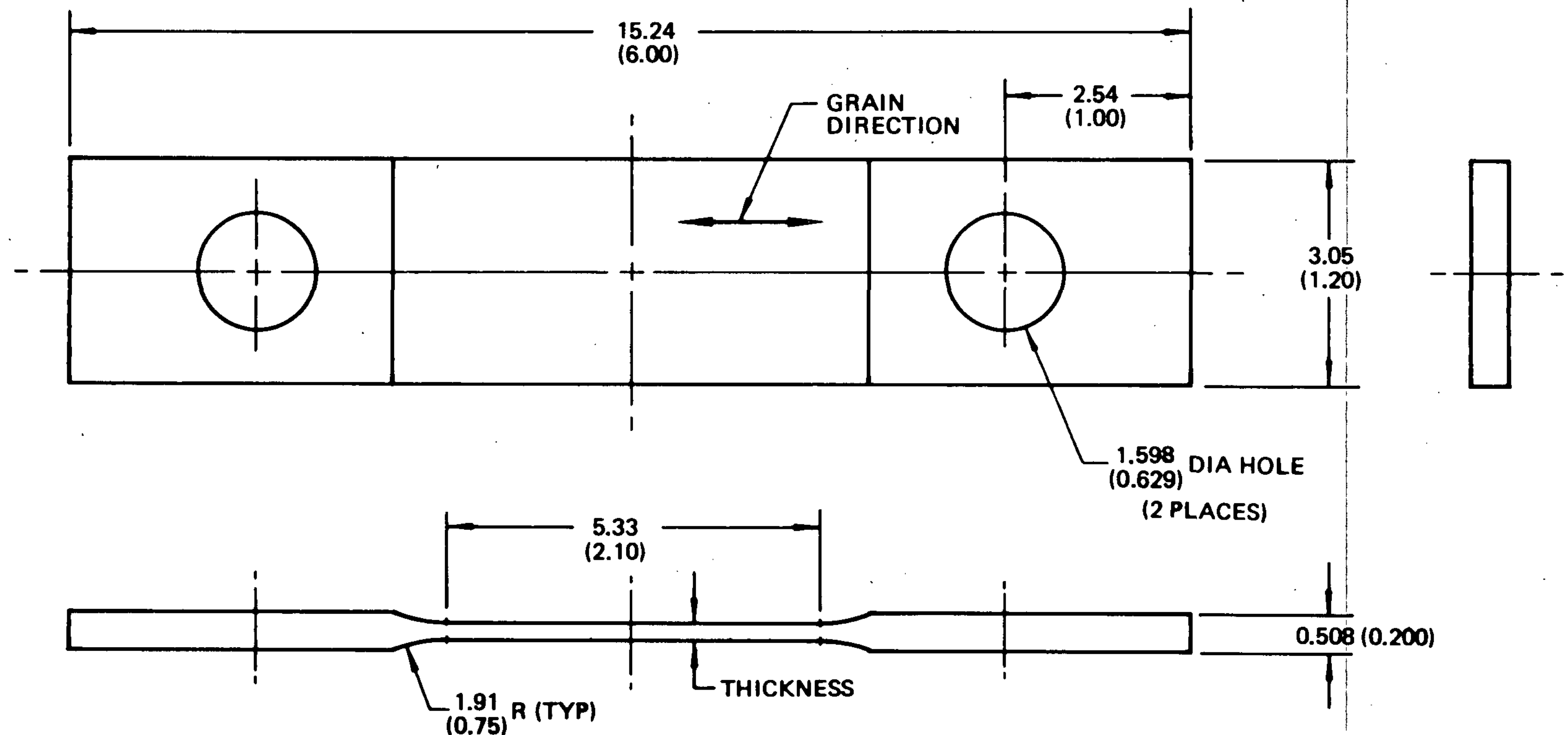

LINEAR DIMENSIONS GIVEN IN CENTIMETERS (INCHES)

SPECIMEN CONF.	THICKNESS
6A	0.254 (0.100)

Figure 10: 5Al-2.5 Sn (ELI) Titanium (20^{o}K/–423^{o}F) Specimen Configuration

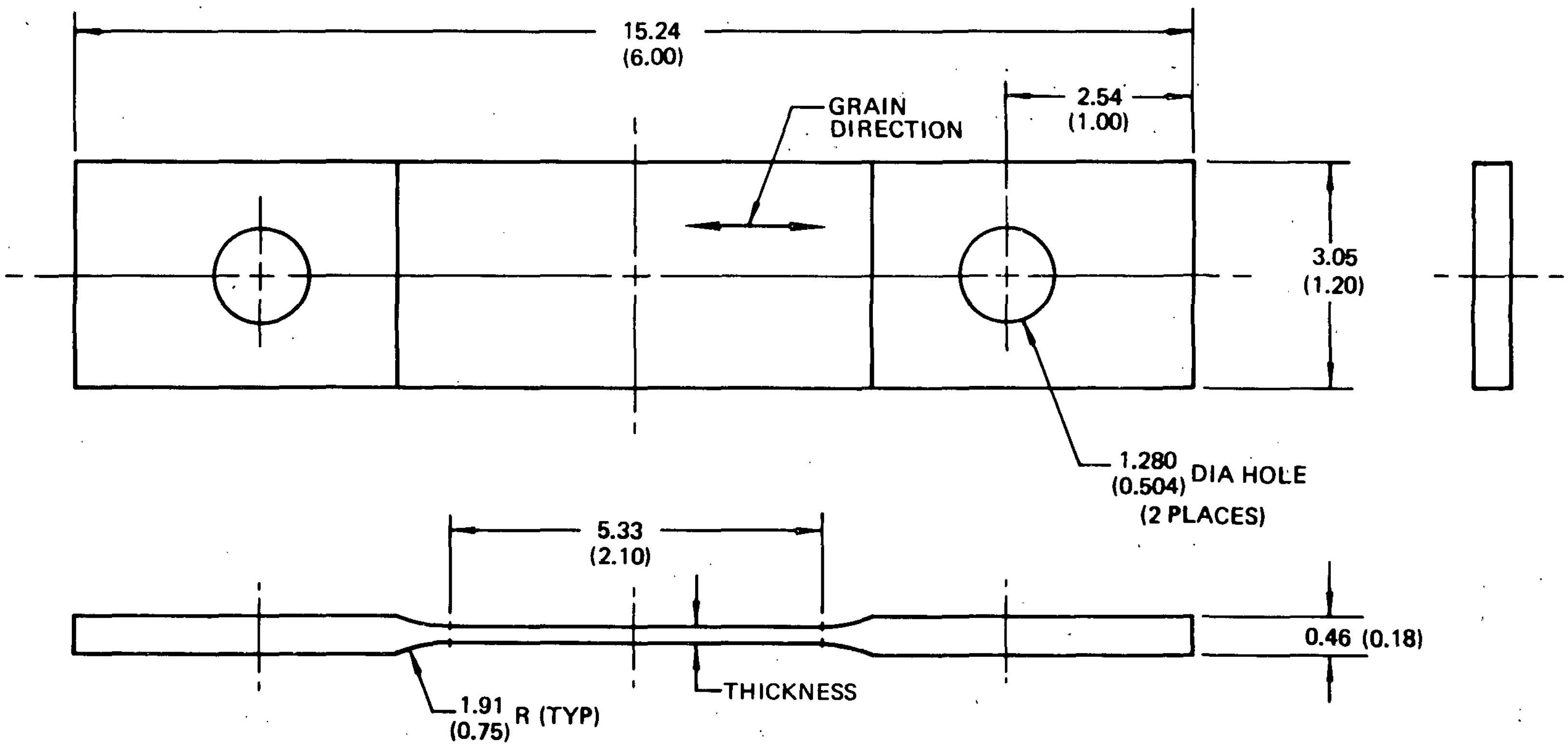

LINEAR DIMENSIONS GIVEN IN CENTIMETERS (INCHES)

SPECIMEN CONF.	THICKNESS
5A	0.168 (0.066)
5B	0.254 (0.100)

Figure 11: 6Al-4V (ELI) STA Titanium (295°K/72°F) and 5Al-2.5 Sn ELI Titanium (20°K/-423°F) Specimen Configurations

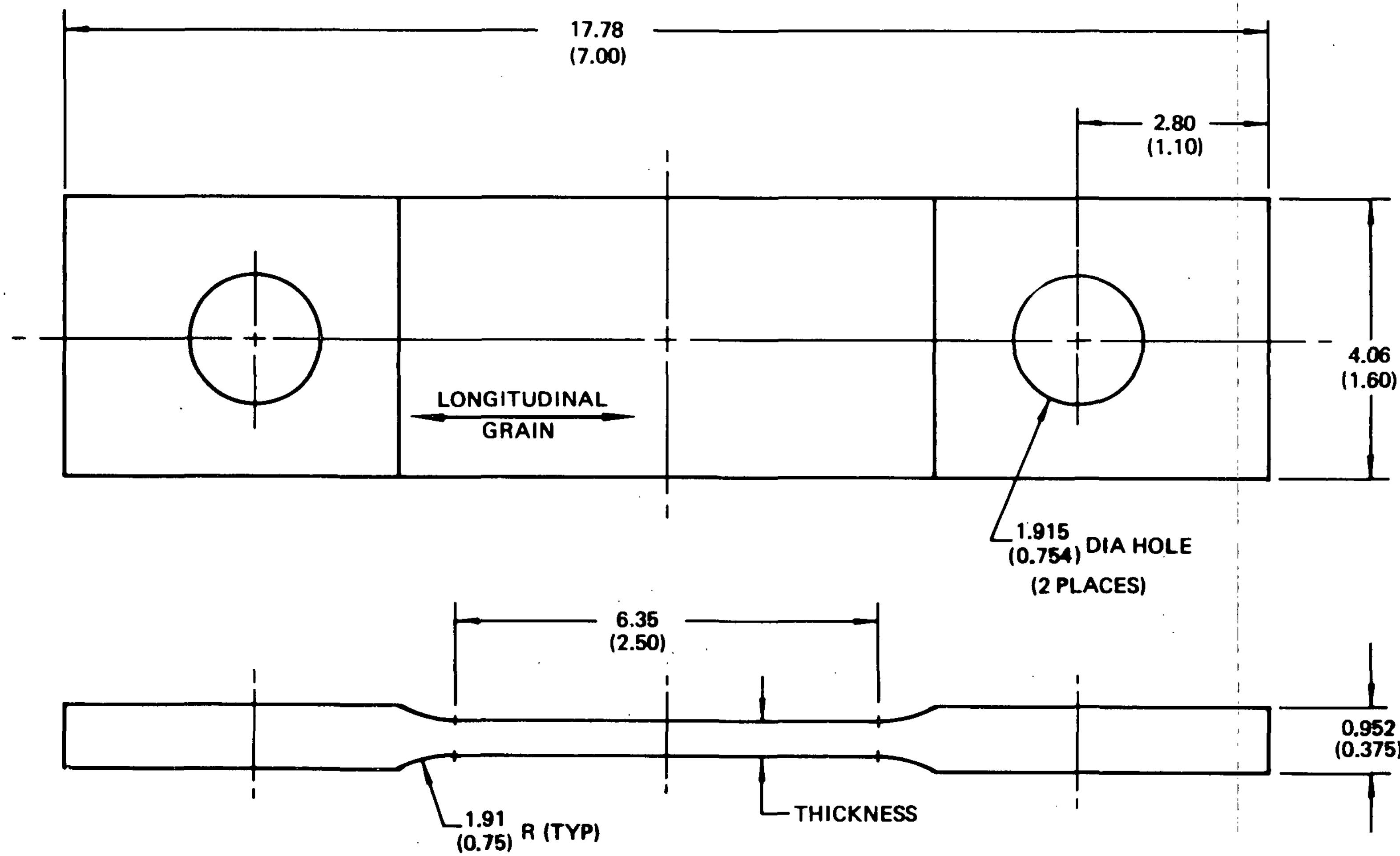

LINEAR DIMENSIONS GIVEN IN CENTIMETERS (INCHES)

SPECIMEN CONF.	THICKNESS
7A	0.508 (0.200)

Figure 12: 6Al-4V (ELI) STA Titanium (295° K/72° F) Specimen Configuration

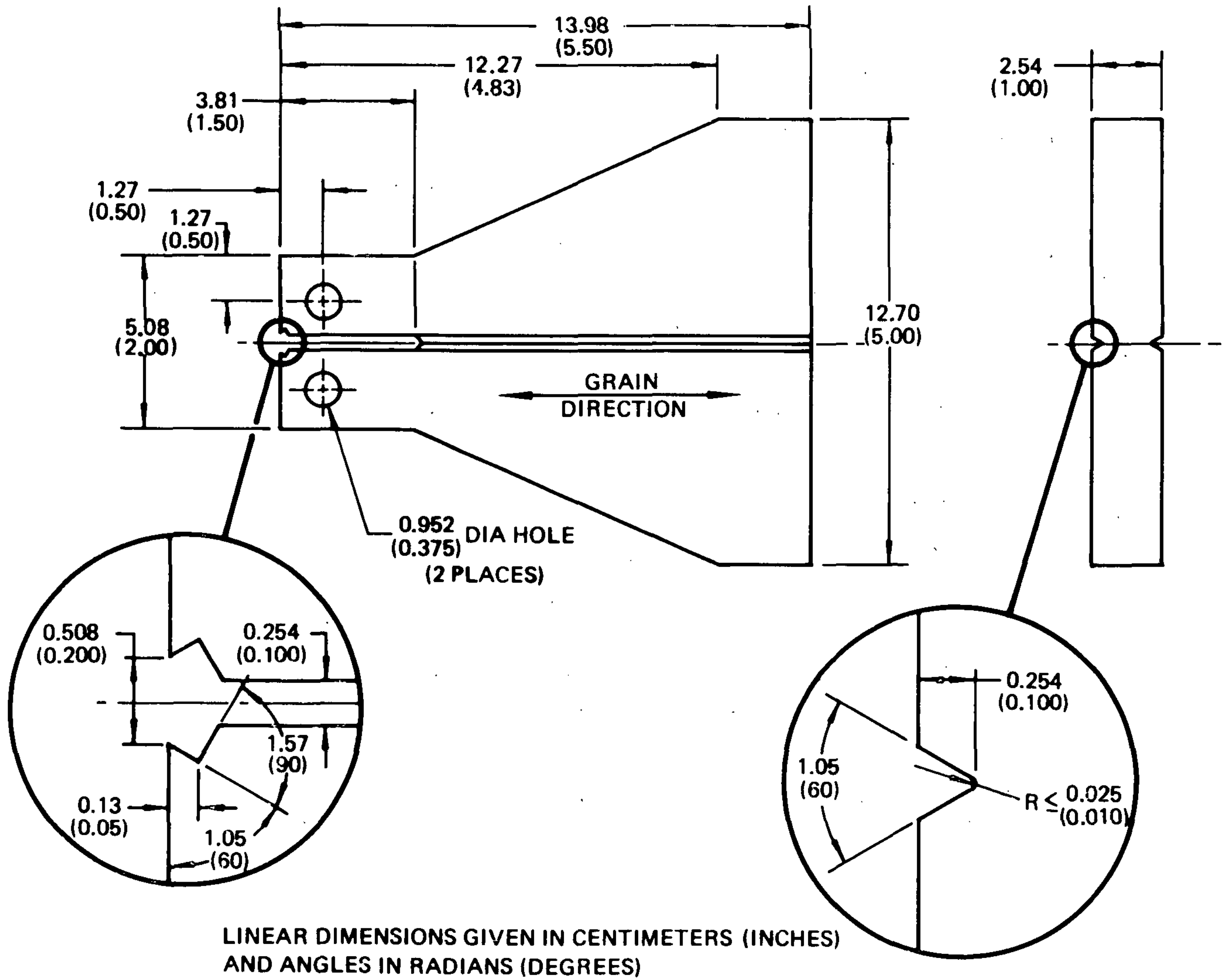

Figure 13: 2219-T87 Aluminum Tapered Double Cantilever Beam Specimen

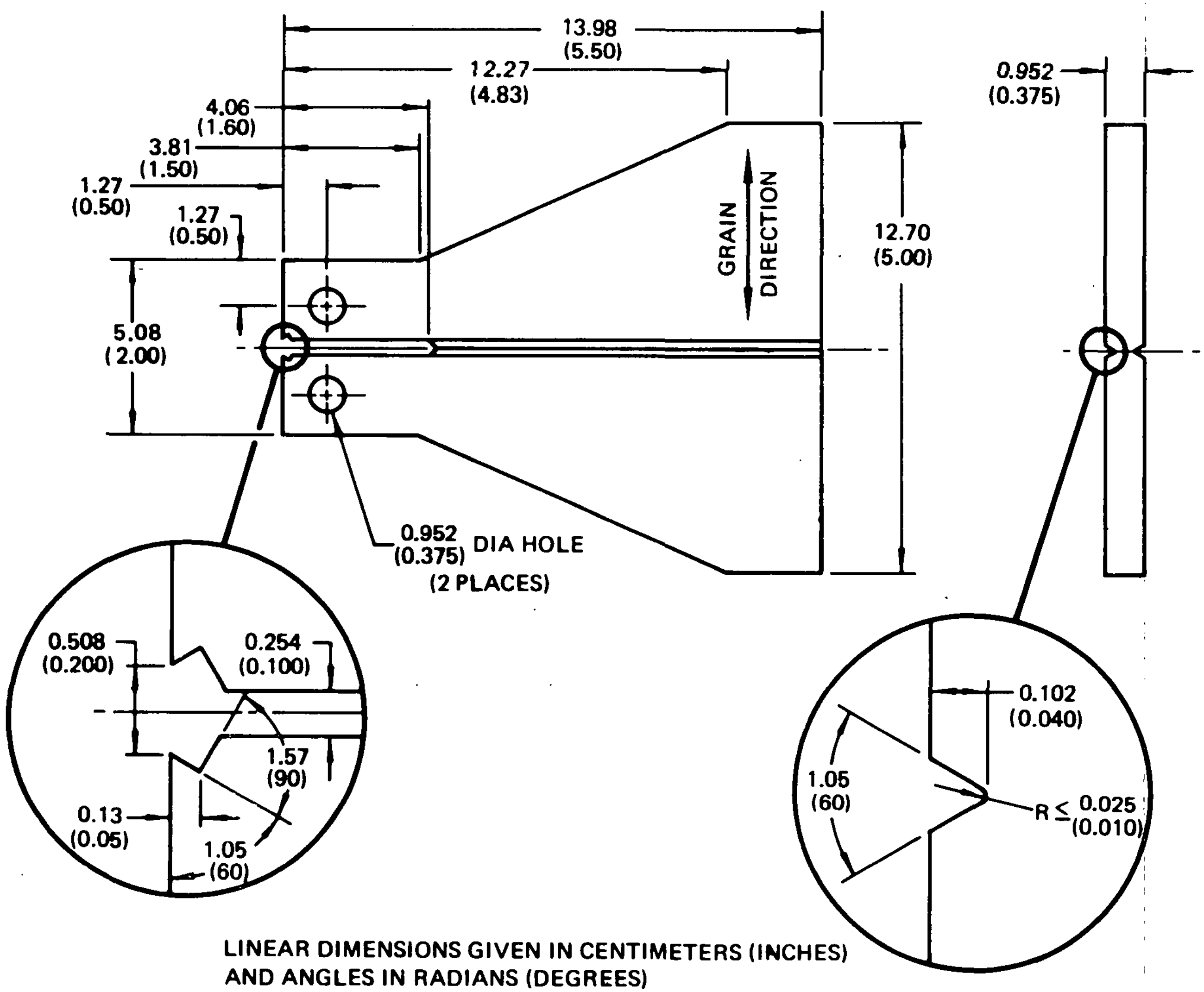

Figure 14: 6Al-4V (ELI) STA Titanium Tapered Double Cantilever Beam Specimen

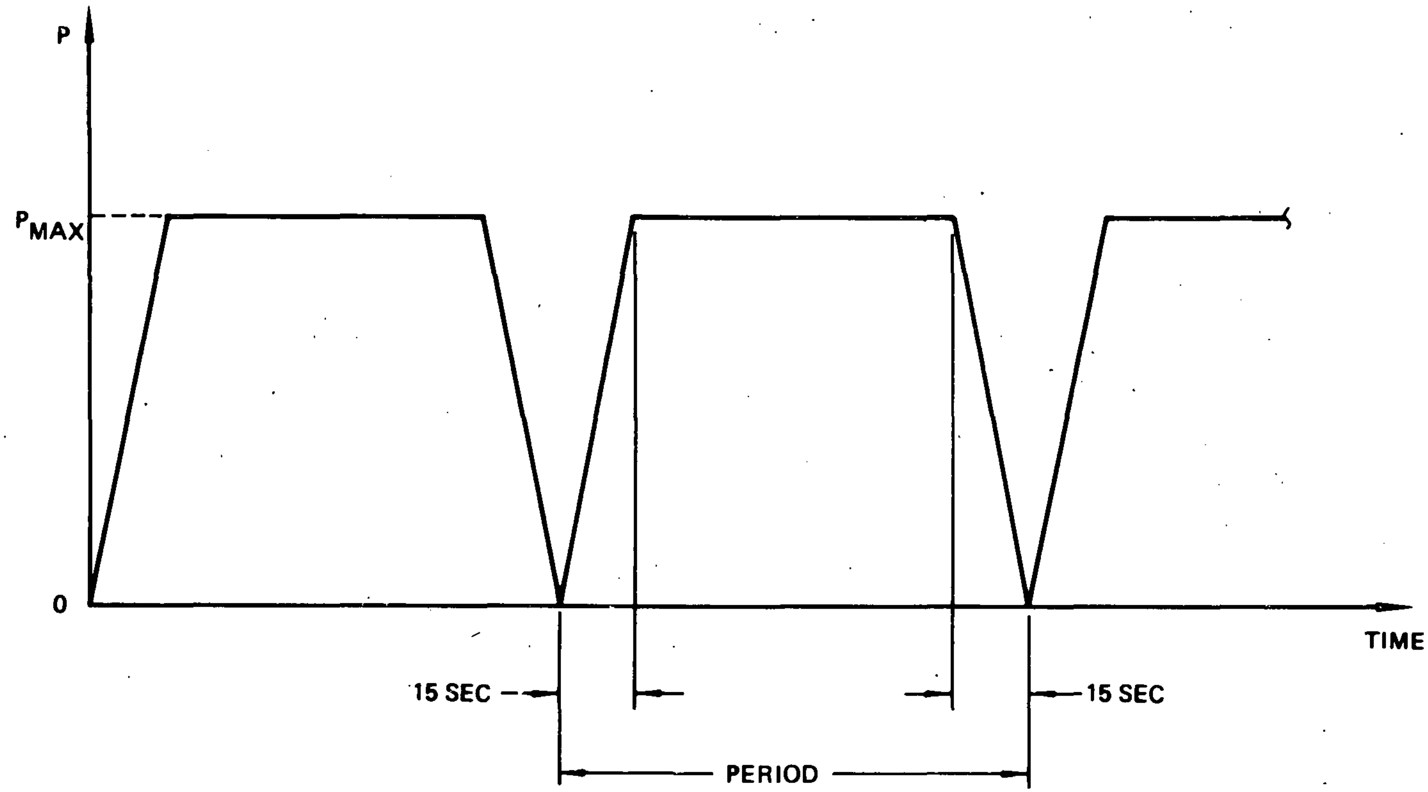

Figure 15: Trapezoidal Loading Profiles

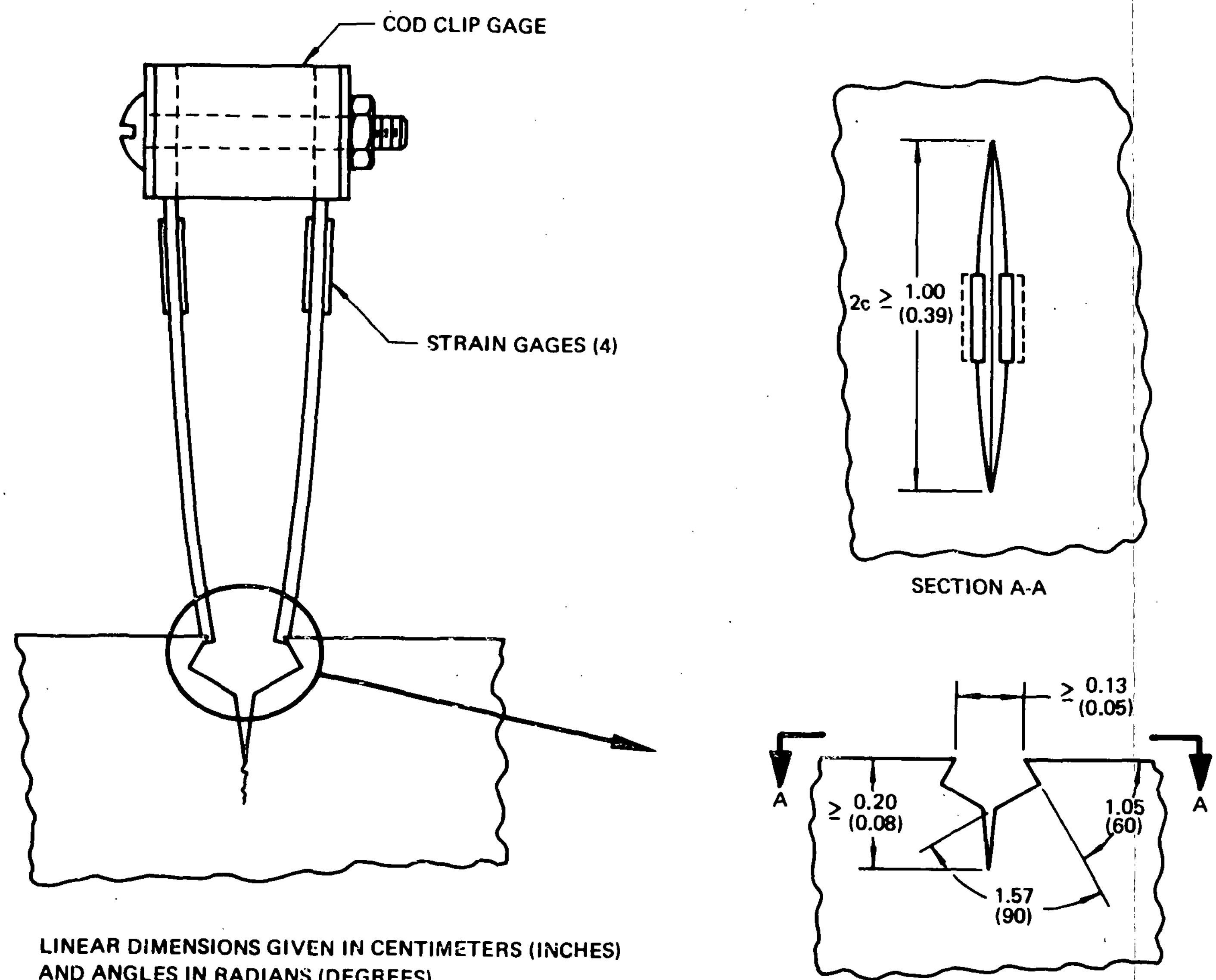

Figure 16: Clip Gage Instrumentation for Large Surface Flaws

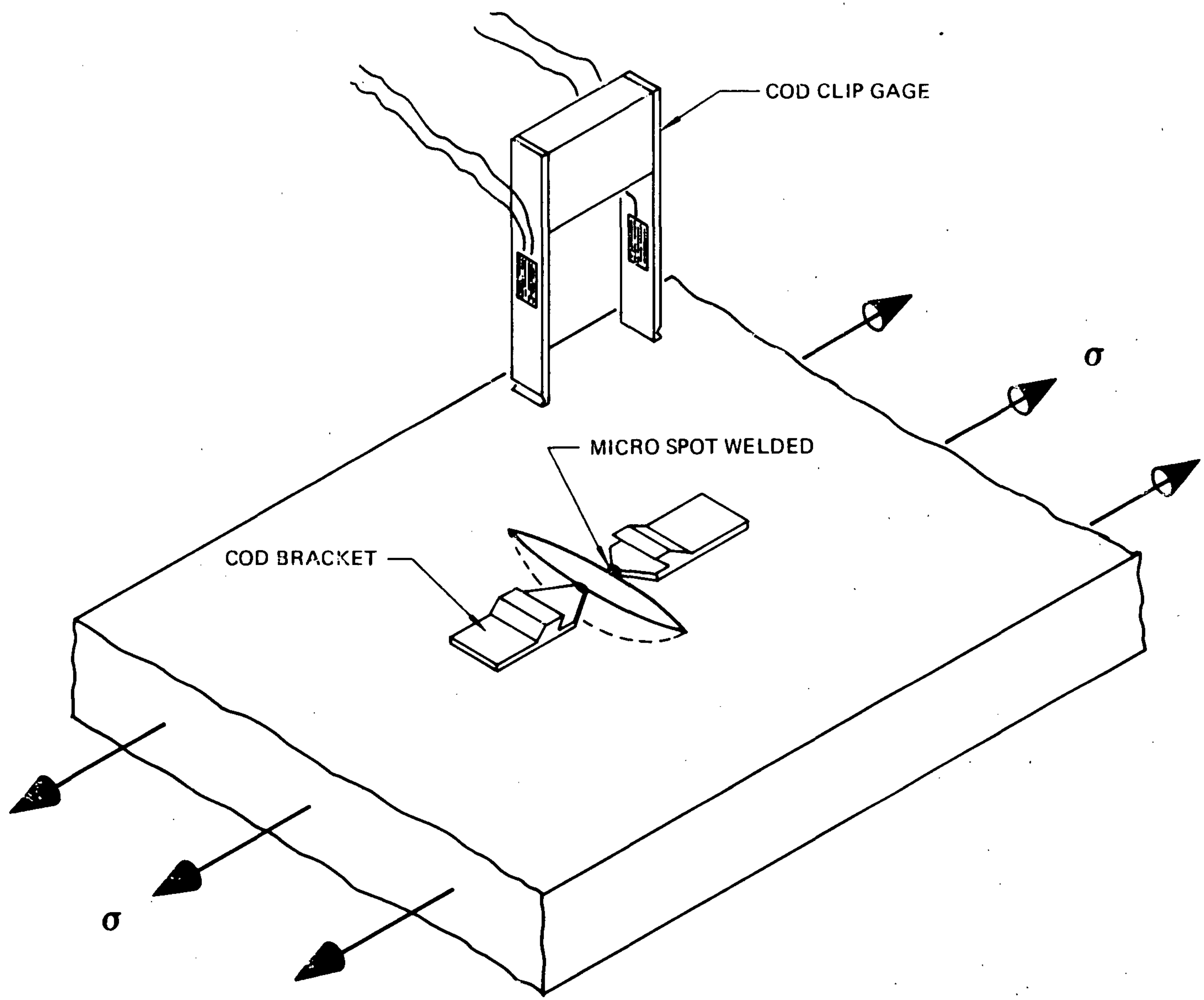

Figure 17: Clip Gage Instrumentation for Small Surface Flaws

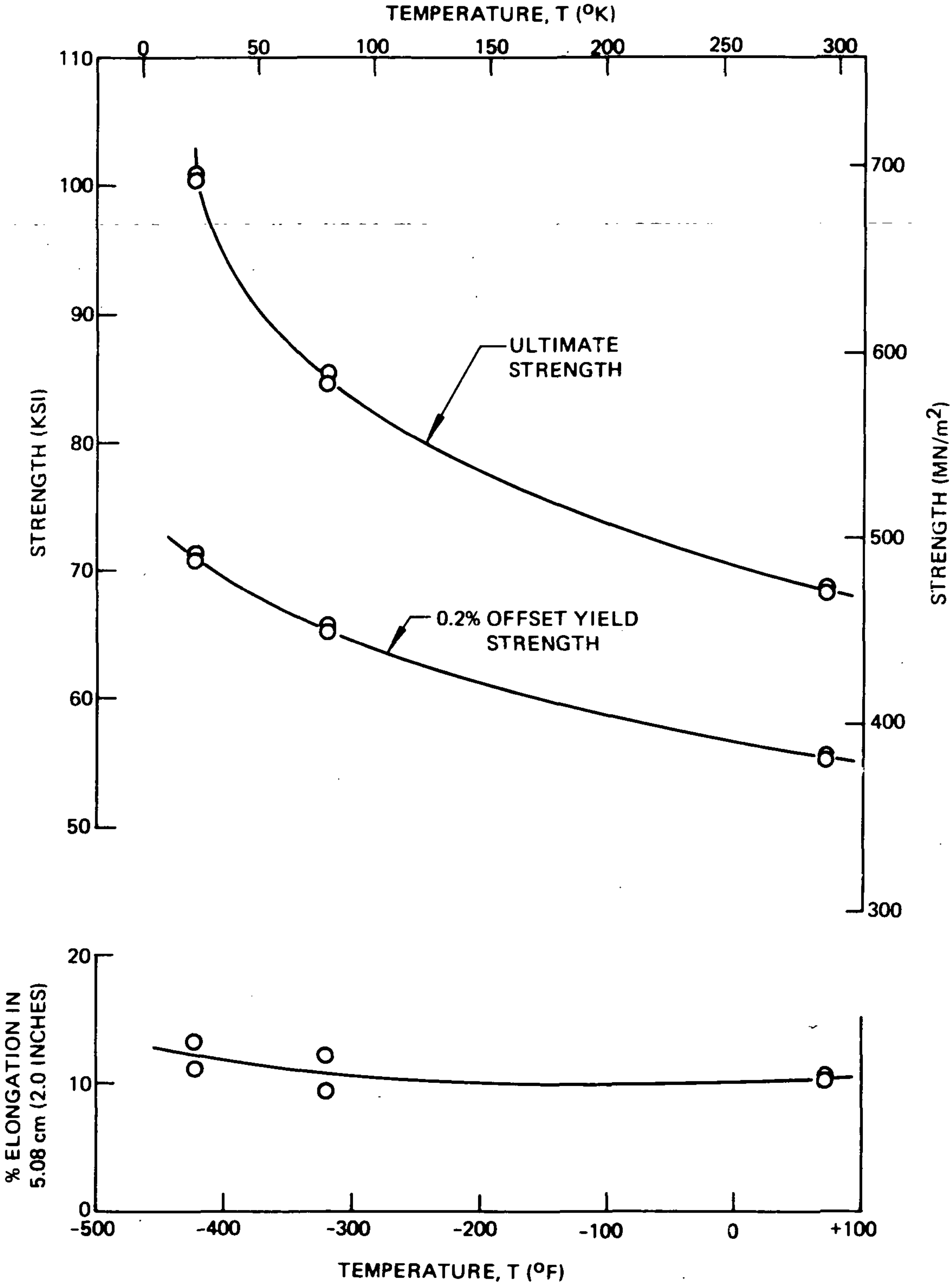

Figure 18: Mechanical Properties of 2219-T87 Aluminum Plate (Transverse Grain)

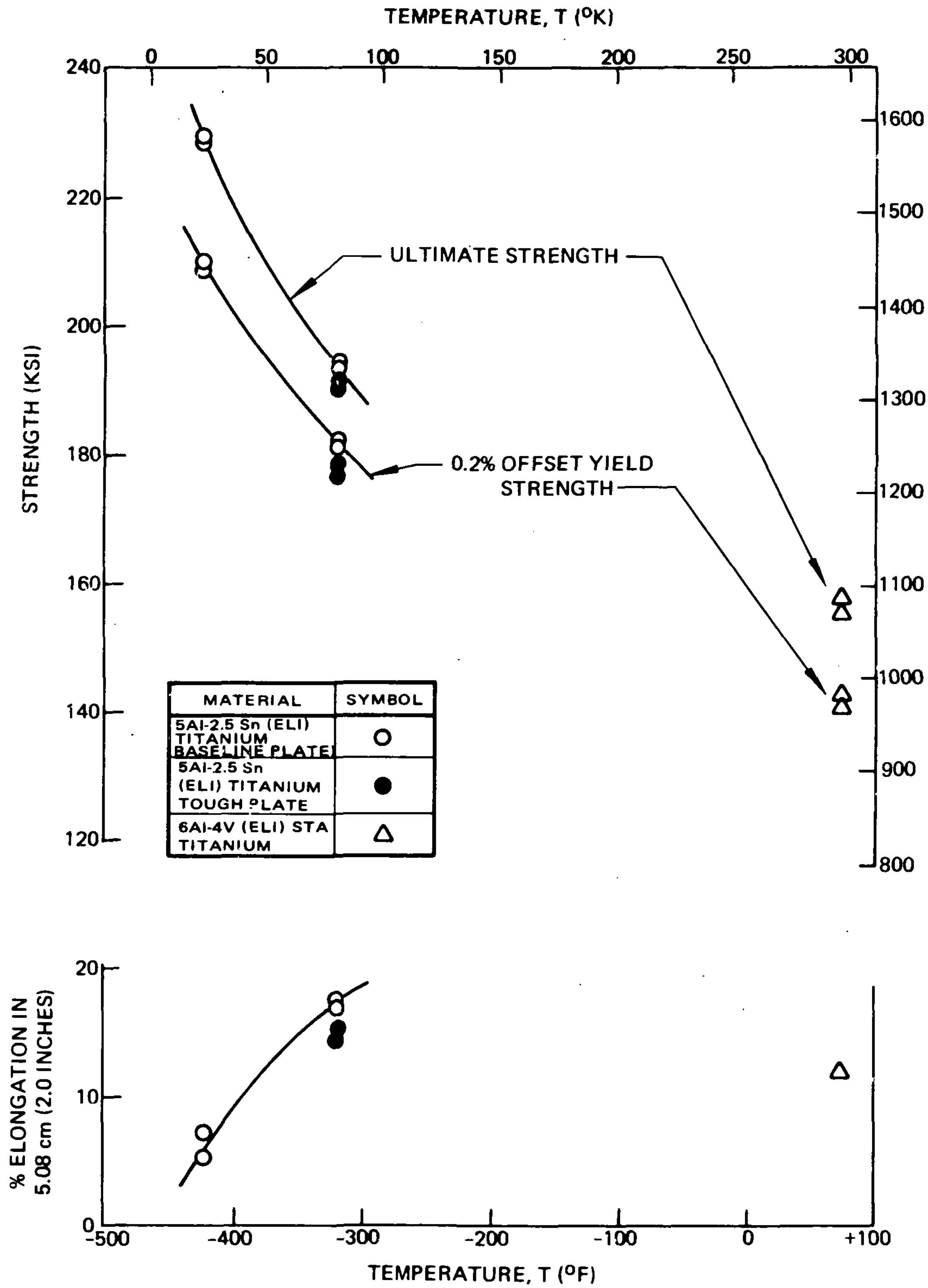

Figure 19: Mechanical Properties of 5Al-2.5 Sn (ELI) Titanium and 6Al-4V (ELI) STA Titanium (Longitudinal Grain)

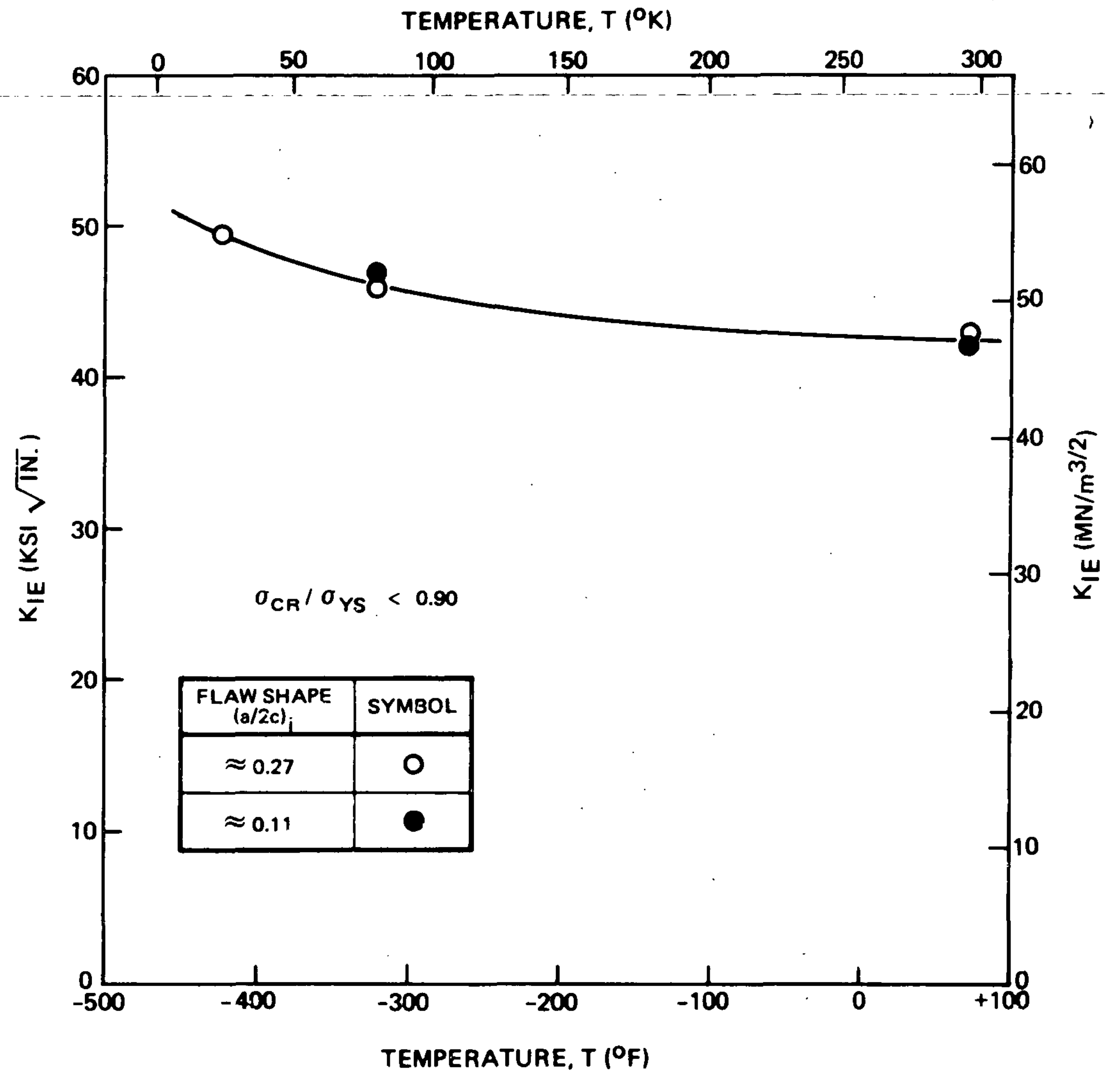

Figure 20: Critical Stress Intensity of 2219-T87 Aluminum Plate (Surface Flawed Specimens—WT Direction)

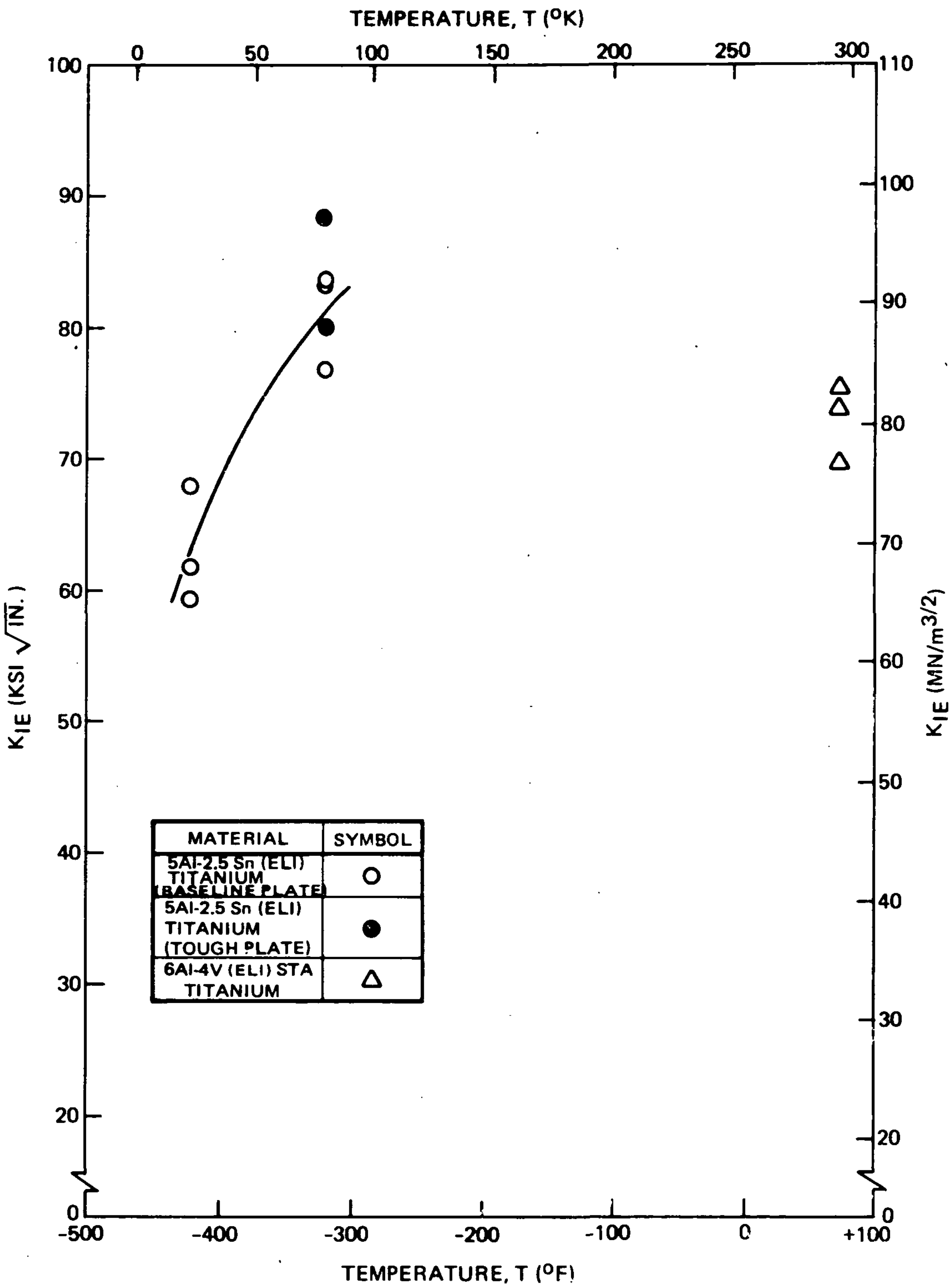

Figure 21: Critical Stress Intensity of 5Al-2.5 Sn (ELI) Titanium and 6Al-4V (ELI) STA Titanium Plate (RT Direction)

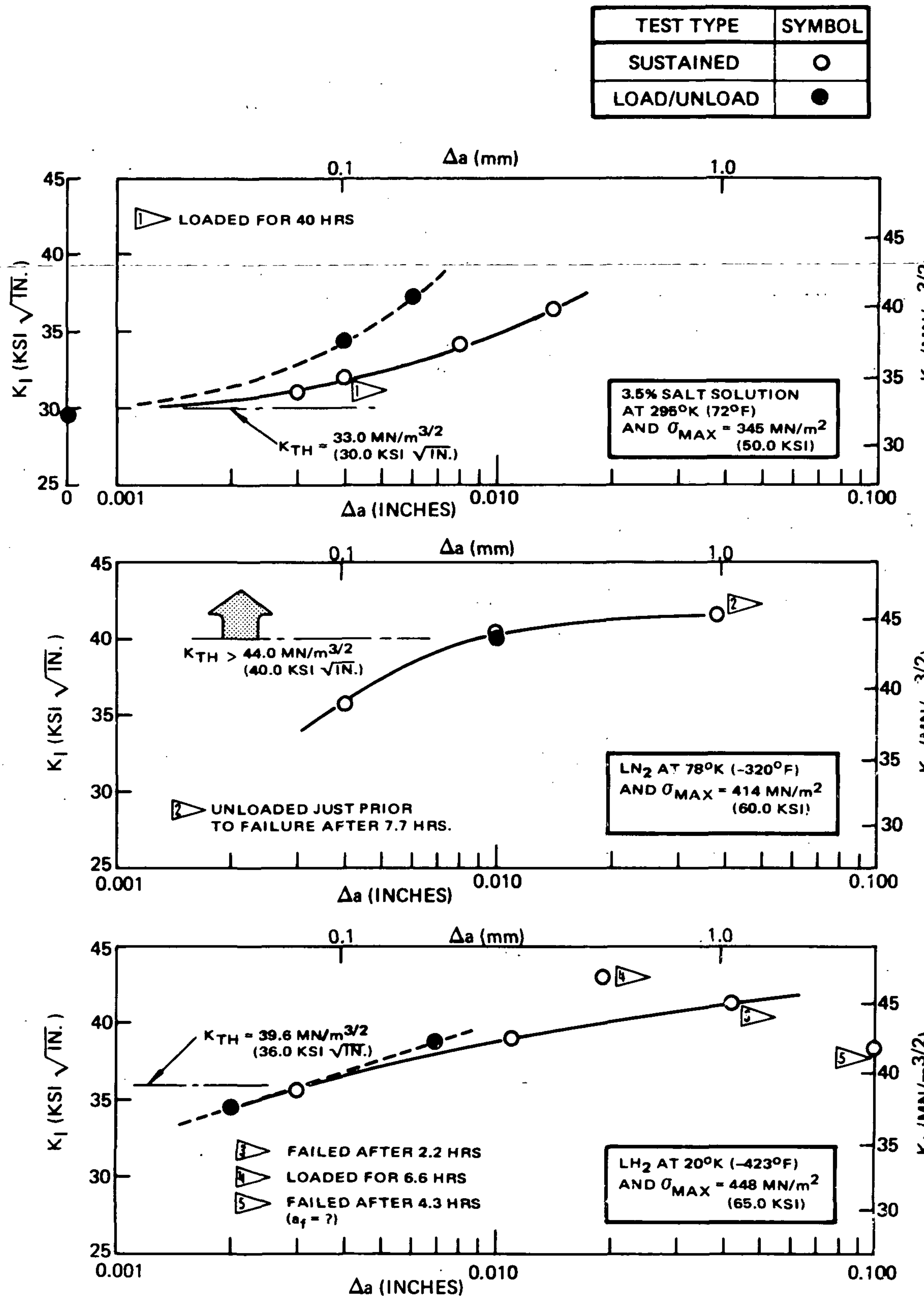

Figure 22: Flaw Depth Growth During 10 Hour Sustained Load and Load/Unload Tests of 2219-T87 Aluminum Surface Flawed Plate (WT Direction)

TEST TYPE	σ_{MAX}, MN/m^2 (KSI)		
	951 (137.9)	1089 (158.0)	1131 (164.0)
10 HR SUSTAINED	○	△	□
LOAD/UNLOAD			■

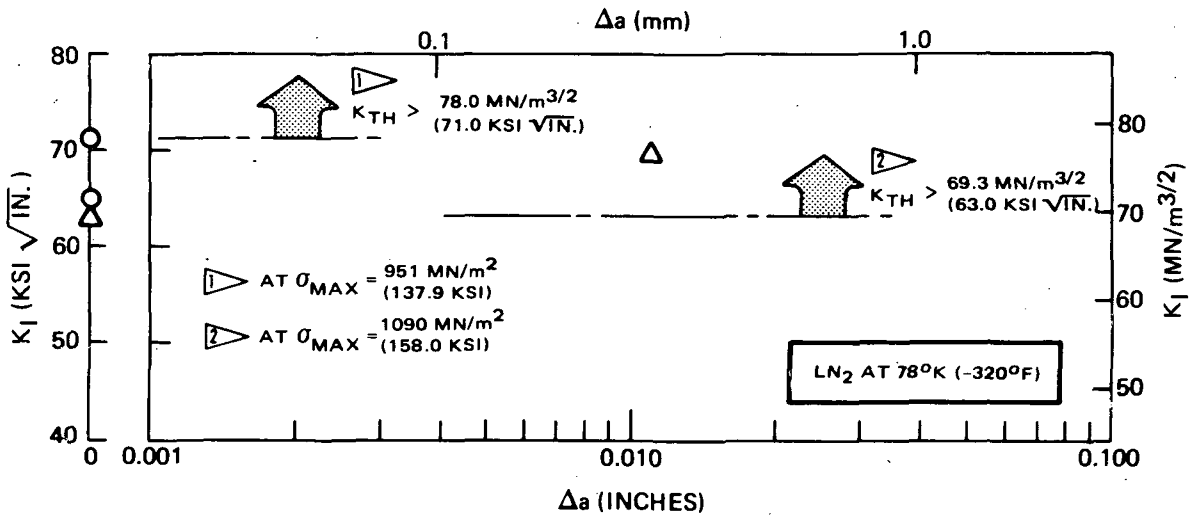

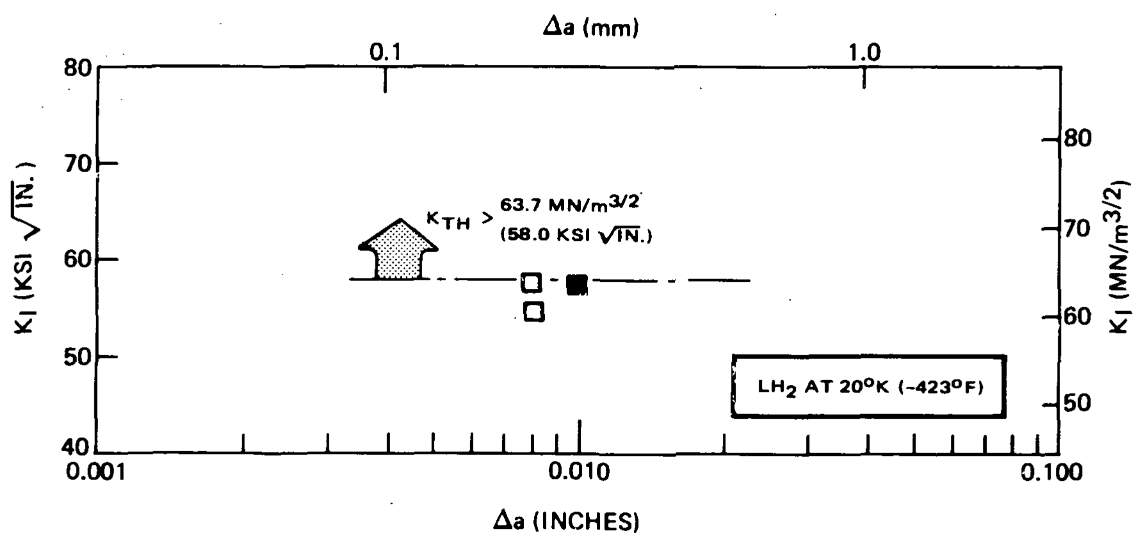

Figure 23: Flaw Depth Growth During 10 Hour Sustained Load and Load/Unload Tests of 5Al-2.5 Sn (ELI) Titanium Surface Flawed Plate (RT Direction)

TEST TYPE	σ_{MAX}, MN/m^2 (KSI)		
	848 (123.0)	772 (112.0)	648 (94.0)
10 HR SUSTAINED	○	△	□
LOAD/UNLOAD IN AIR	●	▲	

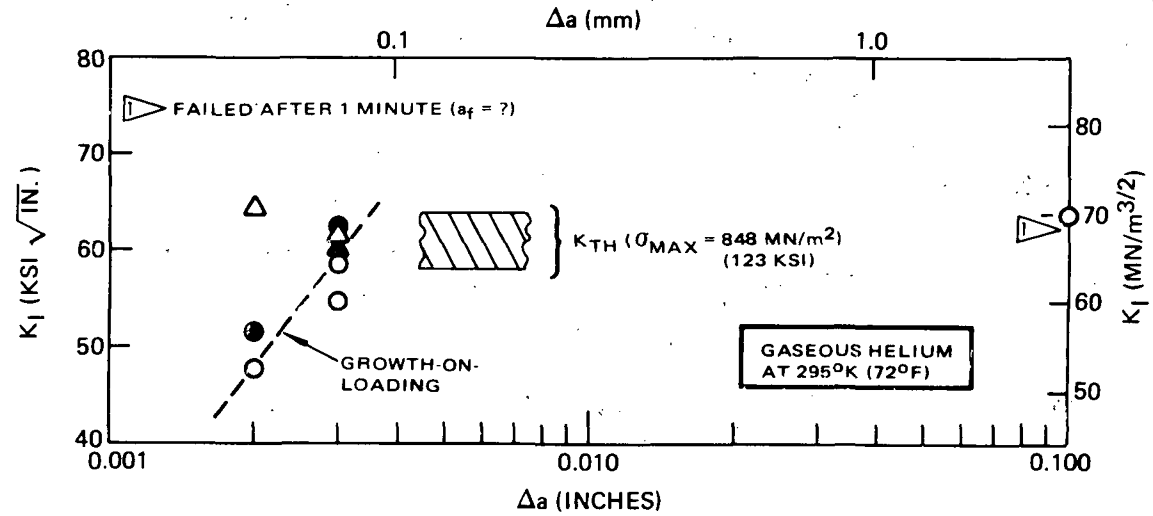

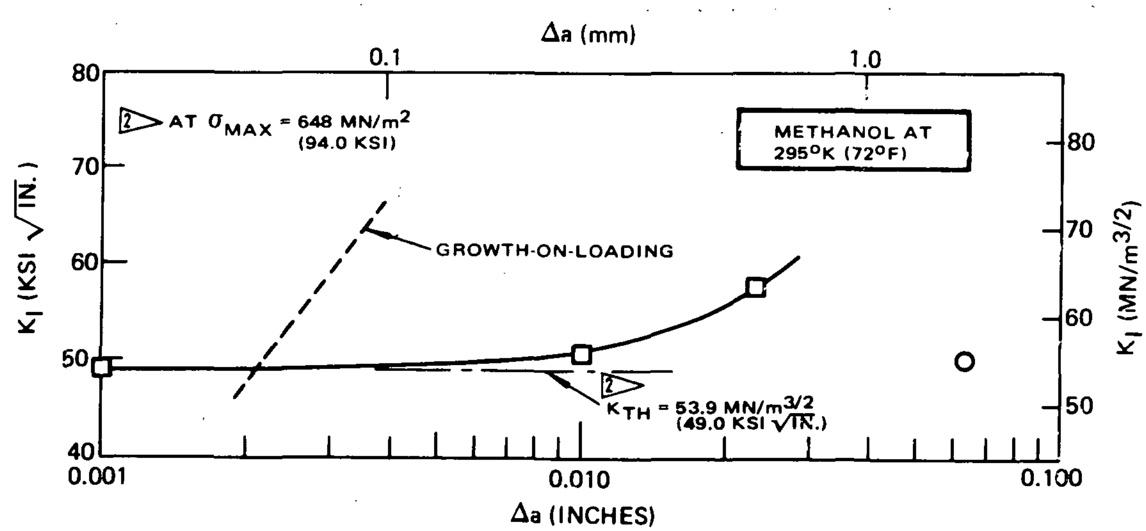

Figure 24: Flaw Depth Growth During 10 Hour Sustained Load and Load/Unload Tests of 6Al-4V (ELI) STA Titanium Surface Flawed Plate (RT Direction)

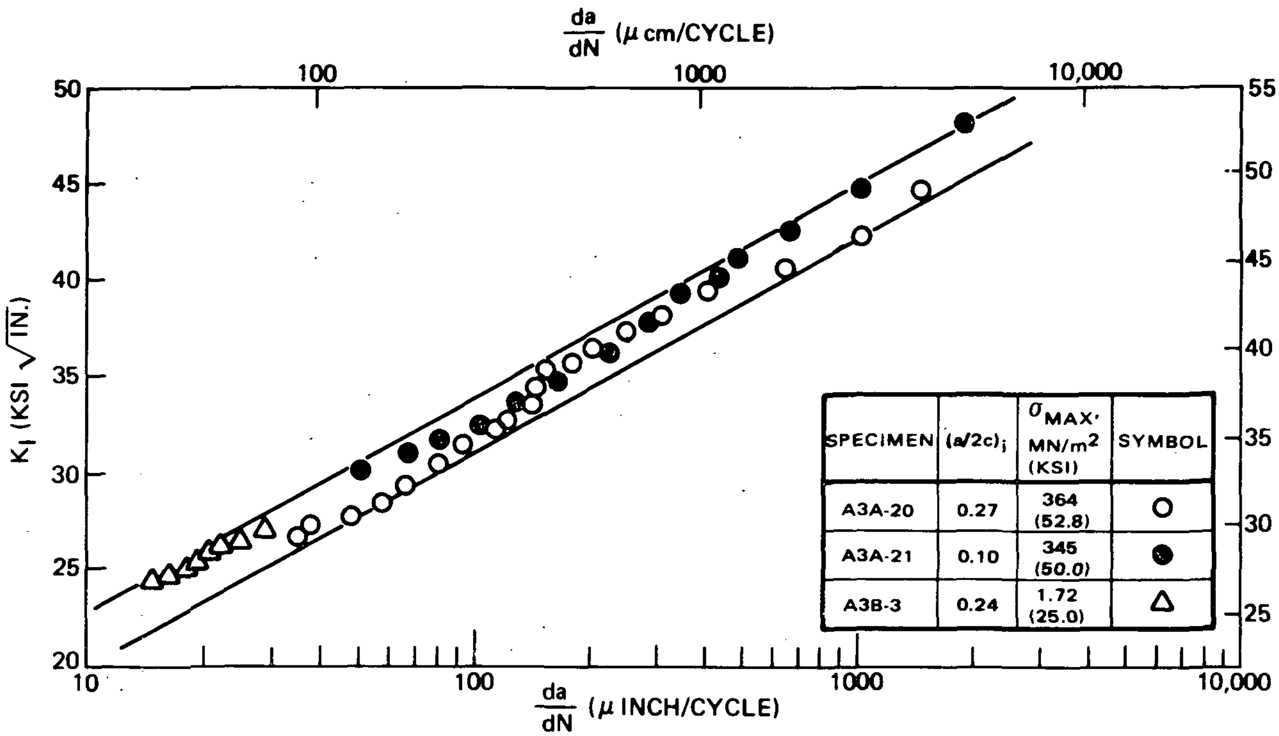

Figure 25: Surface Flaw Fatigue Growth Rates of 2219-T87 Aluminum Plate (WT Direction) in Gaseous Helium at 295°K (72°F) and 333 mHz (20 CPM)

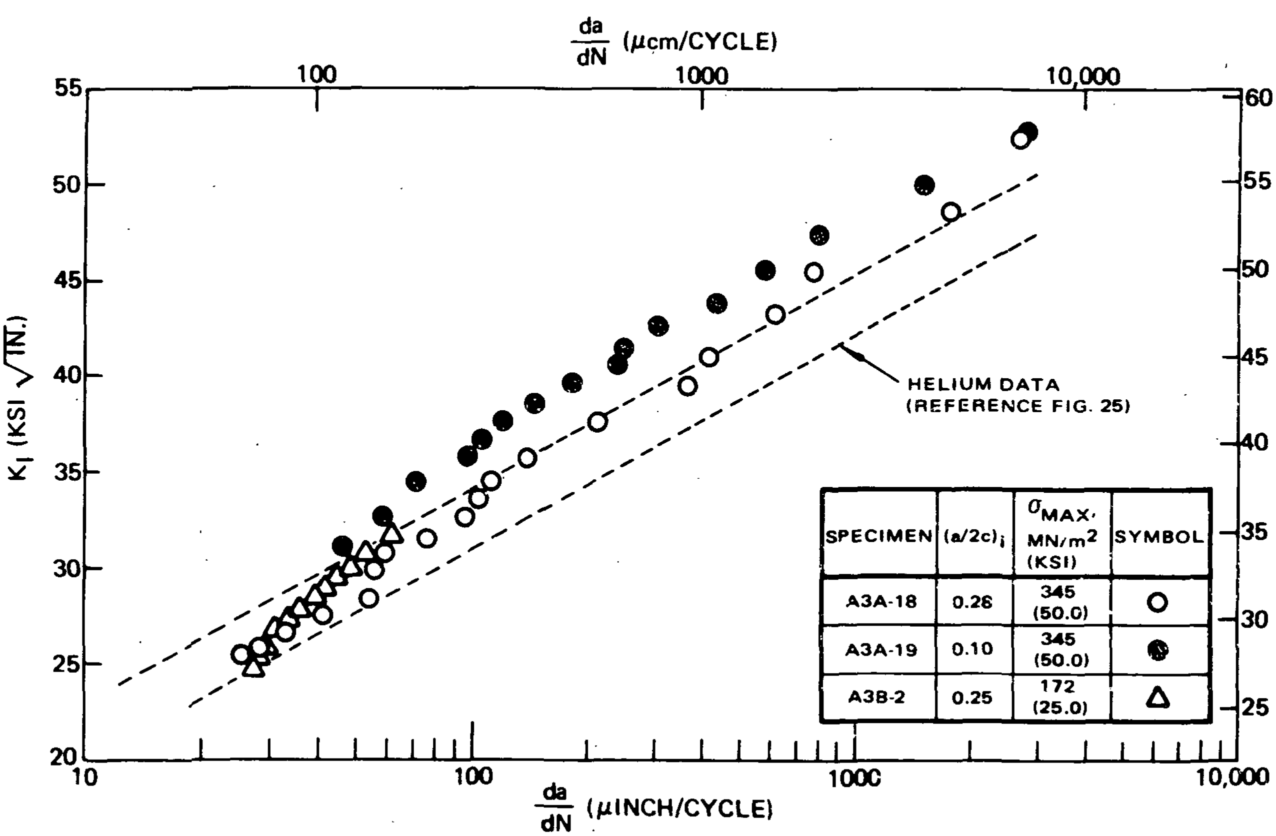

Figure 26: Surface Flaw Fatigue Growth Rates of 2219-T87 Aluminum Plate (WT Direction) in Air at 295°K (72°F) and 333 mHz (20 CPM)

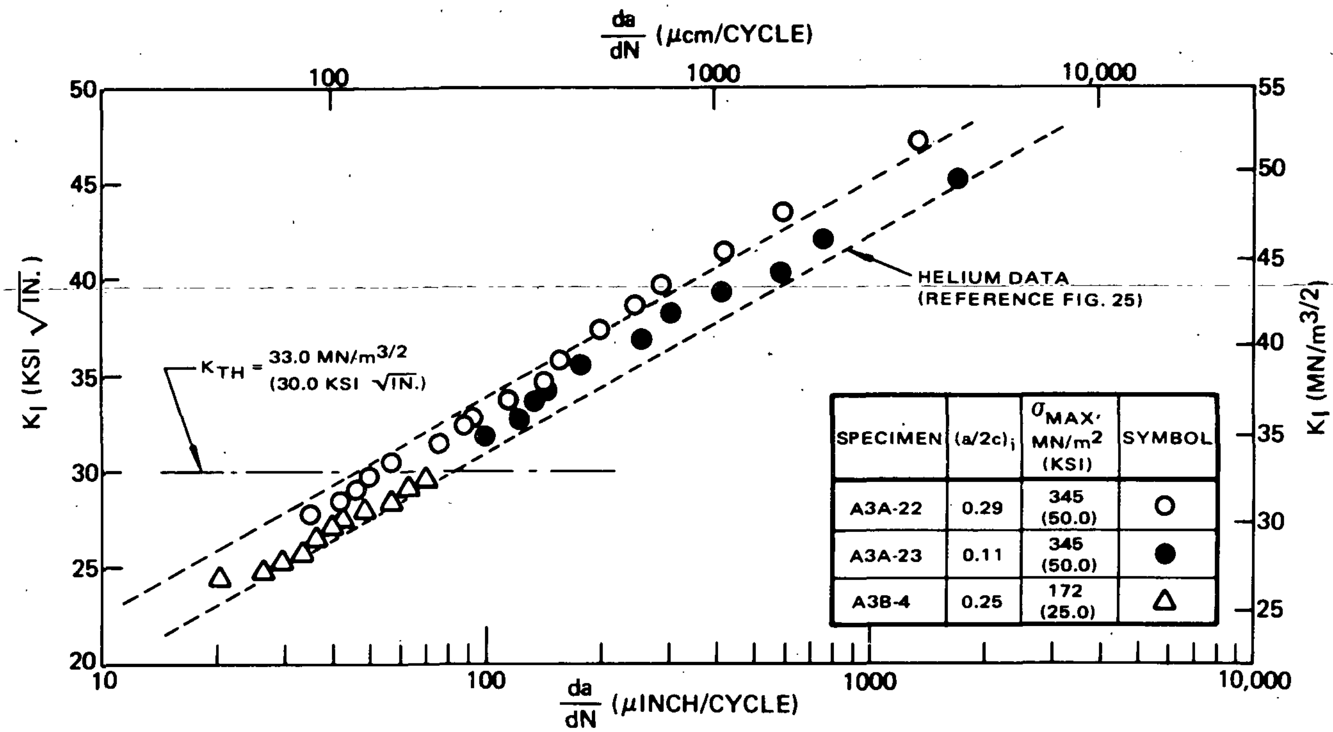

Figure 27: Surface Flaw Fatigue Growth Rates of 2219-T87 Aluminum Plate (WT Direction) in 3.5% Salt Solution at 295° K (72° F) and 333 mHz (20 CPM)

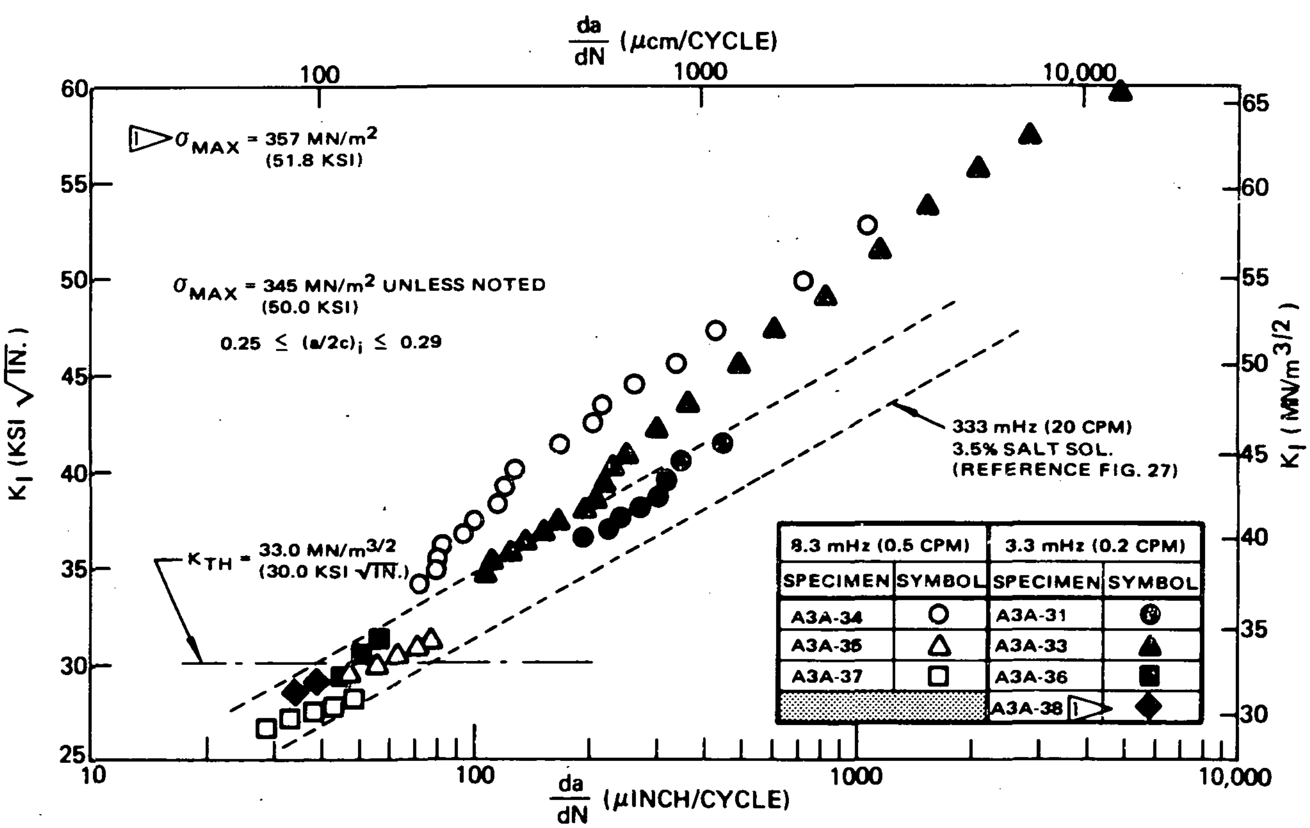

Figure 28: Surface Flaw Fatigue Growth Rates Under Combined Cyclic/Sustained Loading for 2219-T87 Aluminum Plate (WT Direction) in 3.5% Salt Solution at 295° K (72° F) and Frequencies of 8.3 mHz (0.5 CPM) and 3.3 mHz (0.2 CPM)

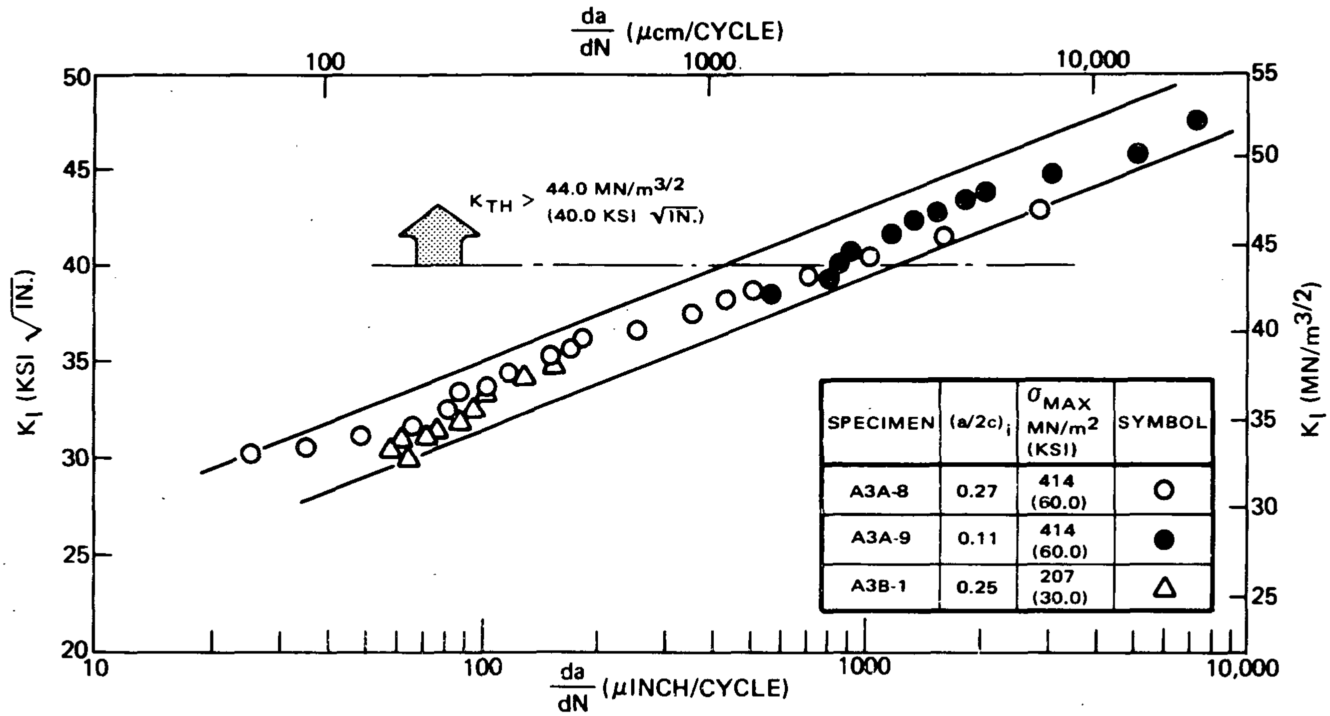

Figure 29: Surface Flaw Fatigue Growth Rates of 2219-T87 Aluminum Plate (WT Direction) in Liquid Nitrogen at 78°K (-320°F) and 333 mHz (20 CPM)

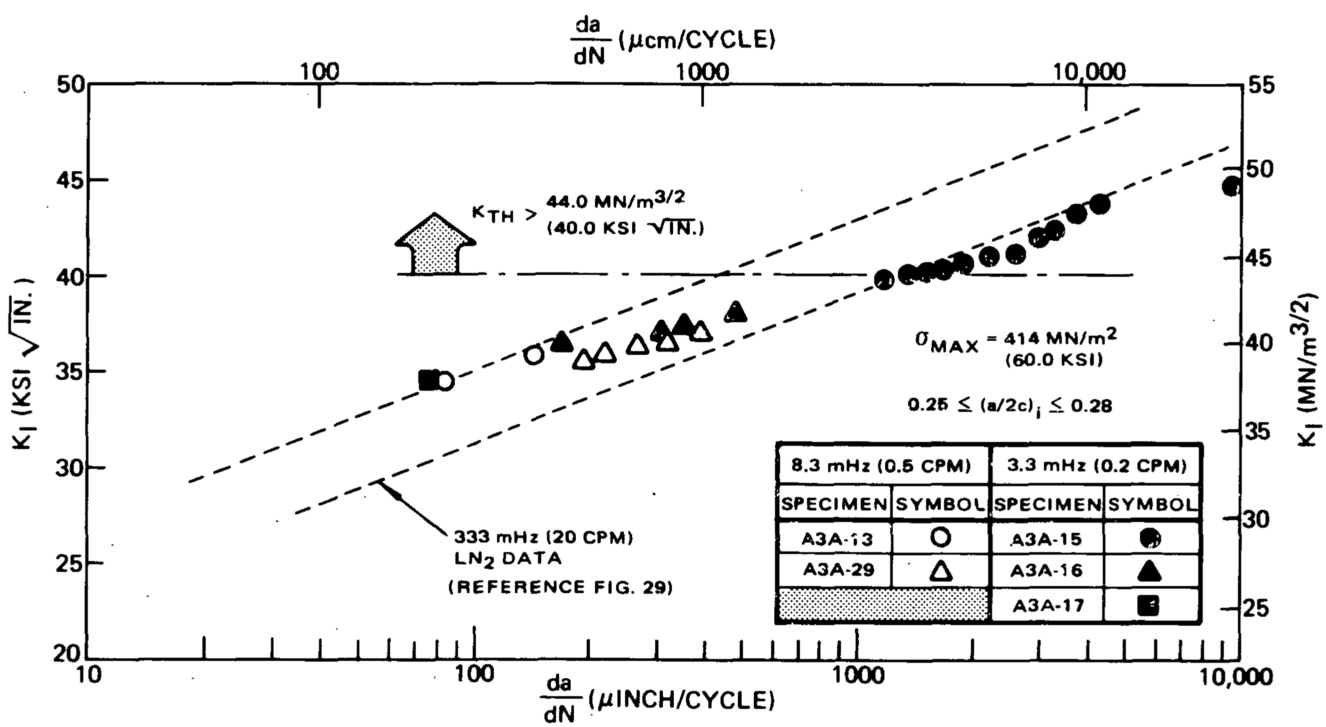

Figure 30: Surface Flaw Fatigue Growth Rates Under Combined Cyclic/Sustained Loading for 2219-T87 Aluminum Plate (WT Direction) in Liquid Nitrogen at 78°K (-320°F) and Frequencies of 8.3 mHz (0.5 CPM) and 3.3 mHz (0.2 CPM)

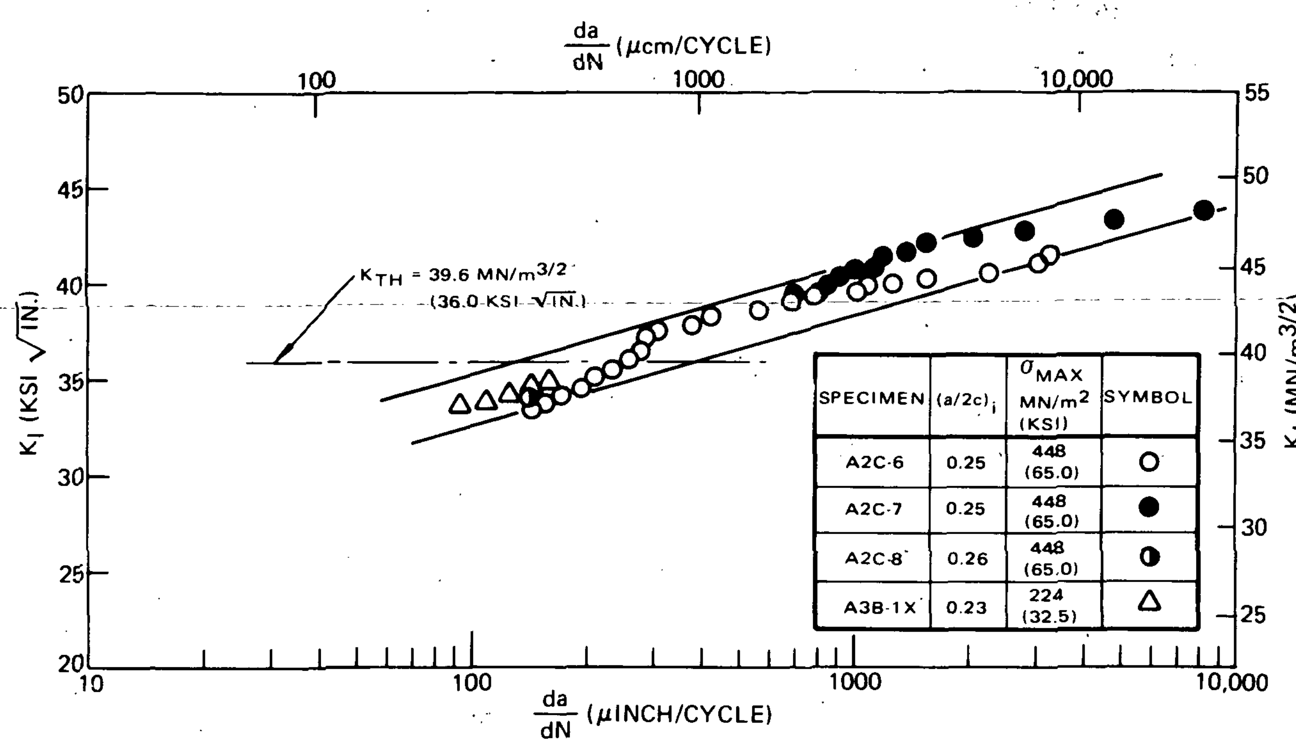

Figure 31: Surface Flaw Fatigue Growth Rates of 2219-T87 Aluminum Plate (WT Direction) in Liquid Hydrogen at 20° K (-423° F) and 333 mHz (20 CPM)

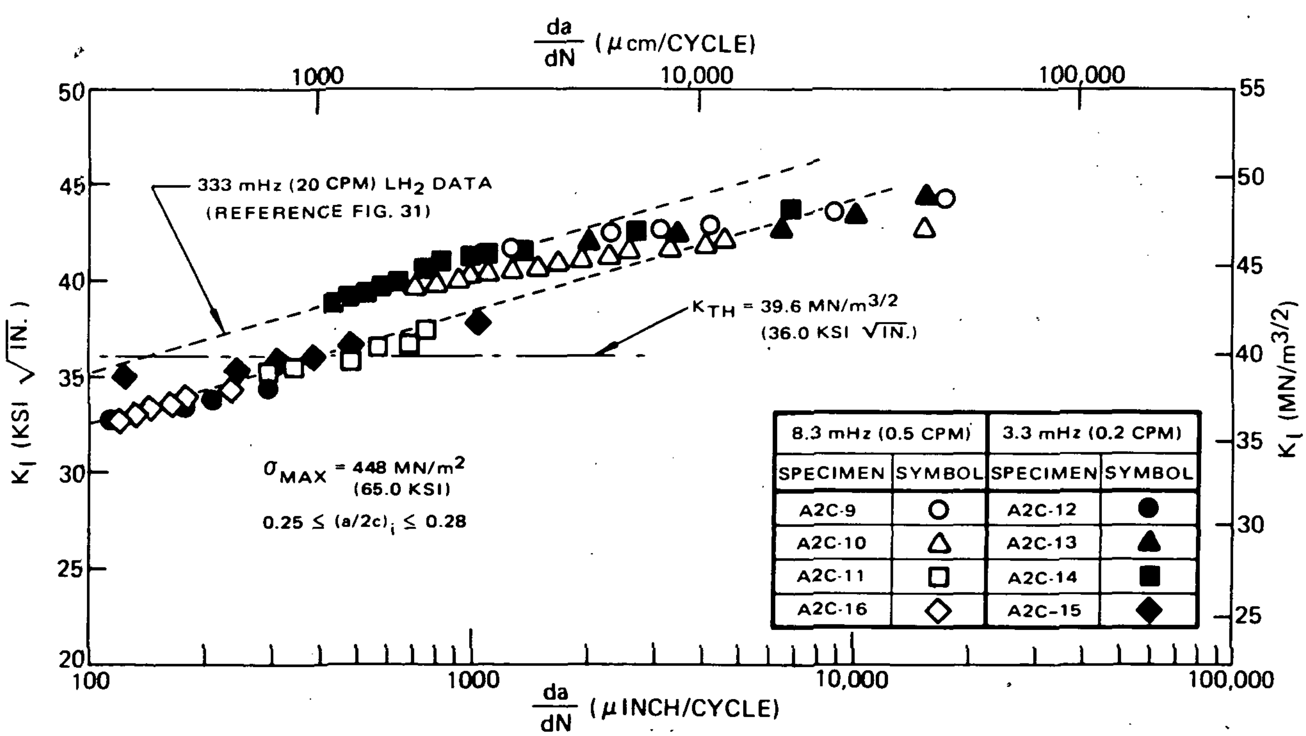

Figure 32: Surface Flaw Fatigue Growth Rates Under Combined Cyclic/Sustained Loading for 2219-T87 Aluminum Plate (W T Direction) in Liquid Hydrogen at 20° K (-423° F) and Frequencies of 8.3 mHz (0.5 CPM) and 3.3 mHz (0.2 CPM)

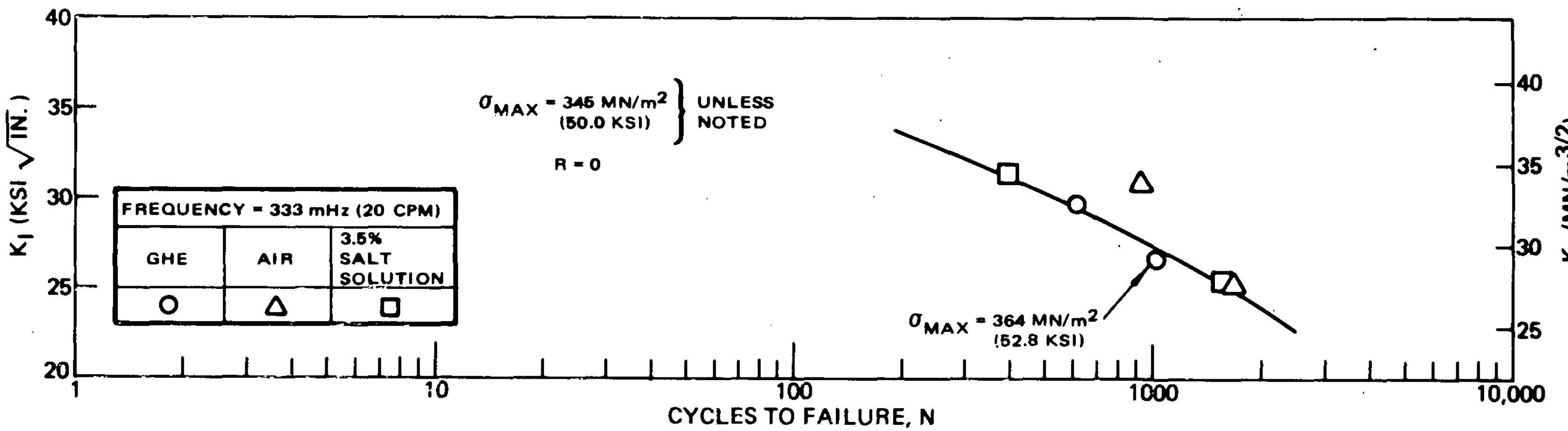

Figure 33: Cycles to Failure for Surface Flawed 2219-T87 Aluminum Plate (WT Direction) at 295°K (72°F)

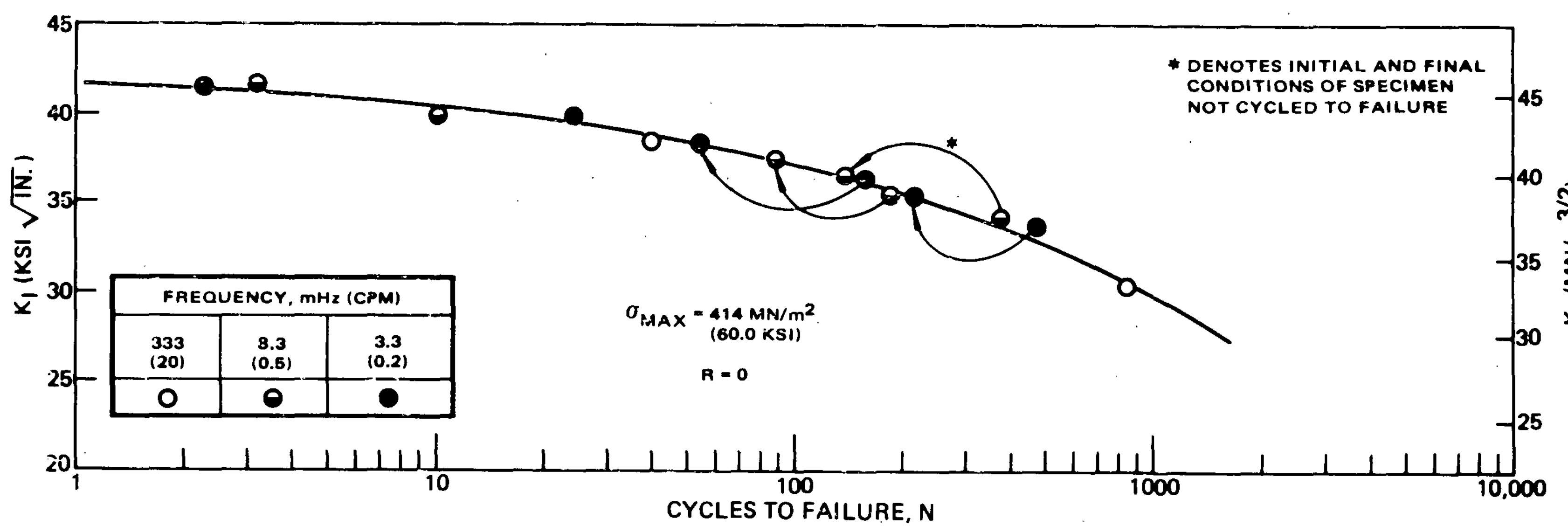

Figure 34: Cycles to Failure for Surface Flawed 2219-T87 Aluminum Plate (WT Direction) in Liquid Nitrogen at 76°K (-320°F)

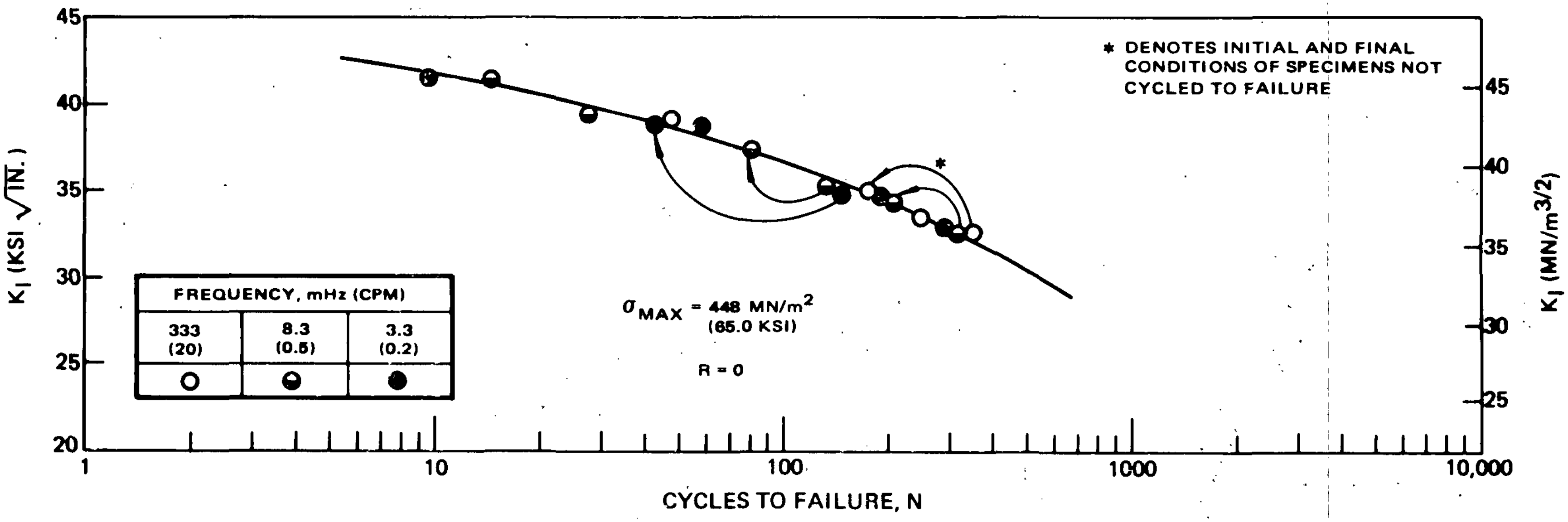

Figure 35: Cycles to Failure for Surface Flawed 2219-T87 Aluminum Plate (WT Direction) in Liquid Hydrogen at 20^{0}K (–423^{0}F)

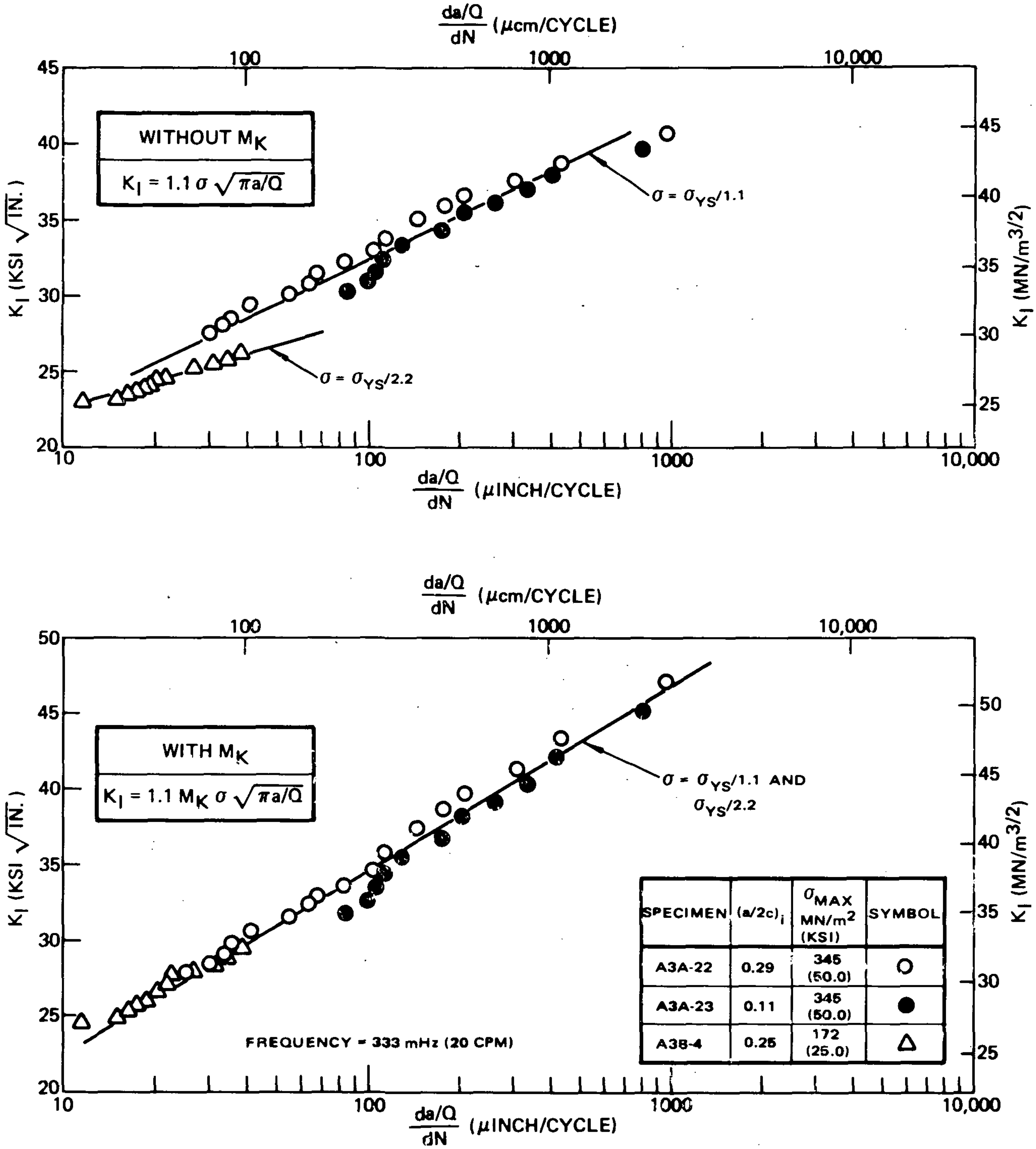

Figure 36: Effect of Stress Intensity Factor Calculations on Surface Flaw Growth Rate Correlations for 2219-T87 Aluminum Alloy Plate (WT Direction) in 3.5% Salt Solution

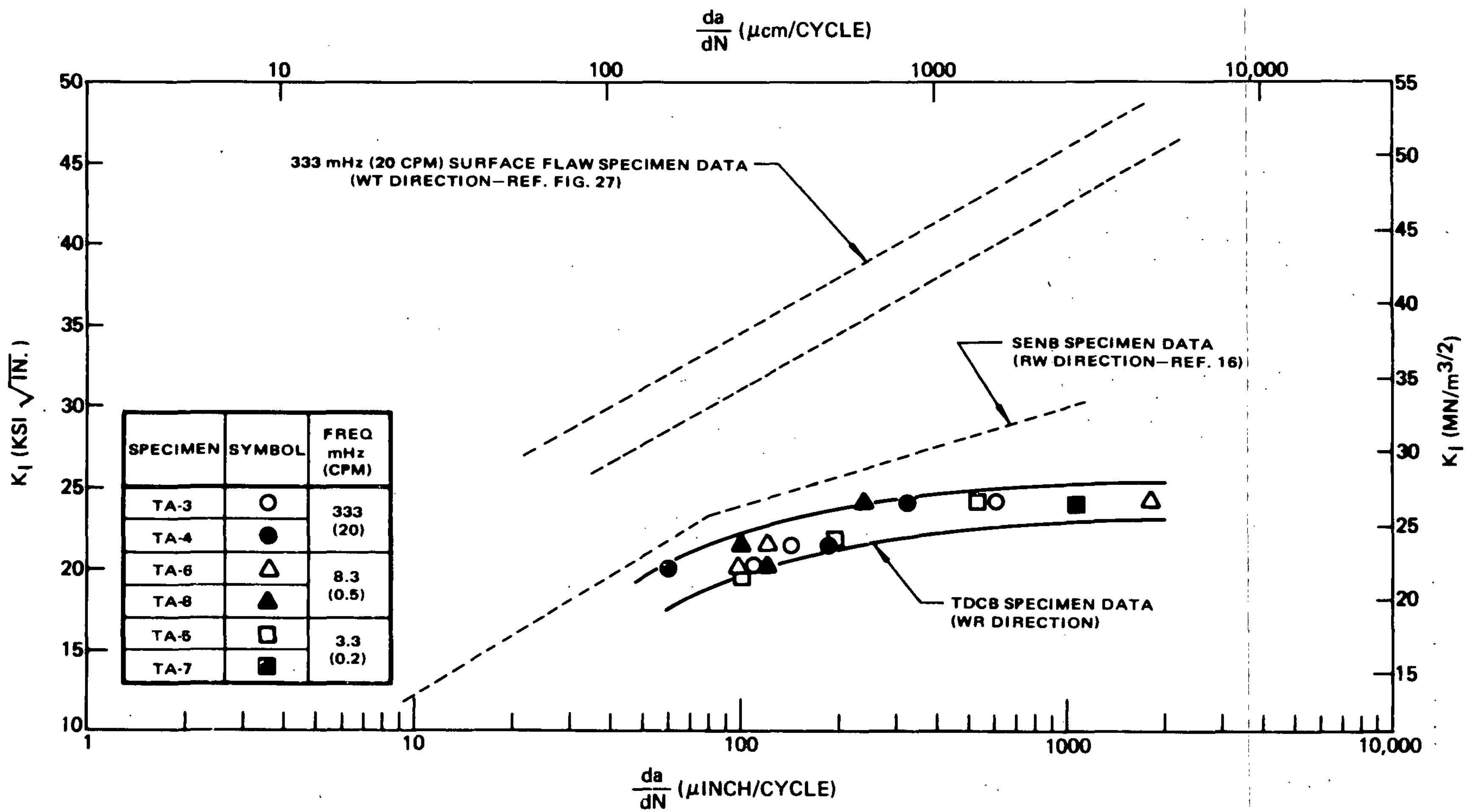

Figure 37: Comparison of Fatigue Crack Growth Rates for 2219-T87 Aluminum Plate in a 3.5% Salt Solution at 295°K (72°F)

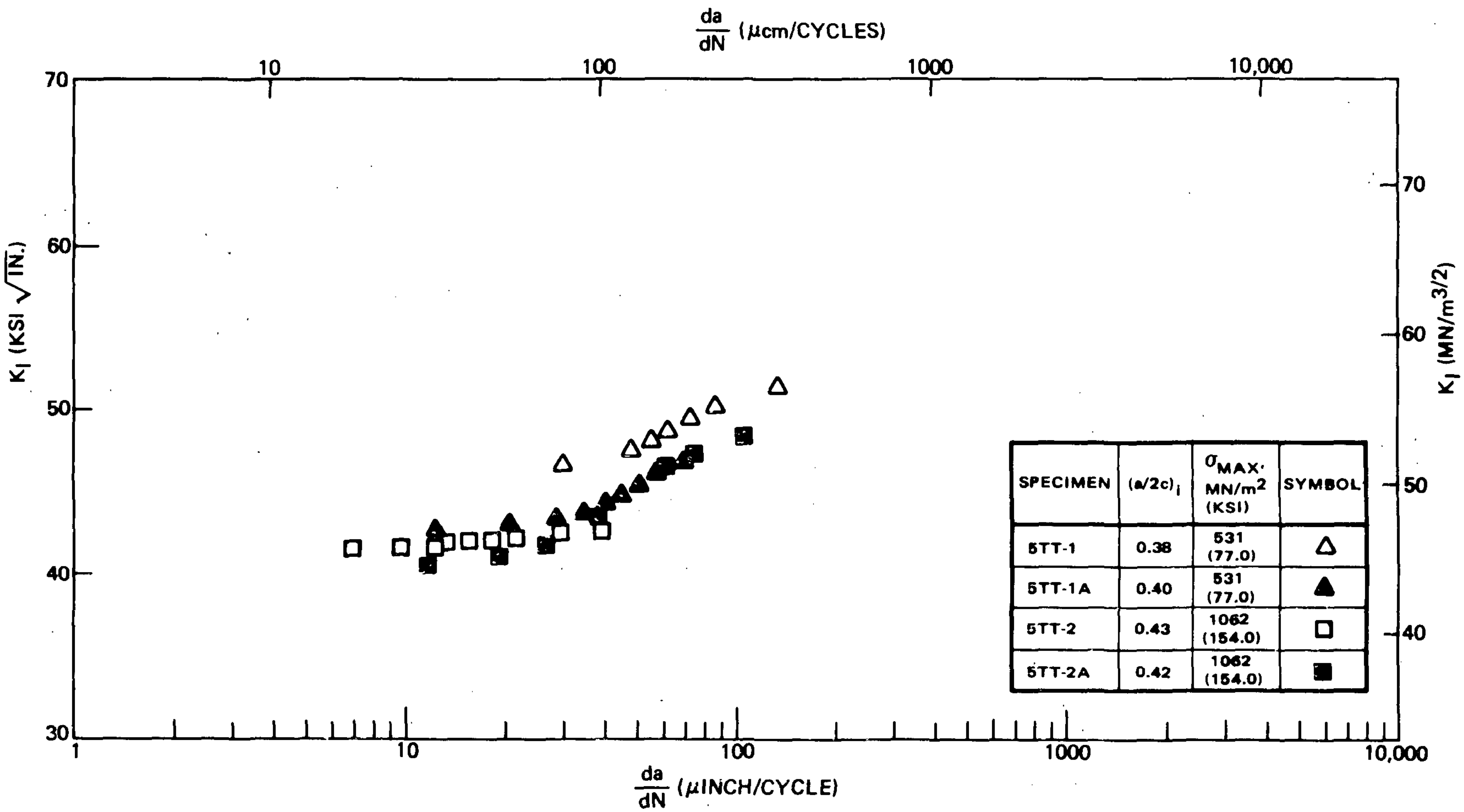

Figure 38: Surface Flaw Fatigue Growth Rates of 5Al-2.5 Sn (ELI) Titanium Plate (RT Direction) in Liquid Nitrogen at 78°K (-320°F) and 333 mHz (20 CPM)

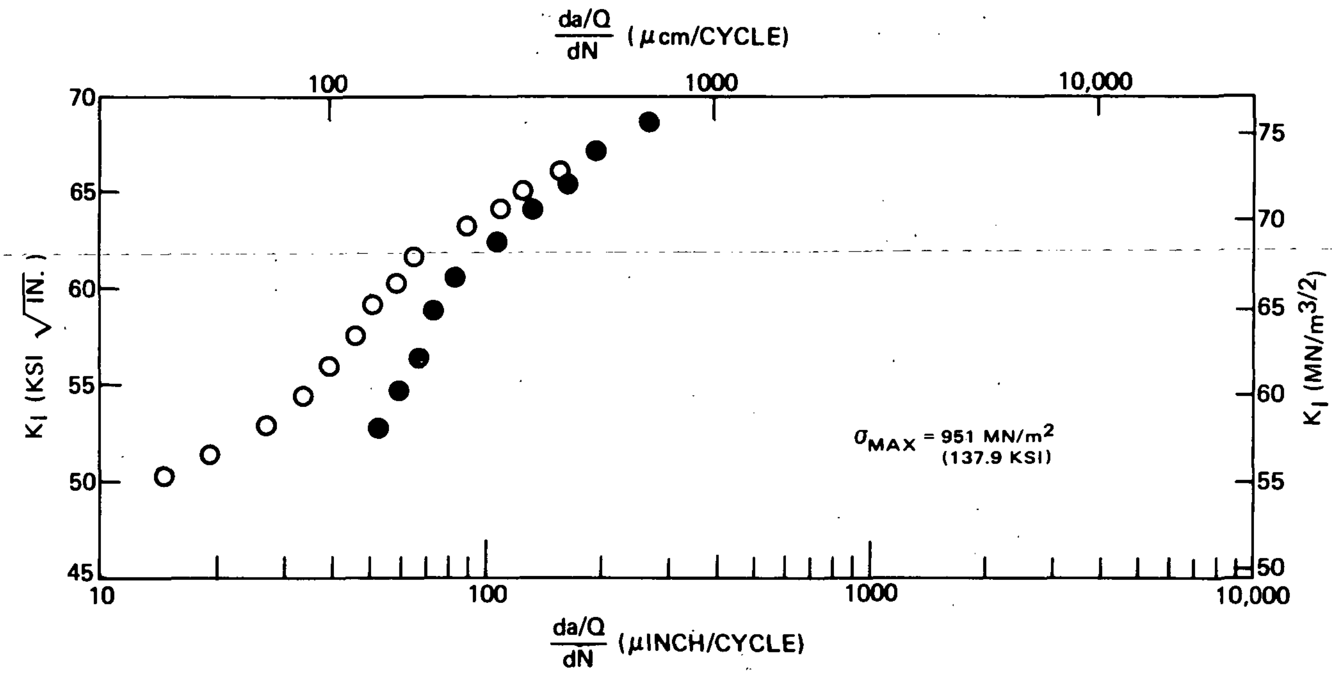

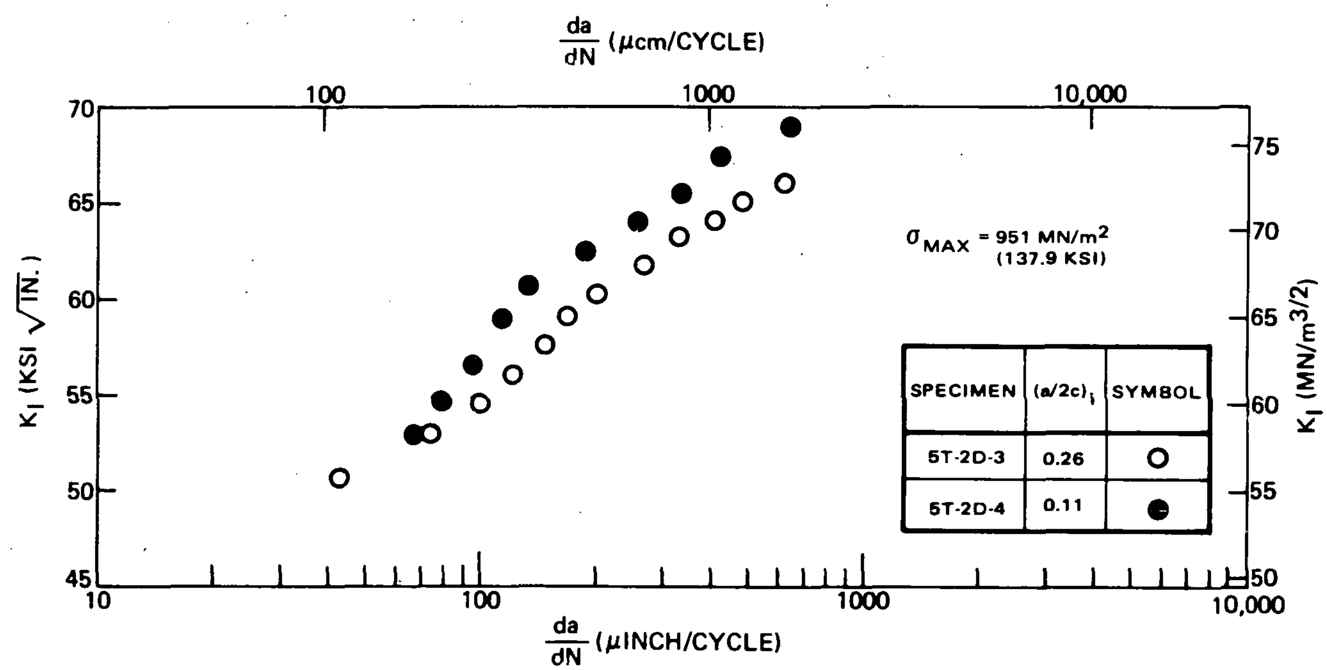

Figure 39: Effect of Flaw Shape on the Fatigue Crack Growth Rates of 5Al-2.5 Sn (ELI) Titanium Plate (RT Direction) in Liquid Nitrogen at 78°K (-320°F) and 333 mHz (20 CPM)

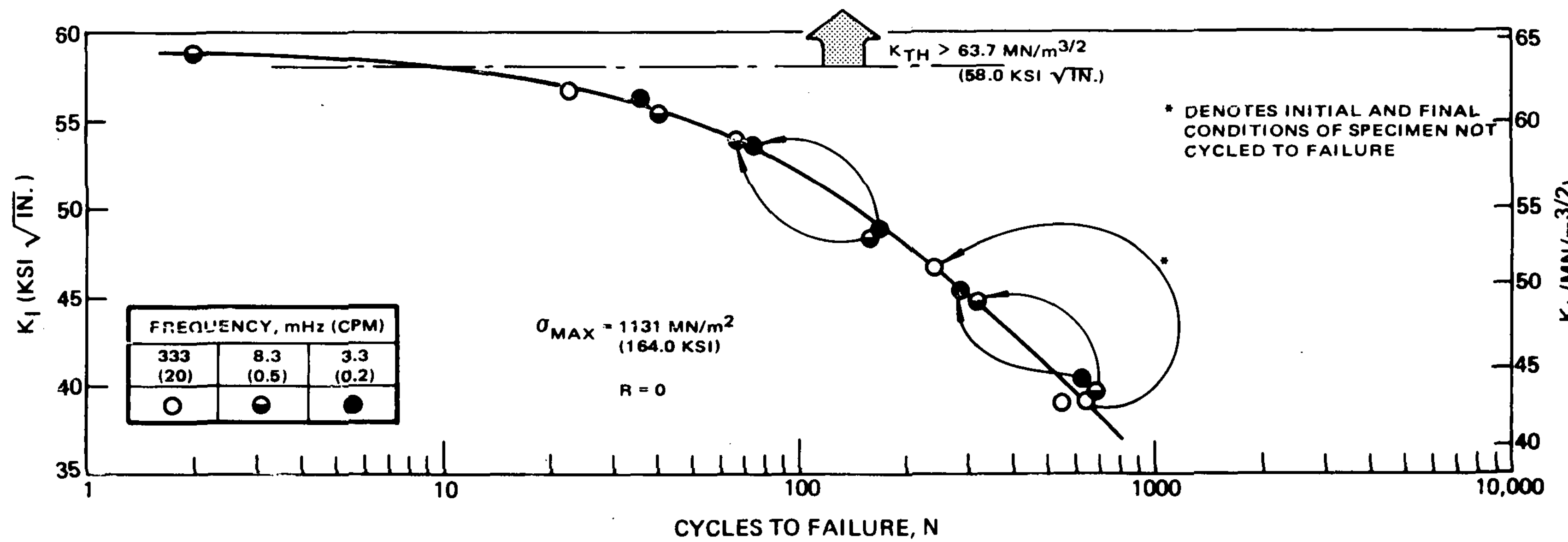

Figure 40: Cycles to Failure for Surface Flawed 5Al-2.5 Sn (ELI) Titanium Plate (RT Direction) in Liquid Hydrogen at 20°K (-423°F)

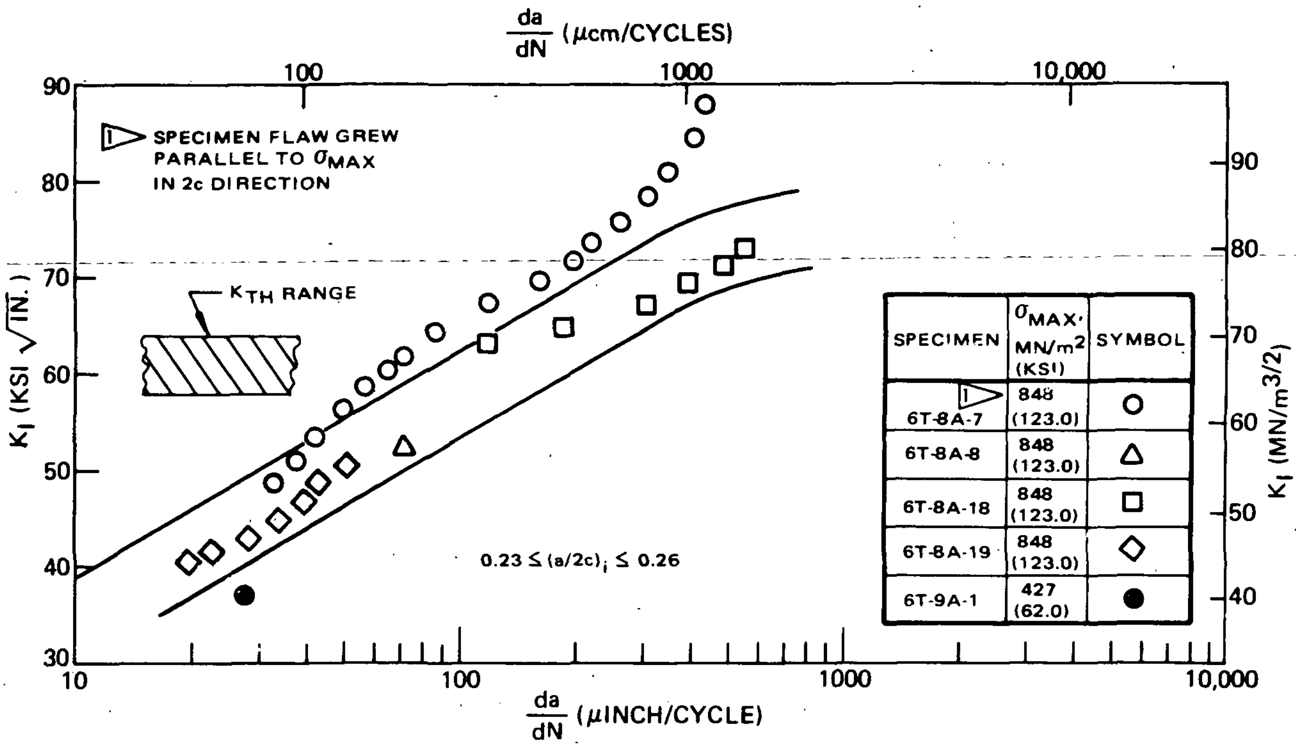

Figure 41: Surface Flaw Fatigue Growth Rates of 6Al-4V (ELI) STA Titanium Plate (RT Direction) in Gaseous Helium at 295°K (72°F) and 333 mHz (20 CPM)

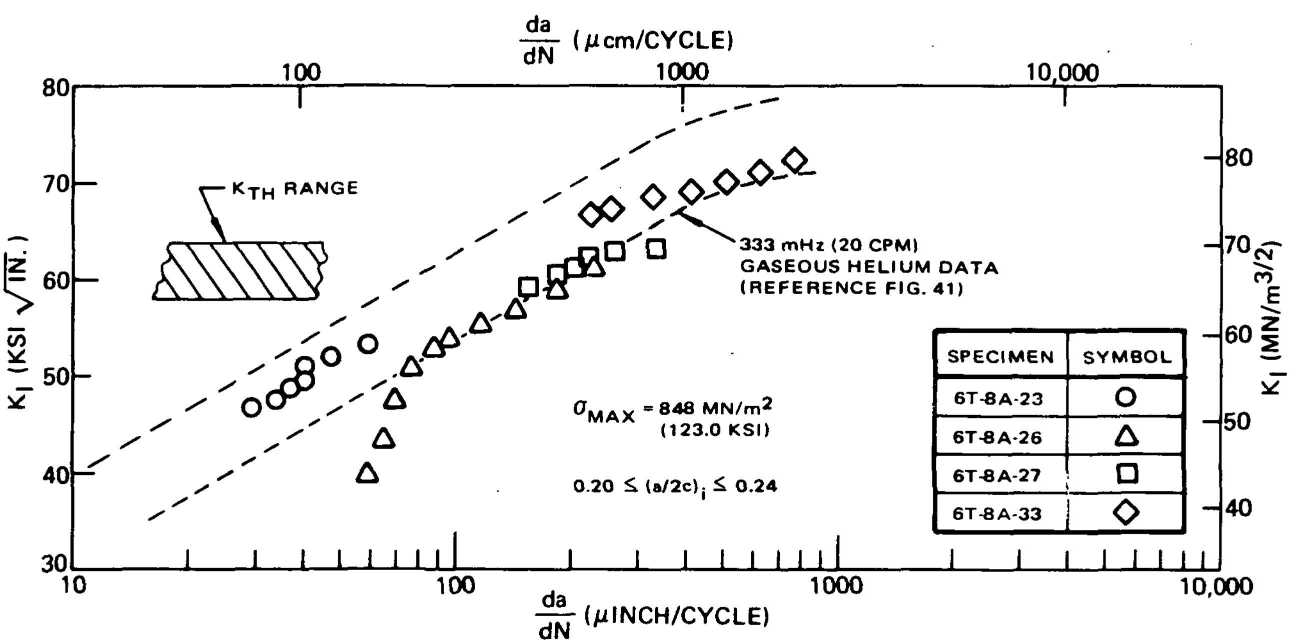

Figure 42: Surface Flaw Fatigue Growth Rates Under Combined Cyclic/Sustained Loading for 6Al-4V (ELI) STA Titanium Plate (RT Direction) in Gaseous Helium at 295°K (72°F) and 8.3 mHz (0.5 CPM)

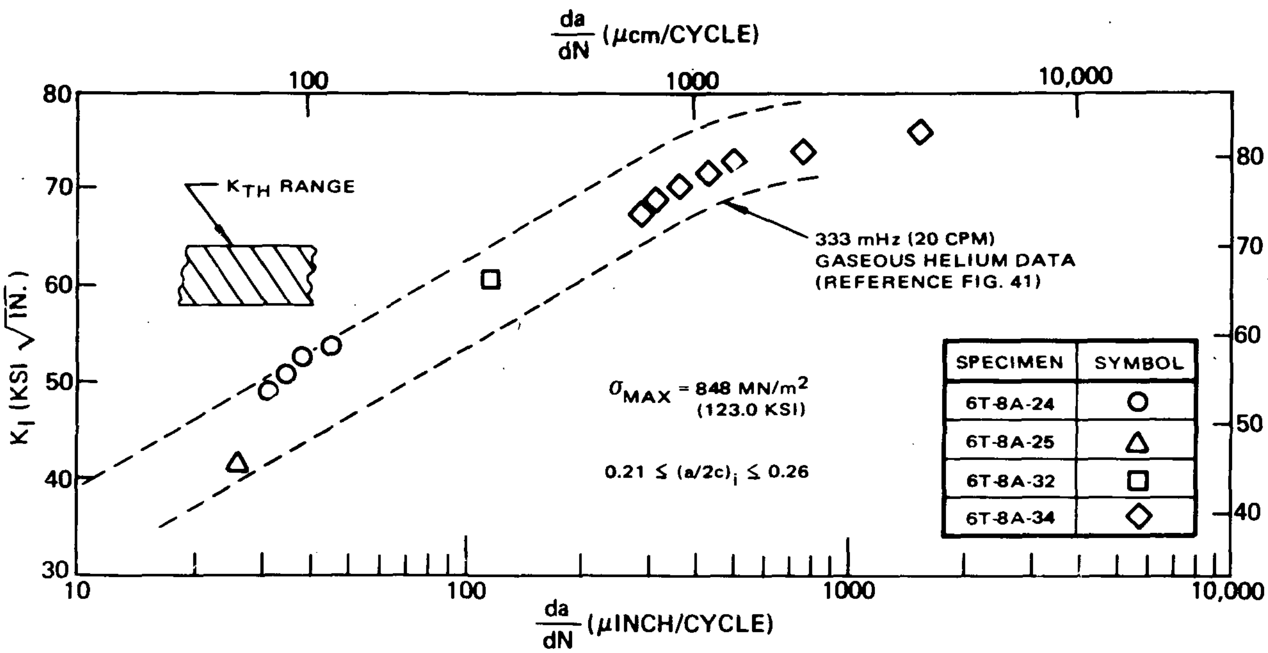

Figure 43: Surface Flaw Fatigue Growth Rates Under Combined Cyclic/Sustained Loading for 6Al-4V (ELI) STA Titanium Plate (RT Direction) in Gaseous Helium at 295°K (72°F) and 3.3 mHz (0.2 CPM)

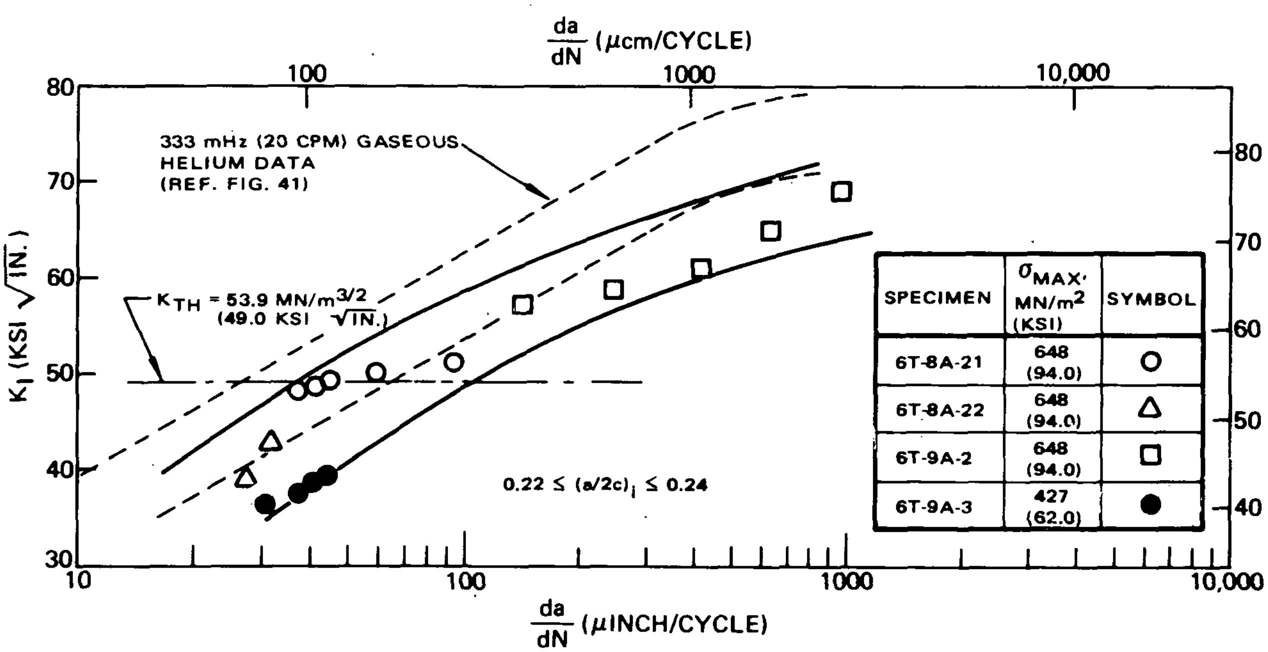

Figure 44: Surface Flaw Fatigue Growth Rates of 6Al-4V (ELI) STA Titanium Plate (RT Direction) in Methanol at 295°K (72°F) and 333 mHz (20 CPM)

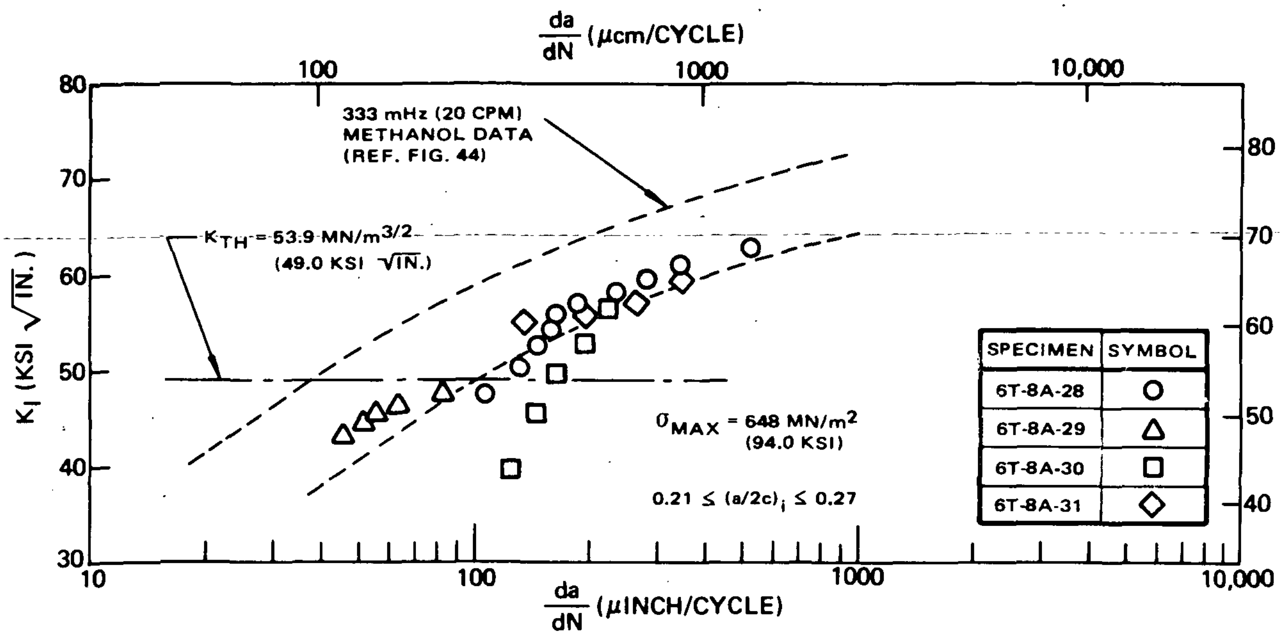

Figure 45: Surface Flaw Fatigue Growth Rates Under Combined Cyclic/Sustained Loading for 6Al-4V (ELI) STA Titanium Plate (RT Direction) in Methanol at 295°K (72°F) and 8.3 mHz (0.5 CPM)

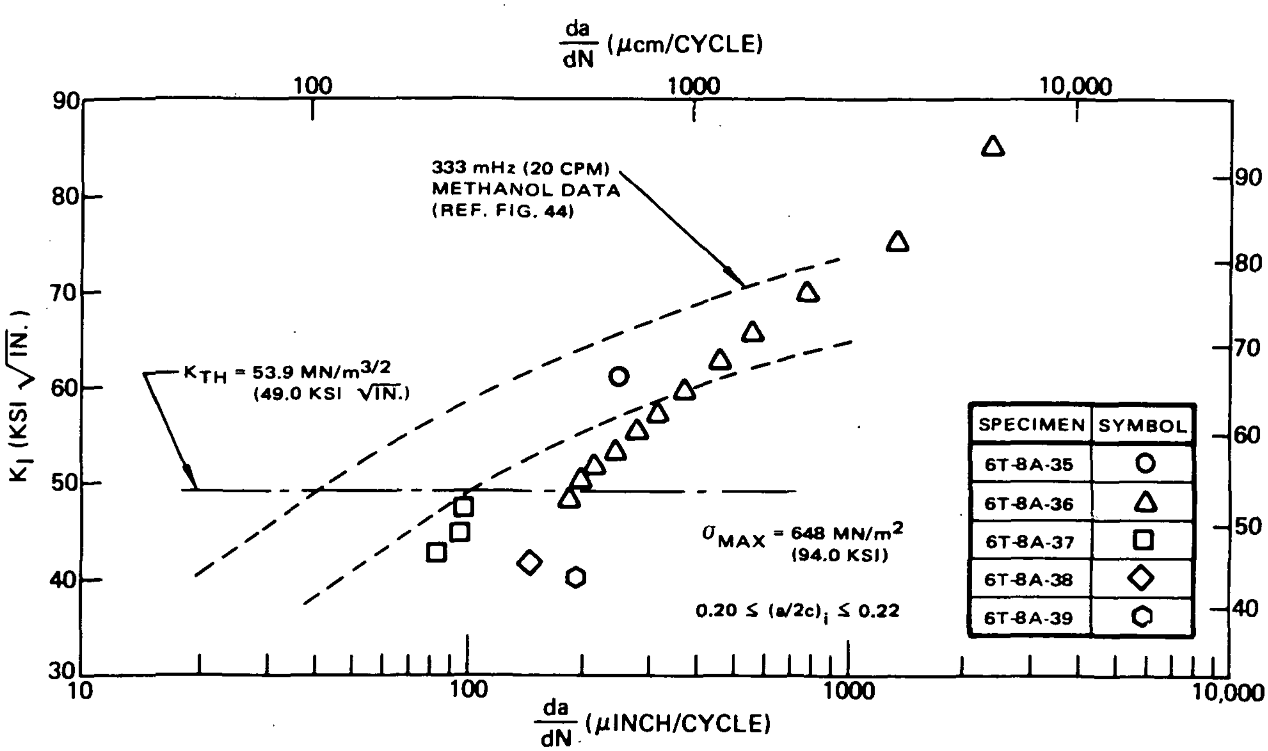

Figure 46: Surface Flaw Fatigue Growth Rates Under Combined Cyclic/Sustained Loading for 6Al-4V (ELI) STA Titanium Plate (RT Direction) in Methanol at 295°K (72°F) and 3.3 mHz (0.2 CPM)

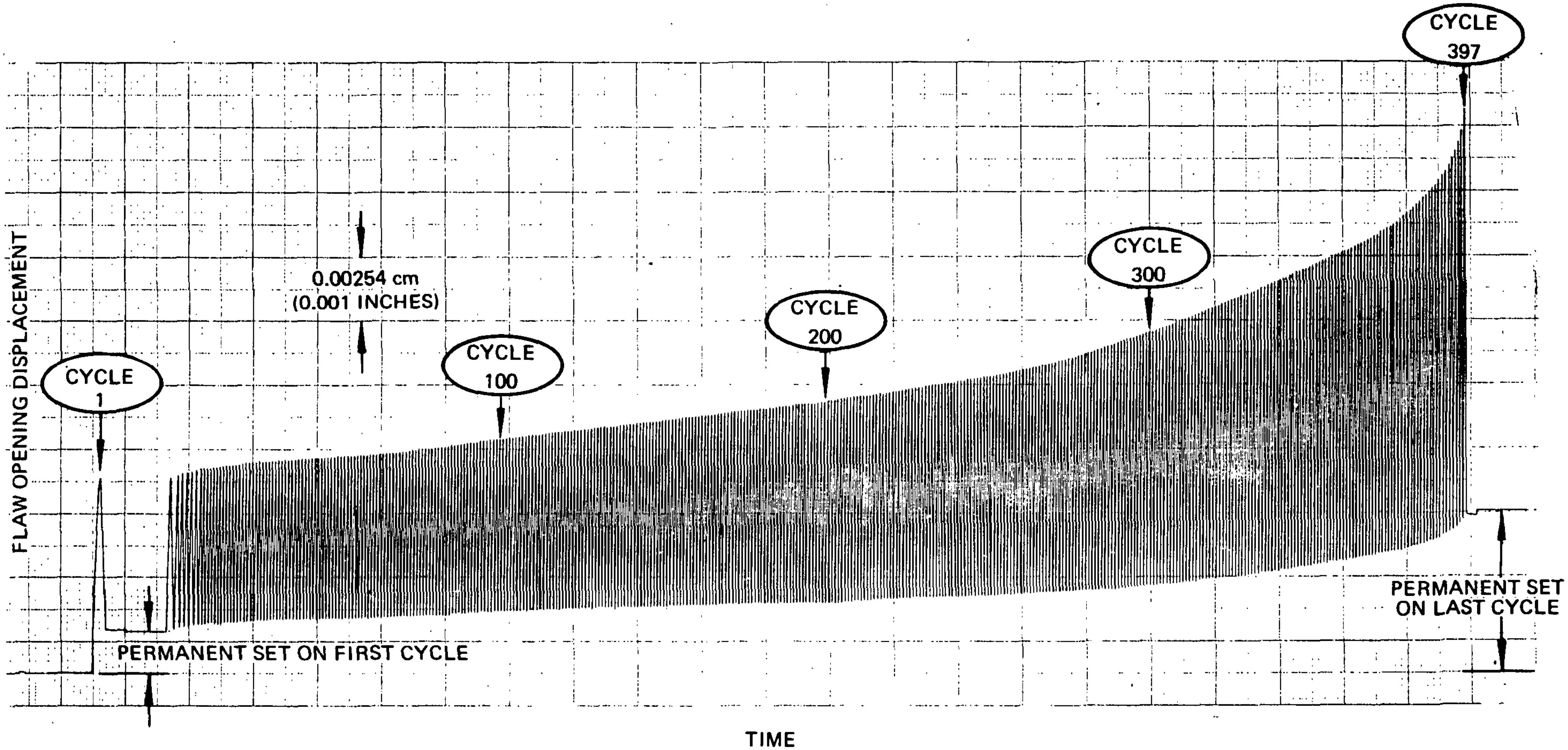

Figure A-1: Flaw Opening Displacement Record for Specimen A3A-23

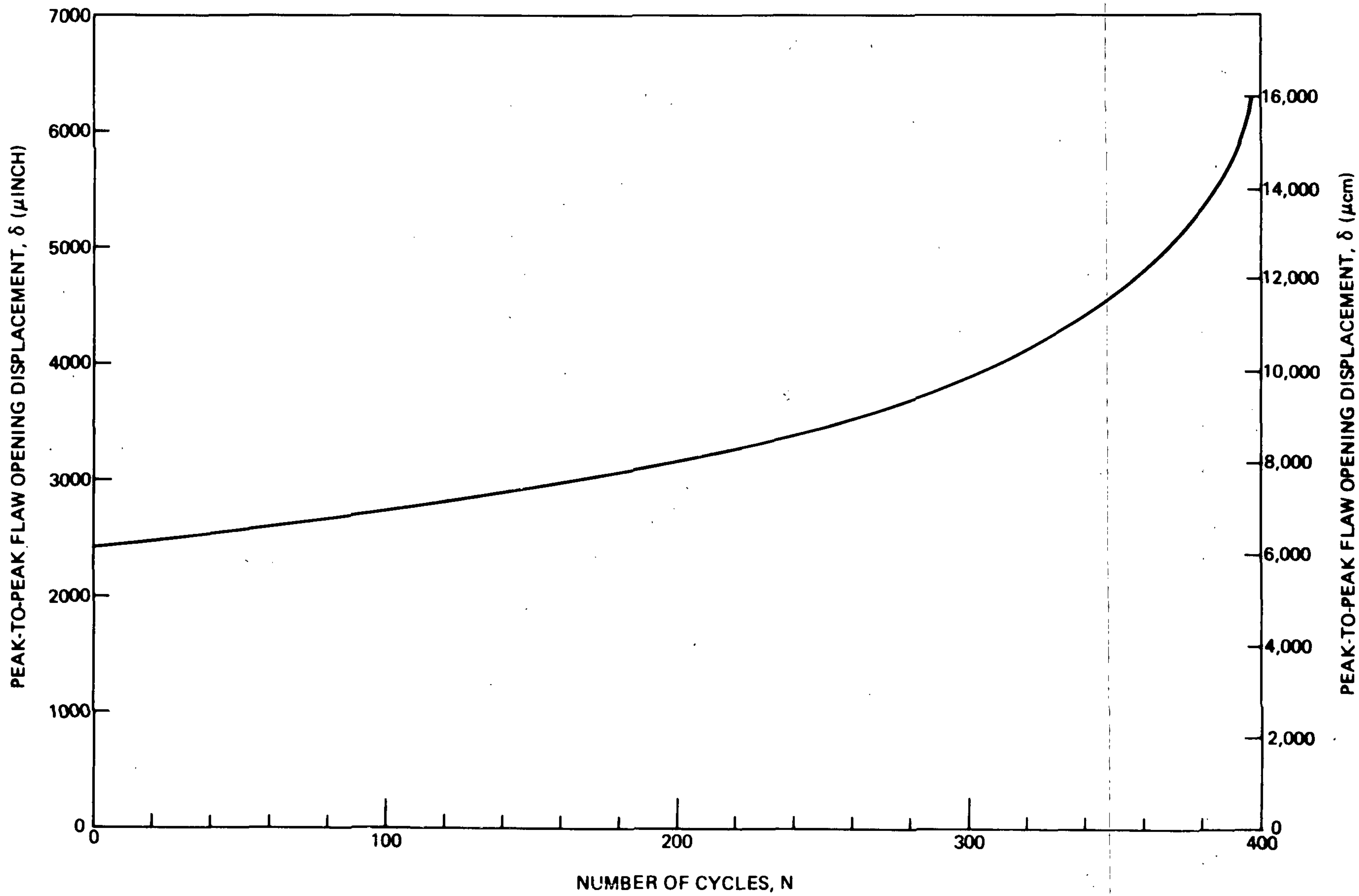

Figure A-2: Flaw Opening Displacement for Specimen A3A-23

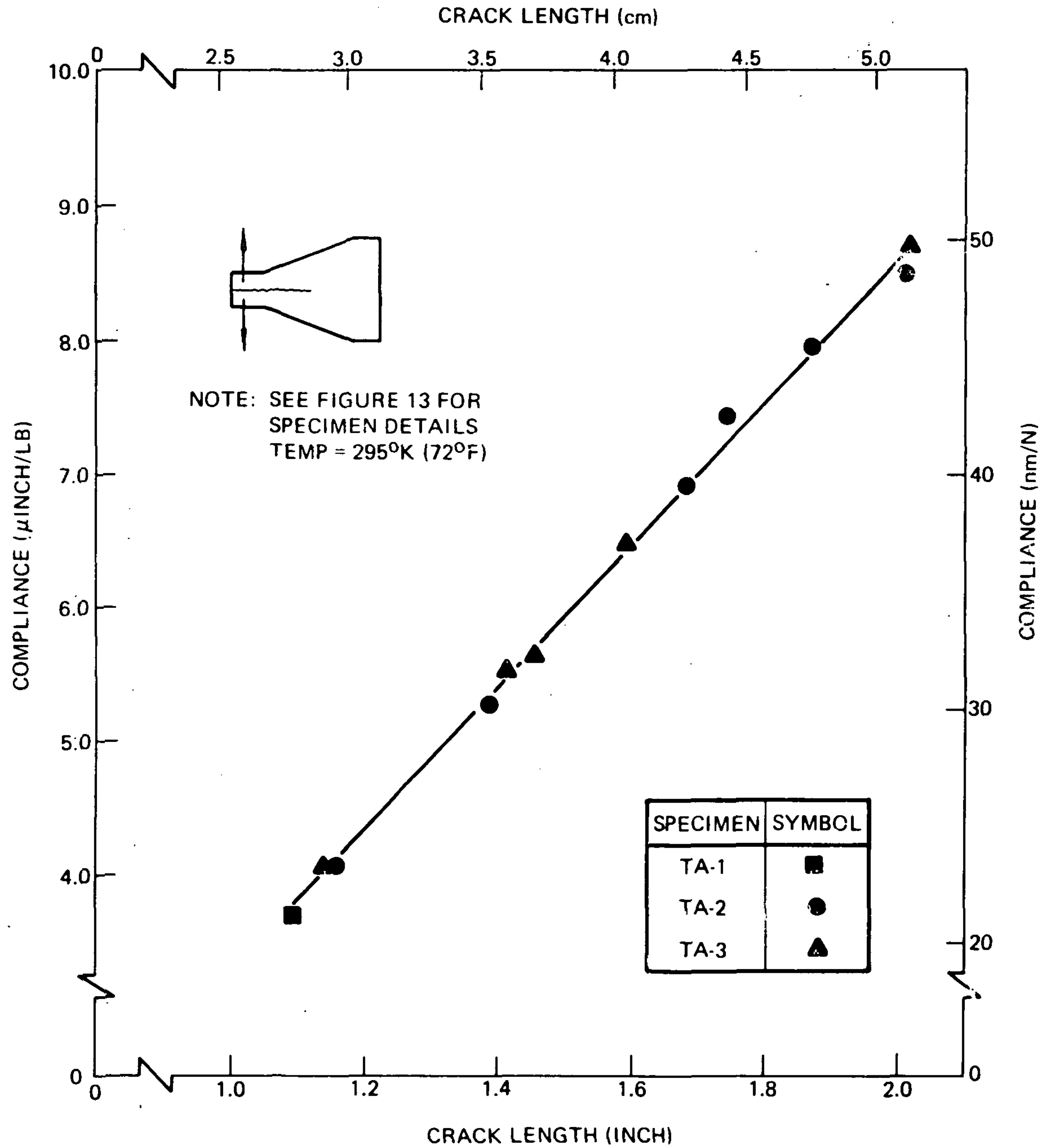

Figure B-1: Compliance Values for 2219-T87 Aluminum Tapered Double Cantilever Beam Specimens

Table 1: Test Program Summary

MATERIAL	TEST TEMPERATURE °K (°F)	TEST ENVIRONMENT	TENSILE TESTS	SURFACE FLAWED SPECIMEN TESTS [1]: STATIC FRACTURE	LOAD/ UNLOAD	SUSTAINED LOAD	CYCLIC LOAD, TEST FREQUENCY mHz (CPM): 333 (20)	8.3 (0.5)	3.3 (0.2)	TDCB CYCLIC TESTS
2219-T87 ALUMINUM	295 (72)	GHe					$a/2c \cong 0.25, 0.10$ $\sigma = \sigma_{YS}/1.10, \sigma_{YS}/2.20$			
		AIR	✓	$a/2c \cong 0.25, 0.10$	$\sigma_{YS}/1.10$		$a/2c \cong 0.25, 0.10$ $\sigma = \sigma_{YS}/1.10, \sigma_{YS}/2.20$			
		3.5% SALT SOLUTION				$\sigma = \sigma_{YS}/1.10$	$a/2c \cong 0.25, 0.10$ $\sigma = \sigma_{YS}/1.10, \sigma_{YS}/2.20$	$\sigma = \sigma_{YS}/1.10$	$\sigma = \sigma_{YS}/1.10$	FREQ = 333 mHz, 8.3 mHz, 3.3 mHz
	78 (-320)	LN_2	✓	$a/2c \cong 0.25, 0.10$	$\sigma_{YS}/1.10$	$\sigma = \sigma_{YS}/1.10$	$a/2c \cong 0.25, 0.10$ $\sigma = \sigma_{YS}/1.10, \sigma_{YS}/2.20$	$\sigma = \sigma_{YS}/1.10$	$\sigma = \sigma_{YS}/1.10$	
	20 (-423)	LH_2	✓	✓	$\sigma_{YS}/1.10$	$\sigma = \sigma_{YS}/1.10$	$\sigma = \sigma_{YS}/1.10, \sigma_{YS}/2.20$	$\sigma = \sigma_{YS}/1.10$	$\sigma = \sigma_{YS}/1.10$	
5AL-2.5 Sn (ELI) TITANIUM	78 (-320)	LN_2	✓	$a/2c \cong 0.25, 0.10$		$\sigma = \sigma_{ULT}/1.40, \sigma_{YS}/1.15$	$a/2c \cong 0.40, 0.25, 0.10$ $\sigma = \sigma_{ULT}/1.40, \sigma_{YS}/1.15, \sigma_{YS}/2.30$			
	20 (-423)	LH_2	✓	✓	$\sigma = \sigma_{ULT}/1.40$	$\sigma = \sigma_{ULT}/1.40$	$\sigma = \sigma_{ULT}/1.40$	$\sigma = \sigma_{ULT}/1.40$	$\sigma = \sigma_{ULT}/1.40$	
6AL-4V (ELI) STA TITANIUM	295 (72)	GHe				$\sigma = \sigma_{ULT}/1.40, \sigma_{YS}/1.15$	$\sigma = \sigma_{YS}/1.15, \sigma_{YS}/2.30$	$\sigma = \sigma_{YS}/1.15$	$\sigma = \sigma_{YS}/1.15$	
		AIR	✓	✓	$\sigma = \sigma_{ULT}/1.40, \sigma_{YS}/1.15$					
		METHANOL				$\sigma = \sigma_{ULT}/1.50, \sigma_{YS}/1.15$	$\sigma = \sigma_{ULT}/1.50, \sigma_{YS}/2.30$	$\sigma = \sigma_{ULT}/1.50$	$\sigma = \sigma_{ULT}/1.50$	FREQ = 333 mHz, 8.3 mHz, 3.3 mHz

[1] $a/2c \cong 0.25$ UNLESS NOTED

Table 2: Threshold Stress Intensity Ratio Comparison for Surface Flawed 2219-T87 Aluminum Plate (WT Direction)

ENVIRONMENT	TEMPERATURE °K (°F)	K_{TH}/K_{IE} RATIO					
		REFERENCE			PRESENT INVESTIGATION		
		σ/σ_{YS}	GROWTH ON LOADING	GROWTH TO FAILURE	σ/σ_{YS}	GROWTH ON LOADING	GROWTH TO FAILURE
AIR	295 (72)	< 0.72	0.63	0.90	–	–	–
3.5% SALT SOLUTION	295 (72)	0.80	–	[1] > 0.90	0.91	0.70	0.70
LN_2	78 (-320)	< 0.72	0.72	0.81	0.91	≃0.62	> 0.86
LH_2	20 (-423)	< 0.72	≃ 0.7	≃ 0.9	0.91	≃0.65	0.73

[1] REFERENCE DATA

Table 3: Threshold Stress Intensity Ratio Comparison for Surface Flawed 5Al-2.5 Sn (ELI) Titanium Plate (RT Direction)

ENVIRONMENT	TEMPERATURE °K (°F)	K_{TH}/K_{IE} RATIO			
		REFERENCE		PRESENT INVESTIGATION	
		σ/σ_{YS}	GROWTH TO FAILURE	σ/σ_{YS}	GROWTH TO FAILURE
LN_2	78 (-320)	0.84→0.97	0.82	0.87	> 0.78
		0.44→0.83	0.98	0.76	> 0.88
LH_2	20 (-423)	0.40→0.85	0.82	0.78	> 0.92

Table 4: Mechanical Properties of 2219-T87 Aluminum Plate (Transverse Grain)

SPECIMEN NUMBER	THICKNESS, t cm (INCH)	WIDTH, w cm (INCH)	TEST TEMPERATURE, T °K (°F)	[1] 0.2% OFFSET YIELD STRENGTH, σ_{YS} MN/m² (KSI)	ULTIMATE STRENGTH, σ_{ULT} MN/m² (KSI)	[1] ELONGATION %	REDUCTION IN AREA %
A1-1	0.960 (0.378)	1.262 (0.497)	295 (72)	383 (55.5)	473 (68.6)	10	16
A1-6	0.958 (0.377)	1.265 (0.498)	295 (72)	383 (55.5)	474 (68.7)	10	13
A1-3	0.953 (0.375)	1.265 (0.498)	78 (-320)	454 (65.9)	583 (84.6)	9	14
A1-4	0.955 (0.376)	1.262 (0.497)	78 (-320)	452 (65.5)	590 (85.6)	12	15
A1-2	0.950 (0.374)	1.265 (0.498)	20 (-423)	494 (71.7)	694 (100.7)	11	12
A1-5	0.967 (0.381)	1.265 (0.498)	20 (-423)	488 (70.8)	696 (101.0)	13	14

[1] MEASURED IN 5.08 cm (2.0 INCH) GAGE LENGTH

Table 5: Mechanical Properties of 5Al-2.5 Sn (ELI) Titanium Plate (Longitudinal Grain)

SPECIMEN NUMBER	THICKNESS, t cm (INCH)	WIDTH, w cm (INCH)	TEST TEMPERATURE, T °K (°F)	0.2% OFFSET YIELD STRENGTH, σ_{YS} MN/m² (KSI) 1	ULTIMATE STRENGTH, σ_{ULT} MN/m² (KSI)	ELONGATION % 1	REDUCTION IN AREA %
5T-1-1	0.460 (0.181)	1.271 (0.500)	78 (-320)	1256 (182.1)	1331 (193.1)	17	31
5T-1-2	0.462 (0.182)	1.278 (0.503)	78 (-320)	1249 (181.2)	1330 (192.9)	17	33
5T-1-3	0.460 (0.181)	1.278 (0.503)	20 (-423)	1453 (210.7)	1574 (228.3)	5	22
5T-1-4	0.457 (0.180)	1.272 (0.501)	20 (-423)	1438 (208.6)	1584 (229.7)	7	24
2 5TT-1-1	0.958 (0.377)	1.280 (0.504)	78 (-320)	1218 (176.6)	1316 (190.8)	15	25
2 5TT-1-2	0.958 (0.377)	1.274 (0.502)	78 (-320)	1231 (178.5)	1315 (190.7)	14	28

1 MEASURED IN 5.08 cm (2.0 INCH) GAGE LENGTH

2 TOUGH TITANIUM PLATE

Table 6: Mechanical Properties of 6Al-4V (ELI) STA Titanium (Longitudinal Grain)

SPECIMEN NUMBER	THICKNESS, t cm (INCH)	WIDTH, w cm (INCH)	TEST TEMPERATURE, T °K (°F)	0.2% OFFSET YIELD STRENGTH, σ_{YS} MN/m² (KSI) 1	ULTIMATE STRENGTH, σ_{ULT} MN/m² (KSI)	ELONGATION % 1	REDUCTION IN AREA %
6T-1-1	0.945 (0.372)	1.266 (0.498)	295 (72)	968 (140.4)	1069 (155.0)	12	40
6T-1-2	0.945 (0.372	1.260 (0.496)	295 (72)	980 (142.2)	1086 (157.5)	12	50

1 MEASURED IN 5.08 cm (2.0 INCH) GAGE LENGTH

Table 7: Static Fracture Tests of 2219-T87 Aluminum

SPECIMEN NUMBER	THICKNESS, t cm (INCH)	WIDTH, W cm (INCH)	SPECIMEN LOADING SEQUENCE	FLAW DEPTH, a cm (INCH)	FLAW LENGTH, 2c cm (INCH)	a / 2c	STRESS, σ MN/m^2 (KSI)	YIELD STRENGTH, σ_{ys} MN/m^2 (KSI)	σ / σ_{ys}	SHAPE PARAMETER, Q	FLAW SIZE, a/Q cm (INCH)	a / t	MAGNIFICATION FACTOR, M_K	TEST TEMPERATURE, T ^oK (^oF)	ENVIRONMENT	STRESS INTENSITY, K_I $MN/m^{3/2}$ (KSI$\sqrt{IN}$)	REMARKS
A3A-1	1.016 (0.400)	12.713 (5.005)	FAILURE	0.416 (0.164)	1.80 (0.709)	0.231	358 (52.0)	382 (55.5)	0.937	1.222	0.340 (0.134)	0.410	1.078	295 (72)	AIR	44.0 (40.0)	$(K_{IE})_{AVG}$ = 46.8 $MN/m^{3/2}$ (42.6 KSI $\sqrt{IN.}$) FOR σ/σ_{YS} < 0.90
A3A-4	1.021 (0.402)	12.707 (5.003)	FAILURE	0.396 (0.156)	2.89 (1.410)	0.111	332 (48.2)	382 (55.5)	0.868	0.963	0.411 (0.162)	0.388	1.103	295 (72)	AIR	45.9 (41.8)	
AR-1	1.539 (0.606)	15.24 (6.00)	FAILURE	0.602 (0.237)	2.32 (0.915)	0.259	341 (49.5)	382 (55.5)	0.892	1.323	0.455 (0.179)	0.390	1.060	295 (72)	AIR	47.6 (43.3)	
A3A-2	1.013 (0.399)	12.715 (5.006)	FAILURE	0.381 (0.150)	1.54 (0.608)	0.247	413 (59.9)	453 (65.7)	0.911	1.282	0.297 (0.117)	0.376	1.060	78 (-320)	LN_2	46.7 (42.5)	$(K_{IE})_{AVG}$ = 50.9 $MN/m^{3/2}$ (46.4 KSI $\sqrt{IN.}$) FOR σ/σ_{YS} < 0.90
A3A-3	1.024 (0.403)	12.713 (5.005)	FAILURE	0.404 (0.159)	3.78 (1.490)	0.107	369 (53.6)	453 (65.7)	0.816	0.969	0.416 (0.164)	0.396	1.108	78 (-320)	LN_2	51.4 (46.8)	
B-1	1.542 (0.607)	15.16 (5.97)	FAILURE	0.635 (0.250)	2.34 (0.920)	0.272	360 (52.2)	453 (65.7)	0.794	1.396	0.455 (0.179)	0.413	1.065	78 (-320)	LN_2	50.4 (45.9)	
A2C-1	1.016 (0.400)	5.715 (2.250)	FAILURE	0.345 (0.136)	1.40 (0.553)	0.246	457 (66.4)	491 (71.3)	0.931	1.271	0.272 (0.107)	0.340	1.058	20 (-423)	LH_2	49.2 (44.8)	$(K_{IE})_{AVG}$ = 54.0 $MN/m^{3/2}$ (49.1 KSI $\sqrt{IN.}$) FOR σ/σ_{YS} < 0.90
A2C-2	1.013 (0.399)	5.715 (2.250)	FAILURE	0.376 (0.148)	1.48 (0.584)	0.253	446 (64.7)	491 (71.3)	0.907	1.298	0.289 (0.114)	0.371	1.059	20 (-423)	LH_2	49.6 (45.1)	
H-6	1.524 (0.600)	15.24 (6.00)	FAILURE	0.632 (0.249)	2.34 (0.920)	0.271	389 (56.4)	491 (71.3)	0.790	1.399	0.450 (0.177)	0.415	1.065	20 (-423)	LH_2	54.0 (49.1)	

Table 8: Static Fracture Tests of 5Al-2.5 Sn (ELI) Titanium

SPECIMEN NUMBER	THICKNESS, t cm (INCH)	WIDTH, W cm (INCH)	SPECIMEN LOADING SEQUENCE	FLAW DEPTH, a cm (INCH)	FLAW LENGTH, 2c cm (INCH)	a / 2c	STRESS, σ MN/m^2 (KSI)	YIELD STRENGTH, σ_{ys} MN/m^2 (KSI)	σ / σ_{ys}	SHAPE PARAMETER, Q	FLAW SIZE, a/Q cm (INCH)	a / t	MAGNIFICATION FACTOR, M_K	TEST TEMPERATURE, T ^oK (^oF)	ENVIRONMENT	STRESS INTENSITY, K_I $MN/m^{3/2}$ (KSI$\sqrt{IN}$)	REMARKS
5T-2A-1	0.386 (0.152)	5.715 (2.250)	FAILURE	0.170 (0.067)	0.777 (0.306)	0.219	1077 (156.2)	1253 (181.7)	0.861	1.218	0.140 (0.055)	0.441	1.166	78 (-320)	LN_2	91.8 (83.3)	$(K_{IE})_{AVG}$ = 89.4 $MN/m^{3/2}$ (81.3 KSI $\sqrt{IN.}$)
5T-2A-2	0.386 (0.152)	5.715 (2.250)	FAILURE	0.142 (0.056)	0.139 (0.546)	0.103	991 (143.7)	1253 (181.7)	0.792	0.966	0.147 (0.058)	0.368	1.143	78 (-320)	LN_2	84.5 (76.9)	
5T-2A-3	0.386 (0.152)	5.715 (2.250)	FAILURE	0.183 (0.072)	0.820 (0.323)	0.223	1025 (148.6)	1253 (181.7)	0.818	1.241	0.147 (0.058)	0.474	1.202	78 (-320)	LN_2	92.0 (83.7)	
5TT-2A-1	0.386 (0.152)	5.715 (2.250)	FAILURE	0.170 (0.067)	0.737 (0.290)	0.231	1152 (167.1)	1225 (177.6)	0.943	1.218	0.138 (0.055)	0.441	1.159	78 (-320)	LN_2	97.3 (88.5)	$(K_{IE})_{AVG}$ = 92.8 $MN/m^{3/2}$ (84.4 KSI $\sqrt{IN.}$)
5TT-2A-2	0.389 (0.153)	5.715 (2.250)	FAILURE	0.152 (0.060)	1.631 (0.642)	0.094	965 (140.0)	1225 (177.6)	0.789	0.952	0.160 (0.063)	0.392	1.172	78 (-320)	LN_2	88.1 (80.2)	
5T-5A-1	0.173 (0.068)	3.048 (1.200)	FAILURE	0.074 (0.029)	0.340 (0.134)	0.216	1227 (178.0)	1446 (209.7)	0.849	1.208	0.061 (0.024)	0.426	1.150	20 (-423)	LH_2	67.8 (61.7)	$(K_{IE})_{AVG}$ = 69.2 $MN/m^{3/2}$ (63.0 KSI $\sqrt{IN.}$)
5T-5A-2	0.168 (0.066)	3.048 (1.200)	FAILURE	0.089 (0.035)	0.371 (0.146)	0.240	427 (168.0)	1446 (209.7)	0.802	1.296	0.067 (0.027)	0.530	1.264	20 (-423)	LH_2	74.7 (68.0)	
5T-6A-11	0.259 (0.102)	3.048 (1.200)	FAILURE	0.094 (0.037)	0.406 (0.160)	0.231	1131 (164.0)	1446 (209.7)	0.782	1.276	0.074 (0.029)	0.363	1.092	20 (-423)	LH_2	61.2 (59.3)	

Table 9: Static Fracture Tests of 6Al-4V (ELI) STA Titanium

SPECIMEN NUMBER	THICKNESS, t cm (INCH)	WIDTH, W cm (INCH)	SPECIMEN LOADING SEQUENCE	FLAW DEPTH, a cm (INCH)	FLAW LENGTH, 2c cm (INCH)	a / 2c	STRESS, σ MN/m^2 (KSI)	YIELD STRENGTH, σ_{ys} MN/m^2 (KSI)	σ / σ_{ys}	SHAPE PARAMETER, Q	FLAW SIZE, a/Q cm (INCH)	a / t	MAGNIFICATION FACTOR, M_K	TEST TEMPERATURE, T ^oK (^oF)	ENVIRONMENT	STRESS INTENSITY, K_I MN/m$^{3/2}$ (KSI$\sqrt{IN}$)	REMARKS
6T-5B-1	0.256 (0.101)	3.04 (1.196)	FAILURE	0.135 (0.053)	0.515 (0.203)	0.261	932 (135.1	974 (141.3)	0.956	1.292	0.104 (0.041)	0.525	1.119	295 (72)	AIR	65.4 (59.4)	$(K_{IE})_{AVG}$ = 80.3 MN/m$^{3/2}$ (73.1 KSI $\sqrt{IN.}$) FOR σ / σ_{YS} < 0.90
6T-2B-1	0.925 (0.388)	5.718 (2.251)	FAILURE	0.361 (0.142)	1.422 (0.560)	0.254	758 (110.0)	974 (141.3)	0.779	1.352	0.267 (0.105)	0.390	1.062	295 (72)	AIR	81.2 (73.9)	
6T-7A-1	0.508 (0.200)	4.049 (1.594)	FAILURE	0.287 (0.113)	1.003 (0.395)	0.286	843 (122.2)	974 (141.3)	0.865	1.430	0.201 (0.079)	0.565	1.124	295 (72)	AIR	83.0 (75.5)	
6T-8A-4	0.645 (0.254)	6.355 (2.501)	FAILURE	0.254 (0.100)	0.986 (0.388)	0.258	848 (123.0)	974 (141.3)	0.870	1.333	0.191 (0.075)	0.394	1.061	295 (72)	AIR	75.7 (69.8)	

Table 10: Load/Unload Tests of 2219-T87 Aluminum

SPECIMEN NUMBER	THICKNESS, t cm (INCH)	WIDTH, W cm (INCH)	SPECIMEN LOADING SEQUENCE	FLAW DEPTH, a cm (INCH)	FLAW LENGTH, 2c cm (INCH)	a / 2c	STRESS, σ MN/m^2 (KSI)	YIELD STRENGTH, σ_{ys} MN/m^2 (KSI)	σ / σ_{ys}	SHAPE PARAMETER, Q	FLAW SIZE, a/Q cm (INCH)	a / t	MAGNIFICATION FACTOR, M_K	TEST TEMPERATURE, T ^oK (^oF)	ENVIRONMENT	STRESS INTENSITY, K_I $MN/m^{3/2}$ (KSI$\sqrt{IN}$)	REMARKS
A3A-2	1.020 (0.401)	12.70 (5.003)	INITIATION	0.414 (0.163)	1.728 (0.680)	0.240	345 (50.0)	383 (55.5)	0.902	1.262	0.327 (0.129)	0.407	1.070	295 (72)	AIR	41.2 (37.4)	Δa = 0.015 cm (0.006 IN.)
			TERMINATION	0.429 (0.169)	1.728 (0.680)	0.249	345 (50.0)	383 (55.5)	0.902	1.286	0.333 (0.131)	0.422	1.073	295 (72)	AIR	41.8 (38.0)	
			FAILURE	0.490 (0.193)	1.912 (0.753)	0.256	360 (52.1)	383 (55.5)	0.938	1.297	0.378 (0.149)	0.482	1.099	295 (72)	AIR	47.5 (43.2)	
A3A-4	1.003 (0.395)	12.70 (5.004)	INITIATION	0.295 (0.116)	1.142 (0.450)	0.258	345 (50.0)	383 (55.5)	0.902	1.317	0.224 (0.088)	0.294	1.029	295 (72)	AIR	32.8 (29.8)	Δa = 0
			TERMINATION	0.295 (0.116)	1.142 (0.450)	0.258	345 (50.0)	383 (55.5)	0.902	1.313	0.224 (0.088)	0.294	1.029	295 (72)	AIR	32.8 (29.8)	
			FAILURE	0.376 (0.148)	1.220 (0.480)	0.308	382 (55.3)	383 (55.5)	0.996	1.444	0.259 (0.102)	0.375	1.039	295 (72)	AIR	39.5 (35.9)	
A2A-27	1.020 (0.400)	12.710 (5.002)	INITIATION	0.363 (0.143)	1.48 (0.570)	0.251	348 (50.0)	383 (55.5)	0.902	1.300	0.279 (0.110)	0.357	1.060	295 (72)	AIR	37.7 (34.3)	Δa = 0.010 cm (0.004 IN.)
			TERMINATION	0.373 (0.147)	1.48 (0.570)	0.258	348 (50.0)	383 (55.5)	0.902	1.314	0.284 (0.112)	0.367	1.052	295 (72)	AIR	38.7 (35.2)	
			FAILURE	0.386 (0.152)	1.47 (0.578)	0.263	430 (62.4)	453 (65.7)	0.949	1.310	0.295 (0.116)	0.380	1.060	78 (-320)	LN_2	48.0 (43.7)	
A3A-25	1.020 (0.399)	12.710 (5.003)	INITIATION	0.335 (0.132)	1.35 (0.531)	0.249	414 (60.0)	453 (65.7)	0.913	1.281	0.262 (0.103)	0.331	1.054	78 (-320)	LN_2	44.0 (40.0)	Δa = 0.025 cm (0.010 IN.)
			TERMINATION	0.361 (0.142)	1.36 (0.535)	0.265	414 (60.0)	453 (65.7)	0.913	1.339	0.269 (0.106)	0.356	1.052	78 (-320)	LN_2	44.2 (40.2)	
			FAILURE	(FATIGUE MARKED THROUGH THE THICKNESS)								—	—	78 (-320)	LN_2	—	
A2C-2X	1.020 (0.403)	5.730 (2.254)	INITIATION	0.229 (0.090)	0.94 (0.370)	0.243	448 (65.0)	492 (71.3)	0.911	1.268	0.180 (0.071)	0.223	1.025	20 (-423)	LH_2	38.0 (34.6)	Δa = 0.005 cm (0.002 IN.)
			TERMINATION	0.234 (0.092)	0.94 (0.370)	0.249	448 (65.0)	492 (71.3)	0.911	1.280	0.183 (0.072)	0.228	1.027	20 (-423)	LH_2	38.2 (34.8)	
			FAILURE	0.351 (0.138)	1.02 (0.402)	0.343	451 (65.4)	453 (65.7)	0.995	1.570	0.224 (0.088)	0.342	1.033	78 (-320)	LN_2	42.9 (39.0)	
A2C-5	1.020 (0.400)	5.720 (2.250)	INITIATION	0.287 (0.113)	1.13 (0.443)	0.255	448 (65.0)	492 (71.3)	0.911	1.298	0.221 (0.087)	0.282	1.042	20 (-423)	LH_2	42.8 (38.9)	Δa = 0.018 cm (0.007 IN.)
			TERMINATION	0.305 (0.120)	1.13 (0.443)	0.271	448 (65.0)	492 (71.3)	0.911	1.348	0.229 (0.089)	0.300	1.047	20 (-423)	LH_2	43.3 (39.4)	
			FAILURE	0.335 (0.230)	1.50 (0.590)	0.390	329 (47.7)	383 (55.5)	0.860	1.811	0.323 (0.127)	0.575	1.051	295 (72)	AIR	38.4 (34.9)	

Table 11: Sustained Load Flaw Growth Tests of 2219-T87 Aluminum in Salt Water at 295^{0}K (72^{0}F)

SPECIMEN NUMBER	THICKNESS, t cm (INCH)	WIDTH, W cm (INCH)	SPECIMEN LOADING SEQUENCE	FLAW DEPTH, a cm (INCH)	FLAW LENGTH, 2c cm (INCH)	a / 2c	STRESS, σ MN/m^2 (KSI)	YIELD STRENGTH, σ_{ys} MN/m^2 (KSI)	σ / σ_{ys}	SHAPE PARAMETER, Q	FLAW SIZE, a/Q cm (INCH)	a / t	MAGNIFICATION FACTOR, M_K	TEST TEMPERATURE, T ^oK (^oF)	ENVIRONMENT	STRESS INTENSITY, K_I MN/m$^{3/2}$ (KSI$\sqrt{IN}$)	REMARKS
A3A-3	1.018 (0.400)	12.70 (5.000)	INITIATION	0.348 (0.137)	1.290 (0.508)	0.270	345 (50.0)	383 (55.5)	0.902	1.356	0.256 (0.101)	0.342	1.039	295 (72)	3.5% NACL	35.4 (32.3)	LOADED FOR 40.0 HRS Δa = 0.010 cm (0.004 IN.)
			TERMINATION	0.358 (0.141)	1.290 (0.508)	0.278	345 (50.0)	383 (55.5)	0.902	1.380	0.259 (0.102)	0.352	1.040	295 (72)	3.5% NACL	35.5 (32.3)	
			FAILURE	0.442 (0.170)	1.525 (0.600)	0.284	372 (53.9)	383 (55.5)	0.972	1.400	0.307 (0.121)	0.425	1.061	295 (72)	AIR	42.7 (38.8)	
A3A-26	1.010 (0.399)	12.70 (5.004)	INITIATION	0.358 (0.141)	1.44 (0.568)	0.248	344 (50.0)	383 (55.5)	0.902	1.293	0.277 (0.109)	0.353	1.057	295 (72)	3.5% NACL	37.5 (34.1)	LOADED FOR 10.0 HOURS Δa = 0.020 cm (0.008 IN.)
			TERMINATION	0.378 (0.149)	1.44 (0.568)	0.262	344 (50.0)	383 (55.5)	0.902	1.330	0.284 (0.112)	0.373	1.056	295 (72)	3.5% NACL	37.9 (34.5)	
			FAILURE	0.477 (0.188)	1.63) (0.642)	0.293	409 (59.3)	453 (65.7)	0.902	1.435	0.333 (0.131)	0.471	1.074	78 (-320)	LN_2	49.5 (45.0)	
A3A-28	1.020 (0.402)	12.70 (5.006)	INITIATION	0.429 (0.169)	1.65 (0.649)	0.260	339 (49.2)	383 (55.5)	0.885	1.330	0.323 (0.127)	0.420	1.069	295 (72)	3.5% NACL	40.2 (36.6)	LOADED FOR 10.0 HOURS Δa = 0.035 cm (0.014 IN.)
			TERMINATION	0.465 (0.183)	1.66 (0.652)	0.281	339 (49.2)	383 (55.5)	0.885	1.396	0.333 (0.131)	0.455	1.074	295 (72)	3.5% NACL	41.0 (37.3)	
			FAILURE	0.540 (0.211)	1.81 (0.712)	0.296	384 (55.7)	453 (65.7)	0.847	1.465	0.366 (0.144)	0.525	1.092	78 (-320)	LN_2	49.7 (45.2)	
A3A-30	1.030 (0.405)	12.70 (5.005)	INITIATION	0.307 (0.121)	1.19 (0.470)	0.257	344 (50.0)	383 (55.5)	0.902	1.315	0.234 (0.092)	0.299	1.048	295 (72)	3.5% NACL	34.1 (31.0)	LOADED FOR 10.0 HOURS Δa = 0.010 cm (0.004 IN.)
			TERMINATION	0.318 (0.125)	1.19 (0.470)	0.266	344 (50.0)	383 (55.5)	0.902	1.339	0.234 (0.092)	0.309	1.050	295 (72)	3.5% NACL	34.2 (31.1)	
			FAILURE	0.373 (0.147)	1.26 (0.498)	0.295	443 (64.2)	453 (65.7)	0.977	1.413	0.264 (0.104)	0.363	1.045	78 (-320)	LN_2	46.5 (42.3)	

Table 12: Sustained Load Flaw Growth Tests of 2219-T87 Aluminum in Liquid Nitrogen at 78°K (-320°F)

SPECIMEN NUMBER	THICKNESS, t cm (INCH)	WIDTH, W cm (INCH)	SPECIMEN LOADING SEQUENCE	FLAW DEPTH, a cm (INCH)	FLAW LENGTH, 2c cm (INCH)	a / 2c	STRESS, σ MN/m^2 (KSI)	YIELD STRENGTH, σ_{ys} MN/m^2 (KSI)	σ / σ_{ys}	SHAPE PARAMETER, Q	FLAW SIZE, a/Q cm (INCH)	a / t	MAGNIFICATION FACTOR, M_K	TEST TEMPERATURE, T °K (°F)	ENVIRONMENT	STRESS INTENSITY, K_I $MN/m^{3/2}$ ($KSI\sqrt{IN}$)	REMARKS
A3A-5	1.000 (0.397)	12.70 (5.006)	INITIATION	0.368 (0.145)	1.34 (0.528)	0.275	414 (60.0	453 (65.7)	0.913	1.367	0.269 (0.106)	0.365	1.051	78 (-320)	LN_2	44.1 (40.1)	LOADED FOR 10.0 HOURS Δa = 0.026 cm (0.010 IN.)
			TERMINATION	0.394 (0.155)	1.34 (0.528)	0.294	414 (60.0)	453 (65.7)	0.913	1.435	0.274 (0.108)	0.390	1.045	78 (-320)	LN_2	44.4 (40.4)	
			FAILURE	0.483 (0.190)	1.51 (0.593)	0.320	421 (61.1)	453 (65.7)	0.930	1.520	0.318 (0.125)	0.479	1.062	78 (-320)	LN_2	49.2 (44.8)	
A3A-6	1.020 (0.400)	12.70 (5.002)	INITIATION	0.381 (0.150)	1.45 (0.570)	0.263	414 (60.0)	453 (65.7)	0.913	1.327	0.287 (0.113)	0.375	1.057	78 (-320)	LN_2	45.6 (41.5)	UNLOAD JUST PRIOR TO FAILURE -7.7 HOURS Δa = 0.096 cm (0.038) SPECIMEN DELAMINATED
			TERMINATION	0.477 (0.188)	1.84 (0.726	0.259	414 (60.0)	453 (65.7)	0.913	1.314	0.363 (0.143)	0.470	1.090	78 (-320)	LN_2	53.1 (48.3)	
			FAILURE	0.610 (0.240)	2.08 (0.820)	0.293	368 (53.3)	453 (65.7)	0.812	1.463	0.417 (0.164)	0.600	1.137	78 (-320)	LN_2	52.8 (48.0)	
A3A-12	1.010 (0.398)	12.70 (5.004)	INITIATION	0.295 (0.116)	1.09 (0.430)	0.270	414 (60.0)	453 (65.7)	0.913	1.348	0.218 (0.086)	0.291	1.042	78 (-320)	LN_2	39.3 (35.8)	LOADED FOR 10.0 HOURS Δa = 0.010 cm (0.004 IN.)
			TERMINATION	0.305 (0.120)	1.09 (0.431)	0.278	414 (60.0)	453 (65.7)	0.913	1.379	0.221 (0.087)	0.302	1.044	78 (-320)	LN_2	39.7 (36.0)	
			FAILURE	0.396 (0.156)	1.19 (0.470)	0.332	439 (63.6)	453 (65.7)	0.968	1.544	0.257 (0.101)	0.392	1.038	78 (-320)	LN_2	44.9 (40.9)	

Table 13: Sustained Load Flaw Growth Tests of 2219-T87 Aluminum in Liquid Hydrogen at 20°K (-423°F)

SPECIMEN NUMBER	THICKNESS, t cm (INCH)	WIDTH, W cm (INCH)	SPECIMEN LOADING SEQUENCE	FLAW DEPTH, a cm (INCH)	FLAW LENGTH, 2c cm (INCH)	a / 2c	STRESS, σ MN/m^2 (KSI)	YIELD STRENGTH, σ_{ys} MN/m^2 (KSI)	σ / σ_{ys}	SHAPE PARAMETER, Q	FLAW SIZE, a/Q cm (INCH)	a / t	MAGNIFICATION FACTOR, M_K	TEST TEMPERATURE, T °K (°F)	ENVIRONMENT	STRESS INTENSITY, K_I $MN/m^{3/2}$ $(KSI\sqrt{IN})$	REMARKS
A2C -3	1.020 (0.400)	5.720 (2.251)	INITIATION	0.335 (0.132)	1.36 (0.537)	0.246	448 (65.0)	492 (71.3)	0.911	1.281	0.262 (0.103)	0.330	1.055	20 (-423)	LH_2	47.3 (43.0)	LOADED FOR 6.8 HOURS Δa = 0.048 cm (0.019 IN.)
			TERMINATION	0.384 (0.151)	1.38 (0.543)	0.278	448 (65.0)	492 (71.3)	0.911	1.385	0.277 (0.109)	0.377	1.052	20 (-423)	LH_2	48.5 (44.1)	1) CRYOSTAT WENT DRY DURING TEST
			FAILURE	0.546 (0.215)	1.59 (0.624)	0.345	328 (47.5)	383 (55.5)	0.856	1.628	0.335 (0.132)	0.537	1.072	295 (72)	AIR	39.6 (36.0)	2) LOAD DROPPED DURING TEST
A2C -4	1.020 (0.399)	5.710 (2.249)	INITIATION	0.277 (0.109)	1.11 (0.438)	0.249	448 (65.0)	492 (71.3)	0.911	1.282	0.216 (0.085)	0.273	1.042	20 (-423)	LH_2	42.2 (38.4)	FAILED AFTER 4.33 HOURS AT LOAD
			TERMINATION	(UNDEFINED)			448 (65.0)	492 (71.3)	0.911	--	--	--	--	20 (-423)	LH_2	--	
A2C -17	1.020 (0.400)	5.720 (2.251)	INITIATION	0.310 (0.122)	1.27 (0.500)	0.244	448 (65.0)	492 (71.3)	0.911	1.270	0.244 (0.096)	0.305	1.052	20 (-423)	LH_2	45.4 (41.3)	FAILED AFTER 2.20 HOURS AT LOAD
			TERMINATION	0.417 [1] (0.164)	1.37 [1] (0.540)	0.304	448 (65.0)	492 (71.3)	0.911	1.464	0.284 (0.112)	0.410	1.048	20 (-423)	LH_2	48.9 (44.5)	Δa = 0.107 cm (0.042 IN.)
A2C -18	1.020 (0.401)	5.720 (2.250)	INITIATION	0.292 (0.115)	1.11 (0.438)	0.263	448 (65.0)	492 (71.3)	0.911	1.321	0.221 (0.087)	0.287	1.043	20 (-423)	LH_2	42.8 (38.9)	LOADED FOR 10.0 HOURS Δa = 0.028 cm (0.011 IN.)
			TERMINATION	0.320 (0.126)	1.13 (0.444)	0.284	448 (65.0)	492 (71.3)	0.911	1.400	0.229 (0.090)	0.314	1.043	20 (-423)	LH_2	43.7 (39.8)	1) TEMPORARY LOAD INCREASE OF 8900 N (2000 LB.) DURING TEST
			FAILURE	0.503 (0.198)	1.35 (0.533)	0.371	342 (49.6)	383 (55.5)	0.894	1.721	0.292 (0.115)	0.494	1.043	295 (72)	AIR	37.6 (34.2)	
A2C -1X	1.020 (0.402)	5.720 (2.251)	INITIATION	0.247 (0.098)	0.96 (0.377)	0.260	448 (65.0)	492 (71.3)	0.911	1.324	0.188 (0.074)	0.244	1.030	20 (-423)	LH_2	39.1 (35.6)	
			TERMINATION	0.257 (0.101)	0.96 (0.377)	0.267	448 (65.0)	492 (71.3)	0.911	1.350	0.191 (0.075)	0.254	1.032	20 (-423)	LH_2	39.3 (35.8)	LOADED FOR 10.0 HOURS
			FAILURE	0.356 (0.140)	1.04 (0.410)	0.342	440 (63.8)	453 (65.7)	0.971	1.584	0.221 (0.087)	0.384	1.022	78 (-320)	LN_2	41.4 (37.7)	Δa = 0.007 cm (0.003 IN.)

[1] ESTIMATED FLAW SIZE

Table 14: 333 mHz (20 CPM) Cyclic Load Flaw Growth Tests of 2219-T87 Aluminum in Gaseous Helium at 295°K (72°F)

SPECIMEN NUMBER	THICKNESS, t cm (INCH)	WIDTH, W cm (INCH)	SPECIMEN LOADING SEQUENCE	FLAW DEPTH, a cm (INCH)	FLAW LENGTH, 2c cm (INCH)	a / 2c	STRESS, σ MN/m² (KSI)	YIELD STRENGTH, σ_{ys} MN/m² (KSI)	σ / σ_{ys}	SHAPE PARAMETER, Q	FLAW SIZE, a/Q cm (INCH)	a / t	MAGNIFICATION FACTOR, M_K	TEST TEMPERATURE, T °K (°F)	ENVIRONMENT	STRESS INTENSITY, K_I MN/m^{3/2} (KSI$\sqrt{IN}$)	REMARKS
A3A -20	1.021 (0.402)	12.705 (5.002)	INITIATION	0.218 (0.086)	0.805 (0.317)	0.271	364 (52.8)	383 (55.5)	0.960	1.343	0.163 (0.064)	0.214	1.020	295 (72)	GHE	28.2 (26.6)	CYCLED FOR 1012 CYCLES – UNLOADED JUST PRIOR TO FAILURE
			TERMINATION	0.594 (0.234)	1.963 (0.773)	0.303	364 (52.8)	383 (55.5)	0.960	1.444	0.411 (0.162)	0.582	1.119	295 (72)	GHE	50.9 (46.3)	
			FAILURE	0.653 (0.257)	2.126 (0.837)	0.307	331 (48.0)	383 (55.5)	0.873	1.494	0.437 (0.172)	0.639	1.149	295 (72)	AIR	49.0 (44.6)	
A3A -21	1.036 (0.408)	12.710 (5.004)	INITIATION	0.206 (0.081)	2.096 (0.825)	0.098	345 (50.0)	383 (55.5)	0.902	0.920	0.224 (0.088)	0.199	1.030	295 (72)	GHE	32.6 (29.7)	CYCLED FOR 617 CYCLES – UNLOADED JUST PRIOR TO FAILURE
			TERMINATION	0.635 (0.250)	2.464 (0.970)	0.258	345 (50.0)	383 (55.5)	0.902	1.315	0.483 (0.190)	0.613	1.178	295 (72)	GHE	55.0 (50.0)	
			FAILURE	0.676 (0.266)	2.560 (1.008)	0.264	318 (46.1)	383 (55.5)	0.830	1.364	0.495 (0.195)	0.652	1.201	295 (72)	AIR	52.4 (47.7)	
A3B -3	2.039 (0.803)	12.715 (5.006)	INITIATION	0.782 (0.308)	3.259 (1.283)	0.240	172 (25.0)	383 (55.5)	0.451	1.393	0.561 (0.221)	0.384	1.065	295 (72)	GHE	26.8 (24.4)	CYCLED FOR 4000 CYCLES
			TERMINATION	0.991 (0.390)	3.673 (1.446)	0.270	172 (25.0)	383 (55.5)	0.451	1.482	0.599 (0.263)	0.486	1.092	295 (72)	GHE	30.0 (27.3)	
			FAILURE	1.079 (0.425)	3.937 (1.550)	0.274	272 (39.4)	383 (55.5)	0.710	1.435	0.752 (0.296)	0.529	1.112	295 (72)	AIR	51.1 (46.5)	

Table 15: 333 mHz (20 CPM) Cyclic Load Flaw Growth Tests of 2219-T87 Aluminum in Air at 295°K (72°F)

SPECIMEN NUMBER	THICKNESS, t cm (INCH)	WIDTH, W cm (INCH)	SPECIMEN LOADING SEQUENCE	FLAW DEPTH, a cm (INCH)	FLAW LENGTH, 2c cm (INCH)	a / 2c	STRESS, σ MN/m^2 (KSI)	YIELD STRENGTH, σ_{ys} MN/m^2 (KSI)	σ / σ_{ys}	SHAPE PARAMETER, Q	FLAW SIZE, a/Q cm (INCH)	a / t	MAGNIFICATION FACTOR, M_K	TEST TEMPERATURE, T °K (°F)	ENVIRONMENT	STRESS INTENSITY, K_I $MN/m^{3/2}$ (KSI$\sqrt{IN}$)	REMARKS
A3A -18	1.021 (0.402)	12.715 (5.006)	INITIATION	0.224 (0.088)	0.81 (0.317)	0.278	345 (50.0)	383 (55.5)	0.902	1.375	0.163 (0.064)	0.219	1.021	295 (72)	AIR	27.5 (25.1)	1685 CYCLES TO FAILURE
			TERMINATION	0.747 ▷ (0.294)	2.54 ▷ (1.000)	0.294	345 (50.0)	383 (55.5)	0.902	1.434	0.521 (0.205)	0.731	1.222	295 (72)	AIR	59.2 (53.9)	
A3A -19	1.018 (0.401)	12.718 (5.007)	INITIATION	0.218 (0.086)	2.12 (0.833)	0.103	345 (50.0)	383 (55.5)	0.902	0.934	0.234 (0.092)	0.214	1.037	295 (72)	AIR	33.7 (30.7)	CYCLED FOR 926 CYCLES –
			TERMINATION	0.640 (0.252)	2.84 (1.116)	0.226	345 (50.0)	383 (55.5)	0.902	1.223	0.523 (0.206)	0.628	1.222	295 (72)	AIR	59.4 (54.0)	UNLOADED JUST PRIOR TO FAILURE
			FAILURE	0.724 (0.285)	3.14 (1.235)	0.231	308 (44.7)	383 (55.5)	0.806	1.272	0.569 (0.224)	0.711	1.283	295 (72)	AIR	58.3 (53.0)	
A3B -2	2.027 (0.798)	12.715 (5.006)	INITIATION	0.797 (0.314)	3.24 (1.276)	0.246	172 (25.0)	383 (55.5)	0.451	1.414	0.564 (0.222)	0.393	1.064	295 (72)	AIR	26.9 (24.5)	CYCLED FOR 4351 CYCLES
			TERMINATION	1.212 (0.477)	4.54 (1.788)	0.267	172 (25.0)	383 (55.5)	0.451	1.476	0.820 (0.323)	0.598	1.158	295 (72)	AIR	35.3 (32.1)	
			FAILURE	1.257 (0.495)	4.81 (1.895)	0.261	241 (35.0)	383 (55.5)	0.637	1.418	0.886 (0.349)	0.620	1.181	295 (72)	AIR	52.3 (47.6)	

▷ ESTIMATED FLAW SIZE

Table 16: 333 mHz (20 CPM) Cyclic Load Flaw Growth Tests of 2219-T87 Aluminum in Salt Water at 295°K (72°F)

SPECIMEN NUMBER	THICKNESS, t cm (INCH)	WIDTH, W cm (INCH)	SPECIMEN LOADING SEQUENCE	FLAW DEPTH, a cm (INCH)	FLAW LENGTH, 2c cm (INCH)	a / 2c	STRESS, σ MN/m² (KSI)	YIELD STRENGTH, σ_{ys} MN/m² (KSI)	σ / σ_{ys}	SHAPE PARAMETER, Q	FLAW SIZE, a/Q cm (INCH)	a/t	MAGNIFICATION FACTOR, M_K	TEST TEMPERATURE, T °K (°F)	ENVIRONMENT	STRESS INTENSITY, K_I MN/m$^{3/2}$ (KSI$\sqrt{IN}$)	REMARKS
A3A -22	1.031 (0.406)	12.715 (5.006)	INITIATION	0.231 (0.091)	0.805 (0.317)	0.287	345 (50.0)	383 (55.5)	0.902	1.421	0.163 (0.064)	0.224	1.022	295 (72)	3.5% NACL	27.8 (25.3)	CYCLED FOR 1595 CYCLES –
			TERMINATION	0.660 (0.260)	2.350 (0.925)	0.281	345 (50.0)	383 (55.5)	0.902	1.390	0.475 (0.187)	0.640	1.175	295 (72)	3.5% NACL	54.4 (49.5)	UNLOADED JUST PRIOR TO FAILURE
			FAILURE	0.710 (0.279)	2.769 (1.090)	0.256	338 (49.0)	383 (55.5)	0.883	1.322	0.536 (0.211)	0.687	1.235	295 (72)	AIR	59.7 (54.3)	
A3A -23	1.013 (0.399)	12.715 (5.006)	INITIATION	0.231 (0.091)	2.070 (0.815)	0.110	345 (50.0)	383 (55.5)	0.902	0.947	0.241 (0.095)	0.226	1.041	295 (72)	3.5% NACL	34.4 (31.3)	CYCLED FOR 396 CYCLES –
			TERMINATION	0.564 (0.222)	2.337 (0.920)	0.241	345 (50.0)	383 (55.5)	0.902	1.268	0.445 (0.175)	0.556	1.153	295 (72)	3.5% NACL	51.8 (47.1)	UNLOADED JUST PRIOR TO FAILURE
			FAILURE	0.577 (0.227)	2.362 (0.930)	0.244	375 (54.4)	453 (65.7)	0.826	1.304	0.442 (0.174)	0.569	1.159	78 (-320)	LN_2	56.4 (51.3)	
A3B -4	2.035 (0.801)	12.713 (5.005)	INITIATION	0.795 (0.313)	3.246 (1.278)	0.245	172 (25.0)	383 (55.5)	0.451	1.409	0.564 (0.222)	0.391	1.065	295 (72)	3.5% NACL	27.0 (24.5)	CYCLED FOR 3430 CYCLES
			TERMINATION	1.140 (0.449)	4.128 (1.625)	0.276	172 (25.0)	383 (55.5)	0.451	1.506	0.757 (0.298)	0.561	1.129	295 (72)	3.5% NACL	33.0 (30.0)	
			FAILURE	(FAILED DURING MARKING)					–	–	–	–	–	78 (-320)	LN_2	–	

Table 17: 8.3 mHz (0.5 CPM) Combined Cyclic/Sustained Load Flaw Growth Tests of 2219-T87 Aluminum in Salt Water at 295^{o}K (72^{o}F)

SPECIMEN NUMBER	THICKNESS, t cm (INCH)	WIDTH, W cm (INCH)	SPECIMEN LOADING SEQUENCE	FLAW DEPTH, a cm (INCH)	FLAW LENGTH, 2c cm (INCH)	a / 2c	STRESS, σ MN/m^2 (KSI)	YIELD STRENGTH, σ_{ys} MN/m^2 (KSI)	σ / σ_{ys}	SHAPE PARAMETER, Q	FLAW SIZE, a/Q cm (INCH)	a / t	MAGNIFICATION FACTOR, M_K	TEST TEMPERATURE, T ^{o}K (^{o}F)	ENVIRONMENT	STRESS INTENSITY, K_I MN/m$^{3/2}$ (KSI$\sqrt{IN}$)	REMARKS
A3A -32	1.013 (0.399)	12.700 (5.000)	INITIATION	0.414 (0.163)	1.560 (0.614)	0.265	241 [1] (35.0)	383 (55.5)	0.631	1.429	0.289 (0.114)	0.409	1.063	295 (72)	3.5% NACL	26.9 (24.5)	CYCLED FOR 42 CYCLES
			TERMINATION	0.429 (0.169)	1.560 (0.614)	0.275	241 (35.0)	383 (55.5)	0.631	1.456	0.295 (0.116)	0.424	1.064	295 (72)	3.5% NACL	27.2 (24.7)	
			INITIATION	0.457 (0.180)	1.595 (0.628)	0.287	345 (50.0)	383 (55.5)	0.902	1.406	0.325 (0.128)	0.451	1.070	295 (72)	3.5% NACL	41.0 (37.3)	CYCLED FOR 20 CYCLES – UNLOADED JUST PRIOR TO FAILURE
			TERMINATION	0.643 (0.253)	2.431 (0.957)	0.264	345 (50.0)	383 (55.5)	0.902	1.338	0.480 (0.189)	0.634	1.187	295 (72)	3.5% NACL	55.3 (50.3)	
			FAILURE	0.732 (0.288)	2.692 (1.060)	0.272	348 (50.4)	453 (65.7)	0.768	1.411	0.518 (0.204)	0.722	1.243	78 (-320)	LN_2	60.7 (55.2)	
A3A -34	1.029 (0.405)	12.713 (5.005)	INITIATION	0.376 (0.148)	1.377 (0.542)	0.273	345 (50.0)	383 (55.5)	0.902	1.370	0.274 (0.108)	0.365	1.052	295 (72)	3.5% NACL	37.2 (33.8)	CYCLED FOR 729 CYCLES – UNLOADED JUST PRIOR TO FAILURE
			TERMINATION	0.693 (0.273)	2.667 (1.050)	0.260	345 (50.0)	383 (55.5)	0.902	1.325	0.523 (0.206)	0.674	1.221	295 (72)	3.5% NACL	59.4 (54.0)	
			FAILURE	0.734 (0.289)	2.832 (1.115)	0.259	378 (54.8)	453 (65.7)	0.835	1.344	0.546 (0.215)	0.714	1.252	78 (-320)	LN_2	68.1 (62.0)	
A3A -35	1.029 (0.405)	12.710 (5.004)	INITIATION	0.292 (0.115)	1.049 (0.413)	0.278	345 (50.0)	383 (55.5)	0.902	1.385	0.211 (0.083)	0.284	1.040	295 (72)	3.5% NACL	32.1 (29.2)	CYCLED FOR 481 CYCLES
			TERMINATION	0.368 (0.145)	1.173 (0.462)	0.314	345 (50.0)	383 (55.5)	0.902	1.510	0.244 (0.096)	0.358	1.040	295 (72)	3.5% NACL	34.6 (31.5)	
			FAILURE	0.371 (0.146)	1.176 (0.463)	0.315	483 (70.0)	453 (65.7)	> 1.0	1.474	0.251 (0.099)	0.360	1.040	78 (-320)	LN_2	49.1 (44.7)	
A3A -37	1.024 (0.403)	12.857 (5.062)	INITIATION	0.247 (0.097)	0.930 (0.366)	0.265	345 (50.0)	383 (55.5)	0.902	1.347	0.183 (0.072)	0.241	1.029	295 (72)	3.5% NACL	29.7 (27.0)	CYCLED FOR 499 CYCLES
			TERMINATION	0.295 (0.116)	0.975 (0.384)	0.302	345 (50.0)	383 (55.5)	0.902	1.469	0.201 (0.079)	0.288	1.036	295 (72)	3.5% NACL	31.3 (28.5)	
			FAILURE	0.300 (0.118)	0.978 (0.385)	0.306	385 (55.9)	383 (55.5)	> 1.0	1.439	0.208 (0.082)	0.293	1.037	295 (72)	AIR	35.6 (32.4)	

[1] STRESS LEVEL ERROR

Table 18: 3.3 mHz (0.2 CPM) Combined Cyclic/Sustained Load Flaw Growth Tests of 2219-T87 Aluminum in Salt Water at 295^{o}K (72^{o}F)

SPECIMEN NUMBER	THICKNESS, t cm (INCH)	WIDTH, W cm (INCH)	SPECIMEN LOADING SEQUENCE	FLAW DEPTH, a cm (INCH)	FLAW LENGTH, 2c cm (INCH)	a / 2c	STRESS, σ MN/m^2 (KSI)	YIELD STRENGTH, σ_{ys} MN/m^2 (KSI)	σ / σ_{ys}	SHAPE PARAMETER, Q	FLAW SIZE, a/Q cm (INCH)	a / t	MAGNIFICATION FACTOR, M_K	TEST TEMPERATURE, T ^{o}K (^{o}F)	ENVIRONMENT	STRESS INTENSITY, K_I MN/m$^{3/2}$ (KSI$\sqrt{IN}$)	REMARKS
A3A -31	1.031 (0.406)	12.710 (5.004)	INITIATION	0.409 (0.161)	1.575 (0.620)	0.260	345 (50.0)	383 (55.5)	0.902	1.319	0.310 (0.122)	0.397	1.061	295 (72)	3.5% NACL	39.7 (36.1)	CYCLED FOR 155 CYCLED – TEST TERMINATED EARLY, WOULD HAVE FAILED AT ≈ 200 CYCLES
			TERMINATION	0.523 (0.206)	1.918 (0.755)	0.273	345 (50.0)	383 (55.5)	0.902	1.364	0.384 (0.151)	0.507	1.101	295 (72)	3.5% NACL	45.8 (41.7)	
			FAILURE	0.579 (0.228)	2.070 (0.815)	0.280	401 (58.2)	453 (65.7)	0.887	1.390	0.417 (0.164)	0.562	1.127	78 (-320)	LN_2	56.8 (51.7)	
A3A -33	1.026 (0.404)	12.713 (5.005)	INITIATION	0.343 (0.135)	1.359 (0.535)	0.252	345 (50.0)	383 (55.5)	0.902	1.298	0.264 (0.104)	0.334	1.054	295 (72)	3.5% NACL	36.4 (33.1)	CYCLED FOR 94 CYCLES [2]
			TERMINATION	0.353 (0.139)	1.359 (0.535)	0.260	345 (50.0)	383 (55.5)	0.902	1.323	0.267 (0.105)	0.344	1.053	295 (72)	3.5% NACL	36.6 (33.3)	
			INITIATION	0.401 (0.158)	1.366 (0.538)	0.294	345 (50.0)	383 (55.5)	0.902	1.436	0.254 (0.110)	0.391	1.048	295 (72)	3.5% NACL	37.3 (33.9)	402 CYCLES TO FAILURE
			TERMINATION	0.757 [1] (0.298)	3.317 [1] (1.235)	0.241	345 (50.0)	383 (55.5)	0.902	1.268	0.597 (0.235)	0.738	1.294	295 (72)	3.5% NACL	67.3 (61.2)	
A3A -36	1.024 (0.403)	12.720 (5.005)	INITIATION	0.284 (0.112)	1.046 (0.412)	0.272	345 (50.0)	383 (55.5)	0.902	1.366	0.208 (0.082)	0.278	1.040	295 (72)	3.5% NACL	31.9 (29.0)	CYCLED FOR 573 CYCLES
			TERMINATION	0.358 (0.141)	1.179 (0.464)	0.304	345 (50.0)	383 (55.5)	0.902	1.189	0.244 (0.096)	0.350	1.042	295 (72)	3.5% NACL	34.6 (31.5)	
			FAILURE	0.366 (0.144)	1.191 (0.469)	0.307	399 (57.8)	383 (55.5)	>1.0	1.144	0.254 (0.100)	0.357	1.042	295 (72)	AIR	40.8 (37.1)	
A3A -38	1.031 (0.406)	12.700 (5.000)	INITIATION	0.249 (0.098)	0.932 (0.367)	0.267	357 (51.8)	383 (55.5)	0.934	1.342	0.185 (0.073)	0.241	1.029	295 (72)	3.5% NACL	31.0 (28.2)	CYCLED FOR 493 CYCLES
			TERMINATION	0.305 (0.120)	1.024 (0.403)	0.298	357 (51.8)	383 (55.5)	0.934	1.429	0.213 (0.084)	0.296	1.039	295 (72)	3.5% NACL	33.3 (30.3)	
			FAILURE	0.312 (0.123)	1.039 (0.409)	0.301	394 (57.1)	383 (55.5)	>1.0	1.414	0.221 (0.087)	0.303	1.040	295 (72)	AIR	37.5 (34.1)	

[1] ESTIMATED FLAW SIZE

[2] TEST TERMINATED DUE TO MACHINE HYDRAULIC LEAK

Table 19: 333 mHz (20 CPM) Cyclic Load Flaw Growth Tests of 2219-T87 Aluminum in Liquid Nitrogen at 78°K (-320°F)

SPECIMEN NUMBER	THICKNESS, t cm (INCH)	WIDTH, W cm (INCH)	SPECIMEN LOADING SEQUENCE	FLAW DEPTH, a cm (INCH)	FLAW LENGTH, 2c cm (INCH)	a / 2c	STRESS, σ MN/m^2 (KSI)	YIELD STRENGTH, σ_{ys} MN/m^2 (KSI)	σ / σ_{ys}	SHAPE PARAMETER, Q	FLAW SIZE, a/Q cm (INCH)	a / t	MAGNIFICATION FACTOR, M_K	TEST TEMPERATURE, T °K (°F)	ENVIRONMENT	STRESS INTENSITY, K_I $MN/m^{3/2}$ (KSI$\sqrt{IN}$)	REMARKS
A3A -8	1.013 (0.399)	12.710 (5.004)	INITIATION	0.216 (0.085)	0.810 (0.319)	0.266	414 (60.0)	453 (68.7)	0.913	1.349	0.160 (0.063)	0.213	1.021	78 (-320)	LN_2	33.1 (30.1)	853 CYCLES TO FAILURE
			TERMINATION	0.597 [1] (0.235)	1.500 [1] (0.590)	0.398	414 (60.0)	453 (65.7)	0.913	1.821	0.328 (0.129)	0.589	1.049	78 (-320)	LN_2	48.4 (44.0)	
A3A -9	1.026 (0.404)	12.713 (5.005)	INITIATION	0.239 (0.094)	2.108 (0.830)	0.113	414 (60.0)	453 (65.7)	0.913	0.949	0.251 (0.099)	0.233	1.045	78 (-320)	LN_2	42.2 (38.4)	40 CYCLES TO FAILURE
			TERMINATION	0.457 [1] (0.180)	2.121 [1] (0.839)	0.216	414 (60.0)	453 (65.7)	0.913	1.192	0.384 (0.151)	0.446	1.101	78 (-320)	LN_2	55.2 (50.2)	
A3B -1	2.029 (0.799)	12.718 (5.007)	INITIATION	0.818 (0.322)	3.327 (1.310)	0.246	207 (30.0)	453 (65.7)	0.457	1.412	0.579 (0.228)	0.403	1.068	78 (-320)	LN_2	32.9 (29.9)	CYCLED FOR 1400 CYCLES
			TERMINATION	1.135 (0.447)	3.597 (1.558)	0.287	207 (30.0)	453 (65.7)	0.457	1.541	0.737 (0.290)	0.559	1.120	78 (-320)	LN_2	38.8 (35.3)	
			FAILURE	1.160 (0.457)	4.064 (1.600)	0.286	270 (39.2)	453 (65.7)	0.597	1.503	0.772 (0.304)	0.572	1.128	78 (-320)	LN_2	52.2 (47.5)	

[1] ESTIMATED FLAW SIZE

Table 20: 8.3 mHz (0.5 CPM) Combined Cyclic/Sustained Load Flaw Growth Tests of 2219-T87 Aluminum in Liquid Nitrogen at 78°K (-320°F)

SPECIMEN NUMBER	THICKNESS, t cm (INCH)	WIDTH, W cm (INCH)	SPECIMEN LOADING SEQUENCE	FLAW DEPTH, a cm (INCH)	FLAW LENGTH, 2c cm (INCH)	a/2c	STRESS, σ MN/m^2 (KSI)	YIELD STRENGTH, σ_{ys} MN/m^2 (KSI)	σ / σ_{ys}	SHAPE PARAMETER, Q	FLAW SIZE, a/Q cm (INCH)	a/t	MAGNIFICATION FACTOR, M_K	TEST TEMPERATURE, T °K (°F)	ENVIRONMENT	STRESS INTENSITY, K_I MN/m$^{3/2}$ (KSI$\sqrt{IN}$)	REMARKS
A3A -10	1.016 (0.400)	12.715 (5.006)	INITIATION	0.391 (0.154)	1.488 (0.570)	0.270	414 (60.0)	453 (65.7)	0.913	1.350	0.290 (0.114)	0.385	1.055	78 (-320)	LN_2	45.8 (41.7)	3.2 CYCLES TO FAILURE
			TERMINATION	0.483 ▷ (0.190)	1.651 ▷ (0.650)	0.292	414 (60.0)	453 (65.7)	0.913	1.428	0.338 (0.133)	0.475	1.076	78 (-320)	LN_2	50.4 (45.9)	
A3A -11	1.013 (0.399)	12.713 (5.005)	INITIATION	0.351 (0.138)	1.346 (0.530)	0.260	414 (60.0)	453 (65.7)	0.913	1.326	0.264 (0.104)	0.346	1.054	78 (-320)	LN_2	43.7 (39.8)	10.1 CYCLES TO FAILURE
			TERMINATION	0.508 ▷ (0.200)	1.600 ▷ (0.630)	0.317	414 (60.0)	453 (65.7)	0.913	1.515	0.335 (0.132)	0.501	1.072	78 (-320)	LN_2	50.1 (45.6)	
A3A -13	1.011 (0.398)	12.716 (5.006)	INITIATION	0.274 (0.108)	0.998 (0.393	0.275	414 (60.0)	453 (65.7)	0.913	1.367	0.201 (0.079)	0.271	1.037	78 (-320)	LN_2	37.5 (34.1)	CYCLED FOR 240 CYCLES
			TERMINATION	0.340 (0.135)	1.100 (0.433)	0.312	414 (60.0)	453 (65.7)	0.913	1.500	0.229 (0.090)	0.339	1.040	78 (-320)	LN_2	40.2 (36.6)	
			FAILURE	0.439 (0.173)	1.295 (0.510)	0.339	438 (63.5)	453 (65.7)	0.967	1.572	0.279 (0.110)	0.435	1.044	78 (-320)	LN_2	47.2 (42.9)	
A3A -29	1.016 (0.400)	12.713 (5.005)	INITIATION	0.274 (0.108)	1.118 (0.440)	0.245	414 (60.0)	453 (65.7)	0.913	1.270	0.216 (0.085)	0.270	1.041	78 (-320)	LN_2	38.9 (35.4)	CYCLED FOR 100 CYCLES
			TERMINATION	0.345 (0.136)	1.153 (0.454)	0.300	414 (60.0)	453 (65.7)	0.913	1.446	0.239 (0.094)	0.340	1.042	78 (-320)	LN_2	41.1 (37.4)	
			FAILURE	0.457 (0.180)	1.306 (0.514)	0.350	429 (62.2)	453 (65.7)	0.946	1.621	0.282 (0.111)	0.450	1.044	78 (-320)	LN_2	46.4 (42.2)	

▷ ESTIMATE FLAW SIZE

Table 21: 3.3 mHz (0.2 CPM) Combined Cyclic/Sustained Load Flaw Growth Tests of 2219-T87 Aluminum in Liquid Nitrogen at 78°K (-320°F)

SPECIMEN NUMBER	THICKNESS, t cm (INCH)	WIDTH, W cm (INCH)	SPECIMEN LOADING SEQUENCE	FLAW DEPTH, a cm (INCH)	FLAW LENGTH, 2c cm (INCH)	a / 2c	STRESS, σ MN/m^2 (KSI)	YIELD STRENGTH, σ_{ys} MN/m^2 (KSI)	σ / σ_{ys}	SHAPE PARAMETER, Q	FLAW SIZE, a/Q cm (INCH)	a / t	MAGNIFICATION FACTOR, M_K	TEST TEMPERATURE, T °K (°F)	ENVIRONMENT	STRESS INTENSITY, K_I $MN/m^{3/2}$ (KSI$\sqrt{IN}$)	REMARKS
A3A -14	1.024 (0.403)	12.712 (5.005)	INITIATION	0.366 (0.144)	1.453 (0.572)	0.252	414 (60.0)	453 (65.7)	0.913	1.297	0.282 (0.111)	0.357	1.060	78 (-320)	LN_2	45.4 (41.3)	2.3 CYCLES TO FAILURE
			TERMINATION	(UNDEFINED)			414 (60.0)	453 (65.7)	0.913	– –	– –	– –	– –	78 (-320)	LN_2	—	
A3A -15	1.003 (0.395)	12.710 (5.004)	INITIATION	0.356 (0.140)	1.339 (0.527)	0.266	414 (60.0)	453 (65.7)	0.913	1.333	0.267 (0.105)	0.354	1.053	78 (-320)	LN_2	43.9 (39.9)	24.4 CYCLES TO FAILURE
			TERMINATION	0.533 ▷ (0.210)	1.600 ▷ (0.630)	0.333	414 (60.0)	453 (65.7)	0.913	1.567	0.340 (0.134)	0.532	1.076	78 (-320)	LN_2	50.6 (46.0)	
A3A -16	1.013 (0.399)	12.712 (5.005)	INITIATION	0.307 (0.121)	1.113 (0.438)	0.276	414 (60.0)	453 (65.7)	0.913	1.375	0.224 (0.088)	0.303	1.045	78 (-320)	LN_2	39.9 (36.3)	CYCLED FOR 100 CYCLES
			TERMINATION	0.376 (0.148)	1.201 (0.473)	0.313	414 (60.0)	453 (65.7)	0.913	1.494	0.251 (0.099)	0.371	1.041	78 (-320)	LN_2	42.1 (38.3)	
			FAILURE	0.399 (0.157)	1.219 (0.480)	0.327	447 (64.9)	453 (65.7)	0.989	1.524	0.262 (0.103)	0.393	1.039	78 (-320)	LN_2	46.5 (42.3)	
A3A -17	1.018 (0.401)	12.717 (5.007)	INITIATION	0.267 (0.105)	0.991 (0.390)	0.269	414 (60.0)	453 (65.7)	0.913	1.346	0.198 (0.078)	0.262	1.035	78 (-320)	LN_2	37.2 (33.8)	CYCLED FOR 258 CYCLES
			TERMINATION	0.318 (0.125)	1.036 (0.408)	0.306	414 (60.0)	453 (65.7)	0.913	1.470	0.216 (0.085)	0.312	1.039	78 (-320)	LN_2	38.9 (35.4)	
			FAILURE	0.330 (0.130)	1.041 (0.410)	0.317	490 (71.0)	453 (65.7)	>1.0	1.477	0.224 (0.088)	0.324	1.038	78 (-320)	LN_2	46.8 (42.6)	

▷ ESTIMATED FLAW SIZE

Table 22: 333 mHz (20 CPM) Cyclic Load Flaw Growth Tests of 2219-T87 Aluminum in Liquid Hydrogen at 20°K (−423°F)

SPECIMEN NUMBER	THICKNESS, t cm (INCH)	WIDTH, W cm (INCH)	SPECIMEN LOADING SEQUENCE	FLAW DEPTH, a cm (INCH)	FLAW LENGTH, 2c cm (INCH)	a / 2c	STRESS, σ MN/m^2 (KSI)	YIELD STRENGTH, σ_{ys} MN/m^2 (KSI)	σ / σ_{ys}	SHAPE PARAMETER, Q	FLAW SIZE, a/Q cm (INCH)	a / t	MAGNIFICATION FACTOR, M_K	TEST TEMPERATURE, T °K (°F)	ENVIRONMENT	STRESS INTENSITY, K_I $MN/m^{3/2}$ (KSI$\sqrt{IN}$)	REMARKS
A2C -6	1.013 (0.399)	5.715 (2.250)	INITIATION	0.218 (0.086)	0.864 (0.340)	0.253	448 (65.0)	492 (71.3)	0.911	1.303	0.168 0.066	0.216	1.022	20 (-423)	LH_2	36.6 (33.3)	244 CYCLES TO FAILURE
			TERMINATION	0.475 [1] (0.187)	1.194 [1] (0.470)	0.398	448 (65.0)	492 (71.3)	0.911	1.833	0.259 0.102	0.469	1.028	20 (-423)	LH_2	45.8 (41.7)	
A2C -7	1.021 (0.402)	5.712 (2.249)	INITIATION	0.295 (0.116)	1.123 (0.442)	0.262	448 (65.0)	492 (71.3)	0.911	1.333	0.221 0.087	0.289	1.044	20 (-423)	LH_2	43.0 (39.1)	47 CYCLES TO FAILURE
			TERMINATION	0.470 [1] (0.185)	1.32 [1] (0.520)	0.356	448 (65.0)	492 (71.3)	0.911	1.651	0.284 0.112	0.460	1.044	20 (-423)	LH_2	48.6 (44.2)	
A2C -8	1.013 (0.399)	5.715 (2.250)	INITIATION	0.213 (0.084)	0.820 (0.323)	0.260	448 (65.0)	492 (71.3)	0.911	1.312	0.163 0.064	0.211	1.020	20 (-423)	LH_2	35.8 (32.6)	CYCLED FOR 175 CYCLES
			TERMINATION	0.277 (0.109)	0.864 (0.340)	0.321	448 (65.0)	492 (71.3)	0.911	1.535	0.180 0.071	0.273	1.030	20 (-423)	LH_2	38.4 (34.9)	
			FAILURE	0.277 (0.109)	0.864 (0.340)	0.321	488 (70.8)	492 (71.3)	0.993	1.493	0.185 0.073	0.273	1.030	20 (-423)	LH_2	42.2 (38.4)	
A3B [2] -1X	2.029 (0.799)	12.700 (5.000)	INITIATION	0.846 (0.333)	3.632 (1.430)	0.233	224 (32.5)	492 (71.3)	0.456	1.370	0.617 0.243	0.417	1.079	20 (-423)	LH_2	37.0 (33.7)	CYCLED FOR 274 CYCLES
			TERMINATION	0.935 (0.368)	3.632 (1.430)	0.257	224 (32.5)	492 (71.3)	0.456	1.460	0.648 0.255	0.460	1.088	20 (-423)	LH_2	38.3 (34.8)	

[1] ESTIMATED FLAW SIZE

[2] TESTED AT 33.3 mHz (2 CPM)

Table 23: 8.3 mHz (0.5 CPM) Combined Cyclic/Sustained Load Flaw Growth Tests of 2219-T87 Aluminum in Liquid Hydrogen at 20°K (−423°F)

SPECIMEN NUMBER	THICKNESS, t cm (INCH)	WIDTH, W cm (INCH)	SPECIMEN LOADING SEQUENCE	FLAW DEPTH, a cm (INCH)	FLAW LENGTH, 2c cm (INCH)	a / 2c	STRESS, σ MN/m² (KSI)	YIELD STRENGTH, σ_{ys} MN/m² (KSI)	σ / σ_{ys}	SHAPE PARAMETER, Q	FLAW SIZE, a/Q cm (INCH)	a / t	MAGNIFICATION FACTOR, M_K	TEST TEMPERATURE, T °K (°F)	ENVIRONMENT	STRESS INTENSITY, K_I MN/m$^{3/2}$ (KSI$\sqrt{IN}$)	REMARKS
A2C-9	1.019 (0.401)	5.715 (2.250)	INITIATION	0.323 (0.127)	0.126 (0.495)	0.257	448 (65.0)	492 (71.3)	0.911	1.309	0.246 (0.097)	0.317	1.051	20 (−423)	LH_2	45.8 (41.5)	14.5 CYCLES TO FAILURE
			TERMINATION	▷ 0.432 (0.170)	▷ 1.372 (0.540)	0.315	448 (65.0)	492 (71.3)	0.911	1.504	0.287 (0.113)	0.424	1.049	20 (−423)	LH_2	49.1 (44.7)	
A2C-10	1.016 (0.400)	5.712 (2.249)	INITIATION	0.299 (0.118)	1.135 (0.447)	0.264	448 (65.0)	492 (71.3)	0.911	1.340	0.224 (0.088)	0.295	1.046	20 (−423)	LH_2	43.3 (39.4)	27.5 CYCLES TO FAILURE
			TERMINATION	▷ 0.439 (0.173)	▷ 1.270 (0.500)	0.346	448 (65.0)	492 (71.3)	0.911	1.616	0.272 (0.107)	0.432	1.042	20 (−423)	LH_2	47.5 (43.2)	
A2C-11	1.016 (0.400)	5.715 (2.250)	INITIATION	0.251 (0.099)	0.912 (0.359)	0.276	448 (65.0)	492 (71.3)	0.911	1.375	0.183 (0.072)	0.247	1.030	20 (−423)	LH_2	38.6 (35.1)	CYCLED FOR 53 CYCLES
			TERMINATION	0.320 (0.126)	0.973 (0.383)	0.329	448 (65.0)	492 (71.3)	0.911	1.555	0.206 (0.081)	0.315	1.035	20 (−423)	LH_2	41.0 (37.3)	
			FAILURE	0.528 (0.208)	1.275 (0.502)	0.414	345 (50.0)	383 (55.5)	0.901	1.908	0.277 (0.109)	0.520	1.029	295 (72)	AIR	36.5 (33.2)	
A2C-16	1.019 (0.401)	5.715 (2.250)	INITIATION	0.216 (0.085)	0.813 (0.320)	0.266	448 (65.0)	492 (71.3)	0.911	1.349	0.160 (0.063)	0.212	1.020	20 (−423)	LH_2	35.8 (32.6)	CYCLED FOR 110 CYCLES
			TERMINATION	0.259 (0.102)	0.846 (0.333)	0.306	448 (65.0)	492 (71.3)	0.911	1.478	0.175 (0.069)	0.254	1.028	20 (−423)	LH_2	37.7 (34.3)	
			FAILURE	0.432 (0.170)	1.057 (0.416)	0.409	383 (52.7)	383 (55.5)	0.949	1.847	0.234 (0.092)	0.424	1.021	295 (72)	AIR	34.8 (31.7)	

▷ ESTIMATED FLAW SIZE

Table 24: 3.3 mHz (0.2 CPM) Combined Cyclic/Sustained Load Flaw Growth Tests of 2219-T87 Aluminum in Liquid Hydrogen at 20°K (−423°F)

SPECIMEN NUMBER	THICKNESS, t cm (INCH)	WIDTH, W cm (INCH)	SPECIMEN LOADING SEQUENCE	FLAW DEPTH, a cm (INCH)	FLAW LENGTH 2c cm (INCH)	a / 2c	STRESS, σ MN/m^2 (KSI)	YIELD STRENGTH, σ_{ys} MN/m^2 (KSI)	σ / σ_{ys}	SHAPE PARAMETER, Q	FLAW SIZE, a/Q cm (INCH)	a / t	MAGNIFICATION FACTOR, M_K	TEST TEMPERATURE, T °K (°F)	ENVIRONMENT	STRESS INTENSITY, K_I $MN/m^{3/2}$ $(KSI\sqrt{IN})$	REMARKS
A2C-12	1.019 (0.401)	5.715 (2.250)	INITIATION	0.213 (0.084)	0.843 (0.332)	0.253	448 (65.0)	492 (71.3)	0.911	1.292	0.165 (0.065)	0.209	1.020	20 (−423)	LH_2	36.2 (32.9)	CYCLED FOR 110 CYCLES
			TERMINATION	0.269 (0.106)	0.859 (0.338)	0.314	448 (65.0)	492 (71.3)	0.911	1.492	0.180 (0.071)	0.264	1.029	20 (−423)	LH_2	38.1 (34.7)	
			FAILURE	0.335 (0.132)	0.904 (0.356)	0.371	377 (54.7)	383 (55.5)	0.986	1.692	0.198 (0.078)	0.329	1.026	295 (72)	AIR	33.6 (30.6)	
A2C-13	1.016 (0.400)	5.718 (2.251)	INITIATION	0.318 (0.125)	1.260 (0.496)	0.252	448 (65.0)	492 (71.3)	0.911	1.302	0.244 (0.096)	0.313	1.051	20 (−423)	LH_2	45.5 (41.4)	9.8 CYCLES TO FAILURE
			TERMINATION	0.432 ▷ (0.170)	1.372 ▷ (0.540)	0.315	448 (65.0)	492 (71.3)	0.911	1.504	0.287 (0.113)	0.425	1.050	20 (−423)	LH_2	49.1 (44.7)	
A2C-14	1.019 (0.401)	5.718 (2.251)	INITIATION	0.284 (0.112)	1.125 (0.443)	0.253	448 (65.0)	492 (71.3)	0.911	1.302	0.218 (0.086)	0.279	1.043	20 (−423)	LH_2	42.6 (38.8)	58 CYCLES TO FAILURE
			TERMINATION	0.470 ▷ (0.185)	1.334 ▷ (0.525)	0.352	448 (65.0)	492 (71.3)	0.911	1.637	0.287 (0.113)	0.461	1.045	20 (−423)	LH_2	48.9 (44.5)	
A2C-15	1.016 (0.400)	5.720 (2.252)	INITIATION	0.234 (0.092)	0.922 (0.363)	0.253	448 (65.0)	492 (71.3)	0.911	1.295	0.180 (0.071)	0.230	1.027	20 (−423)	LH_2	38.0 (34.6)	CYCLED FOR 106 CYCLES
			TERMINATION	0.371 (0.146)	1.046 (0.412)	0.354	448 (65.0)	492 (71.3)	0.911	1.659	0.224 (0.088)	0.365	1.031	20 (−423)	LH_2	42.8 (38.9)	
			FAILURE	0.478 (0.188)	1.138 (0.448)	0.420	353 (51.2)	383 (55.5)	0.923	1.918	0.249 (0.098)	0.470	1.022	295 (72)	AIR	35.2 (32.0)	

▷ ESTIMATED FLAW SIZE

Table 25: Cyclic and Combined Cyclic/Sustained Load Flaw Growth Tests of 2219-T87 Aluminum in Salt Water at 295° K (72° F) Using TDCD Specimens

SPECIMEN NUMBER	TEST FREQUENCY mHz (CPM)	LOAD, P kN (KIPS)	INITIAL CRACK LENGTH, a_i cm (INCH)	FINAL CRACK LENGTH, a_f cm (INCH)	STRESS INTENSITY, $(K_I)_{AVG}$ $MN/m^{3/2}$ (KSI $\sqrt{IN}$)	NUMBER OF CYCLES
TA-3	333 (20)	16.35 (3.675)	4.16 (1.64)	4.86 (1.91)	22.0 (20.0)	2500
		17.44 (3.920)	4.96 (1.95)	5.31 (2.09)	23.6 (21.4)	1000
		19.60 (4.410)	5.79 (2.28)	6.18 (2.43)	26.4 (24.0)	250
TA-4	333 (20)	16.35 (3.675)	4.22 (1.66)	4.29 (1.69)	22.0 (20.0)	500
		17.44 (3.920)	4.52 (1.78)	4.75 (1.87)	23.6 (21.4)	500
		19.60 (4.410)	4.78 (1.88)	4.98 (1.96)	26.4 (24.0)	250
TA-6	8.3 (0.5)	16.35 (3.675)	4.29 (1.69)	4.42 (1.74)	22.0 (20.0)	500
		17.44 (3.920)	4.62 (1.82)	4.78 (1.88)	23.6 (21.4)	500
		19.60 (4.410)	4.91 (1.93)	6.05 (2.38)	26.4 (24.0)	250
TA-8	8.3 (0.5)	16.35 (3.675)	4.24 (1.67)	4.42 (1.74)	22.0 (20.0)	500
		17.44 (3.920)	4.50 (1.77)	4.62 (1.82)	23.6 (21.4)	500
		19.60 (4.410)	4.81 (1.89)	4.96 (1.95)	26.4 (24.0)	250
TA-5	3.3 (0.2)	16.35 (3.675)	4.22 (1.66)	4.34 (1.71)	22.0 (20.0)	500
		17.44 (3.920)	4.65 (1.83)	4.88 (1.92)	23.6 (21.4)	500
		19.60 (4.410)	4.98 (1.96)	5.31 (2.09)	26.4 (24.0)	250
TA-7	3.3 (0.2)	16.35 (3.675)	4.22 (1.66)	[1]	22.0 (20.0)	500
		17.44 (3.920)	[1]	7.42 (2.92)	23.6 (21.4)	500
		19.60 (4.410)	7.75 (3.05)	8.43 (3.32)	26.4 (24.0)	250

[1] INDISTINGUISHABLE DUE TO SURFACE CORROSION

Table 26: Load/Unload Test of 5Al-2.5 Sn (ELI) Titanium

SPECIMEN NUMBER	THICKNESS, t cm (INCH)	WIDTH, W cm (INCH)	SPECIMEN LOADING SEQUENCE	FLAW DEPTH, a cm (INCH)	FLAW LENGTH, 2c cm (INCH)	a / 2c	STRESS, σ MN/m^2 (KSI)	YIELD STRENGTH, σ_{ys} MN/m^2 (KSI)	σ / σ_{ys}	SHAPE PARAMETER, Q	FLAW SIZE, a/Q cm (INCH)	a / t	MAGNIFICATION FACTOR, M_K	TEST TEMPERATURE, T ^oK (^oF)	ENVIRONMENT	STRESS INTENSITY, K_I $MN/m^{3/2}$ ($KSI\sqrt{IN}$)	REMARKS
5T-6A-15	0.254 (0.100)	3.043 (1.198)	INITIATION	0.089 (0.035)	0.381 (0.150)	0.233	1131 (164.0)	1446 (209.7)	0.782	1.296	0.069 (0.027)	0.350	1.083	20 (-423)	LH_2	62.8 (57.1)	Δa = 0.025 cm (0.010 IN.)
			TERMINATION	0.114 (0.045)	0.391 (0.154)	0.292	1131 (164.0)	1446 (209.7)	0.782	1.456	0.079 (0.031)	0.450	1.135	20 (-423)	LH_2	69.7 (63.4)	
			FAILURE	0.226 (0.089)	0.592 (0.233)	0.382	694 (100.7)	763 [1] (110.7)	0.910	1.745	0.130 (0.051)	0.890	1.452	295 (72)	AIR	70.5 (64.1)	

[1] ASSUMED σ_{YS} FROM REFERENCE 2 (NASA CR-54837)

Table 27: Sustained Load Flaw Growth Tests for 5Al-2.5 Sn (ELI) Titanium in Liquid Nitrogen at $78^{0}K$ ($-320^{0}F$)

SPECIMEN NUMBER	THICKNESS, t cm (INCH)	WIDTH, W cm (INCH)	SPECIMEN LOADING SEQUENCE	FLAW DEPTH, a cm (INCH)	FLAW LENGTH, 2c cm (INCH)	a / 2c	STRESS, σ MN/m^2 (KSI)	YIELD STRENGTH, σ_{ys} MN/m^2 (KSI)	σ / σ_{ys}	SHAPE PARAMETER, Q	FLAW SIZE, a/Q cm (INCH)	a / t	MAGNIFICATION FACTOR, M_K	TEST TEMPERATURE, T ^{o}K (^{o}F)	ENVIRONMENT	STRESS INTENSITY, K_I $MN/m^{3/2}$ ($KSI\sqrt{IN}$)	REMARKS
5T-2D-1	0.500 (0.197)	5.715 (2.250)	INITIATION	0.127 (0.050)	0.533 (0.210)	0.238	1089 (158.0)	1253 (181.7)	0.870	1.282	0.099 (0.039)	0.254	1.036	78 (-320)	LN_2	69.6 (63.3)	LOADED FOR 10.0 HOURS $\Delta a = 0$
			TERMINATION	0.127 (0.050)	0.533 (0.210)	0.238	1089 (158.0	1253 (181.7)	0.870	1.282	0.099 (0.039)	0.254	1.036	78 (-320)	LN_2	69.6 (63.3)	
			FAILURE	0.157 (0.062)	0.564 (0.222)	0.279	1189 (172.4)	1253 (181.7)	0.948	1.378	0.114 (0.045)	0.315	1.052	78 (-320)	LN_2	82.8 (75.3)	
5T-2D-2	0.500 (0.197)	5.715 (2.250)	INITIATION	0.173 (0.068)	0.693 (0.273)	0.249	951 (137.9)	1253 (181.7)	0.759	1.333	0.130 (0.051)	0.345	1.076	78 (-320)	LN_2	71.7 (65.2)	LOADED FOR 10.0 HOURS $\Delta a = 0$
			TERMINATION	0.173 (0.068)	0.693 (0.273)	0.249	951 (137.9)	1253 (181.7)	0.759	1.333	0.130 (0.051)	0.345	1.076	78 (-320)	LN_2	71.7 (65.2)	
			FAILURE	0.312 (0.123)	0.813 (0.320)	0.384	747 (108.3)	763 ▷ (110.7)	0.979	1.732	0.180 (0.071)	0.625	1.233	295 (72)	AIR	76.1 (69.2)	
5T-2D-5	0.503 (0.198)	5.715 (2.250)	INITIATION	0.198 (0.078)	0.787 (0.310)	0.252	951 (137.9)	1253 (181.7)	0.759	1.345	0.147 (0.058)	0.394	1.103	78 (-320)	LN_2	78.4 (71.3)	LOADED FOR 10.1 HOURS $\Delta a = 0$
			TERMINATION	0.198 (0.078)	0.787 (0.310)	0.252	951 (137.9)	1253 (181.7)	0.759	1.345	0.147 (0.058)	0.394	1.103	78 (-320)	LN_2	78.4 (71.3)	
			FAILURE	0.391 (0.154)	0.991 (0.390)	0.395	718 (104.1)	763 ▷ (110.1)	0.942	1.812	0.256 (0.085)	0.779	1.355	295 (72)	AIR	88.4 (80.4)	
5T-2D-6	0.500 (0.197)	5.715 (2.250)	INITIATION	0.142 (0.056)	0.655 (0.258)	0.217	1089 (158.0)	1253 (181.7)	0.870	1.217	0.117 (0.046)	0.284	1.051	78 (-320)	LN_2	76.6 (69.7)	LOADED FOR 10.0 HOURS Δa = 0.028 cm (0.011 IN.)
			TERMINATION	0.170 (0.067)	0.665 (0.262)	0.256	1089 (158.0)	1253 (181.7)	0.870	1.314	0.130 (0.051)	0.340	1.072	78 (-320)	LN_2	81.7 (74.3)	
			FAILURE	0.343 (0.135)	0.818 (0.322)	0.419	743 (107.7)	763 ▷ (110.7)	0.973	1.901	0.180 (0.071)	0.684	1.220	295 (72)	AIR	75.2 (68.4)	

▷ ASSUMED σ_{YS} FROM REFERENCE 2 (NASA CR-54837)

Table 28: Sustained Load Flaw Growth Tests of 5Al-2.5 Sn (ELI) Titanium in Liquid Hydrogen at 20°K (-423°F)

SPECIMEN NUMBER	THICKNESS, t cm (INCH)	WIDTH, W cm (INCH)	SPECIMEN LOADING SEQUENCE	FLAW DEPTH, a cm (INCH)	FLAW LENGTH, 2c cm (INCH)	$a/2c$	STRESS, σ MN/m^2 (KSI)	YIELD STRENGTH, σ_{ys} MN/m^2 (KSI)	σ/σ_{ys}	SHAPE PARAMETER, Q	FLAW SIZE, a/Q cm (INCH)	a/t	MAGNIFICATION FACTOR, M_K	TEST TEMPERATURE, T °K (°F)	ENVIRONMENT	STRESS INTENSITY, K_I $MN/m^{3/2}$ (KSI$\sqrt{IN}$)	REMARKS
5T-6A-1	0.259 (0.102)	3.046 (1.199)	INITIATION	0.132 (0.032)	0.371 (0.146)	0.219	1131 (164.0)	1446 (209.7)	0.782	1.231	0.066 (0.026)	0.314	1.065	20 (-423)	LH_2	60.0 (54.6)	LOADED FOR 6.9 HOURS Δa = 0.020 cm (0.008 IN.)
			TERMINATION	0.102 (0.040)	0.371 (0.146)	0.274	1131 (164.0)	1446 (209.7)	0.782	1.429	0.071 (0.028)	0.392	1.095	20 (-423)	LH_2	64.7 (58.9)	
			FAILURE	0.185 (0.073)	0.452 (0.178)	0.410	705 (102.2)	763 [1] (110.7)	0.923	1.872	0.099 (0.039)	0.716	1.266	295 (72)	AIR	54.8 (49.8)	
5T-6A-7	0.257 (0.101)	3.038 (1.196)	INITIATION	0.086 (0.034)	0.401 (0.158)	0.215	1131 (164.0)	1446 (209.7)	0.782	1.214	0.071 (0.028)	0.337	1.080	20 (-423)	LH_2	63.0 (57.3)	LOADED FOR 10.0 HOURS Δa = 0.020 cm (0.008 IN.)
			TERMINATION	0.107 (0.042)	0.401 (0.158)	0.266	1131 (164.0)	1446 (209.7)	0.782	1.400	0.076 (0.030)	0.416	1.117	20 (-423)	LH_2	68.4 (62.2)	
			FAILURE	0.132 (0.052)	0.401 (0.158)	0.329	799 (115.9)	763 [1] (110.7)	>1.0	1.529	0.086 (0.034)	0.515	1.172	295 (72)	AIR	53.9 (49.0)	

[1] ASSUMED σ_{YS} FROM REFERENCE 2 (NASA CR-54837)

Table 29: 333 mHz (20 CPM) Cyclic Load Flaw Growth Tests of 5Al-2.5 Sn (ELI) Titanium in Liquid Nitrogen at 78°K (-320°F)

SPECIMEN NUMBER	THICKNESS, t cm (INCH)	WIDTH, W, cm (INCH)	SPECIMEN LOADING SEQUENCE	FLAW DEPTH, a cm (INCH)	FLAW LENGTH, 2c cm (INCH)	a/2c	STRESS, σ MN/m² (KSI)	YIELD STRENGTH, σ_{ys} MN/m² (KSI)	σ / σ_{ys}	SHAPE PARAMETER, Q	FLAW SIZE, a/Q cm (INCH)	a/t	MAGNIFICATION FACTOR, M_K	TEST TEMPERATURE, T °K (°F)	ENVIRONMENT	STRESS INTENSITY, K_I MN/m$^{3/2}$ (KSI$\sqrt{IN}$)	REMARKS
5T-2D-3	0.493 (0.194)	5.715 (2.250)	INITIATION	0.114 (0.045)	0.437 (0.172)	0.262	951 (137.9)	1253 (181.7)	0.759	1.364	0.084 (0.033)	0.232	1.025	78 (-320)	LN_2	54.7 (49.8)	FAILED ON 470 CYCLE
			TERMINATION	0.267 (0.105)	0.610 (0.240)	0.437	951 (137.9)	1253 (181.7)	0.759	2.059	0.130 (0.051)	0.542	1.096	78 (-320)	LN_2	73.3 (66.7)	
5T-2D-4	0.498 (0.196)	5.715 (2.250)	INITIATION	0.091 (0.036)	0.777 (0.306)	0.118	951 (137.9)	1253 (181.7)	0.759	1.000	0.091 (0.036)	0.184	1.026	78 (-320)	LN_2	57.2 (52.0)	CYCLED FOR 233 CYCLES
			TERMINATION	0.178 (0.070)	0.777 (0.306)	0.229	951 (137.9)	1253 (181.7)	0.759	1.273	0.140 (0.055)	0.357	1.089	78 (-320)	LN_2	75.3 (68.5)	
			FAILURE	0.191 (0.075)	0.777 (0.306)	0.245	774 (112.3)	763 [1] (110.7)	>1.0	1.229	0.155 (0.061)	0.383	1.099	295 (72)	AIR	65.1 (59.2)	
5TT-1	0.963 (0.379)	7.620 (3.000)	INITIATION	0.396 (0.156)	1.041 (0.410)	0.380	531 (77.0)	1225 (177.6)	0.434	1.880	0.211 (0.083)	0.412	1.073	78 (-320)	LN_2	50.9 (46.3)	CYCLED FOR 825 CYCLES
			TERMINATION	0.536 (0.211)	1.219 (0.480)	0.440	531 (77.0)	1225 (177.6)	0.434	2.153	0.249 (0.098)	0.557	1.100	78 (-320)	LN_2	57.0 (51.9)	
			FAILURE	0.546 (0.215)	1.229 (0.484)	0.444	729 (105.8)	1225 (177.6)	0.596	2.129	0.257 (0.101)	0.567	1.098	78 (-320)	LN_2	79.1 (72.0)	
5TT-1A	0.956 (0.377)	5.715 (2.250)	INITIATION	0.363 (0.143)	0.914 (0.360)	0.397	531 (77.0)	1225 (177.6)	0.434	1.959	0.185 (0.073)	0.379	1.055	78 (-320)	LN_2	47.0 (42.8)	CYCLED FOR 867 CYCLES
			TERMINATION	0.450 (0.177)	1.054 (0.415)	0.427	531 (77.0)	1225 (177.6)	0.434	2.082	0.216 (0.085)	0.469	1.075	78 (-320)	LN_2	51.7 (47.0)	
			FAILURE	0.450 (0.177)	1.054 (0.415)	0.427	796 (115.4)	1225 (177.6)	0.650	2.034	0.221 (0.087)	0.469	1.075	78 (-320)	LN_2	78.4 (71.3)	
5TT-2	0.257 (0.101)	5.740 (2.260)	INITIATION	0.089 (0.035)	0.208 (0.082)	0.427	1062 (154.0)	1225 (177.6)	0.867	1.944	0.046 (0.018)	0.347	1.032	78 (-320)	LN_2	45.5 (41.4)	CYCLED FOR 499 CYCLES
			TERMINATION	0.109 (0.043)	0.229 (0.090)	0.478	1062 (154.0)	1225 (177.6)	0.867	2.150	0.051 (0.020)	0.426	1.017	78 (-320)	LN_2	46.9 (42.7)	
			FAILURE	0.109 (0.043)	0.229 (0.090)	0.478	823 (119.2)	763 [1] (110.7)	>1.0	2.150	0.051 (0.020)	0.426	1.017	295 (72)	AIR	36.7 (33.4)	
5TT-2A	0.754 (0.279)	5.715 (2.250)	INITIATION	0.086 (0.034)	0.208 (0.082)	0.415	1062 (154.0)	1225 (177.6)	0.867	1.889	0.046 (0.018)	0.122	1.002	78 (-320)	LN_2	44.1 (40.1)	CYCLED FOR 609 CYCLES
			TERMINATION	0.127 (0.050)	0.307 (0.121)	0.413	1062 (154.0)	1225 (177.6)	0.867	1.923	0.066 (0.026)	0.179	1.004	78 (-320)	LN_2	53.6 (48.8)	
			FAILURE	0.127 (0.050)	0.307 (0.121)	0.413	918 (133.1)	763 [1] (110.7)	>1.0	1.852	0.069 (0.027)	0.179	1.004	295 (72)	AIR	47.0 (42.8)	

[1] ASSUMED σ_{YS} FROM REFERENCE 2 (NASA CR-54837)

Table 30: 333 mHz (20 CPM) Cyclic Load Flaw Growth Tests of 5Al-2.5 Sn (ELI) Titanium in Liquid Hydrogen at 20°K (-423°F)

SPECIMEN NUMBER	THICKNESS, t cm (INCH)	WIDTH, W cm (INCH)	SPECIMEN LOADING SEQUENCE	FLAW DEPTH, a cm (INCH)	FLAW LENGTH, 2c cm (INCH)	a / 2c	STRESS, σ MN/m^2 (KSI)	YIELD STRENGTH, σ_{ys} MN/m^2 (KSI)	σ / σ_{ys}	SHAPE PARAMETER, Q	FLAW SIZE, a/Q cm (INCH)	a/t	MAGNIFICATION FACTOR, M_K	TEST TEMPERATURE, T °K (°F)	ENVIRONMENT	STRESS INTENSITY, K_I MN/m$^{3/2}$ (KSI$\sqrt{IN}$)	REMARKS
5T-6A-4	0.254 (0.100)	3.045 (1.199)	INITIATION	0.046 (0.018)	0.208 (0.082)	0.220	1131 (164.0)	1446 (209.7)	0.782	1.286	0.036 (0.014)	0.180	1.016	20 (-423)	LH_2	42.9 (39.0)	560 CYCLES TO FAILURE
			TERMINATION	(UNDEFINED)		–	1131 (164.0)	1446 (209.7)	0.782	–	–	–	–	20 (-423)	LH_2	–	
5T-6A-5	0.257 (0.101)	1.313 (1.195)	INITIATION	0.091 (0.036)	0.361 (0.142)	0.254	1131 (164.0)	1446 (209.7)	0.782	1.333	0.069 (0.027)	0.356	1.081	20 (-423)	LH_2	62.1 (56.5)	23 CYCLES TO FAILURE
			TERMINATION	(UNDEFINED)		–	1131 (164.0)	1446 (209.7)	0.782	–	–	–	–	20 (-423)	LH_2	–	
5T-6A-6	0.257 (0.101)	3.045 (1.199)	INITIATION	0.046 (0.018)	0.208 (0.082)	0.220	1131 (164.0)	1446 (209.7)	0.782	1.286	0.036 (0.014)	0.178	1.016	20 (-423)	LH_2	42.9 (39.0)	CYCLED FOR 400 CYCLES
			TERMINATION	0.102 (0.040)	0.234 (0.092)	0.435	1131 (164.0)	1446 (209.7)	0.782	2.000	0.051 (0.020)	0.396	1.038	20 (-423)	LH_2	51.2 (46.8)	
			FAILURE	0.127 (0.050)	0.264 (0.104)	0.481	799 (115.9)	763 [1] (110.7)	>1.0	2.174	0.058 (0.023)	0.495	1.023	295 (72)	AIR	38.7 (35.2)	

[1] ASSUMED σ_{YS} FROM REFERENCE 2 (NASA CR-57837)

Table 31: 8.3 mHz (0.5 CPM) Combined Cyclic/Sustained Load Flaw Growth Tests of 5Al-2.5 Sn (ELI) Titanium in Liquid Hydrogen at 20°K (-423°F)

SPECIMEN NUMBER	THICKNESS, t cm (INCH)	WIDTH, W cm (INCH)	SPECIMEN LOADING SEQUENCE	FLAW DEPTH, a cm (INCH)	FLAW LENGTH, 2c cm (INCH)	a / 2c	STRESS, σ MN/m^2 (KSI)	YIELD STRENGTH, σ_{ys} MN/m^2 (KSI)	σ / σ_{ys}	SHAPE PARAMETER, Q	FLAW SIZE, a/Q cm (INCH)	a / t	MAGNIFICATION FACTOR, M_K	TEST TEMPERATURE, T °K (°F)	ENVIRONMENT	STRESS INTENSITY, K_I $MN/m^{3/2}$ $(KSI\sqrt{IN})$	REMARKS
5T-6A-3	0.259 (0.102)	3.043 (1.198)	INITIATION	0.097 (0.038)	0.386 (0.152)	0.250	1131 (164.0)	1446 (209.7)	0.782	1.357	0.071 (0.028)	0.372	1.092	20 (-423)	LH_2	64.7 (58.9)	2 CYCLES TO FAILURE
			TERMINATION	(UNDEFINED)		–	1131 (164.0)	1446 (209.7)	0.782	–	–	–	–	20 (-423)	LH_2	–	
5T-6A-8	0.257 (0.101)	3.048 (1.200)	INITIATION	0.086 (0.034)	0.358 (0.141)	0.241	1131 (164.0)	1446 (209.7)	0.782	1.308	0.066 (0.026)	0.338	1.073	20 (-423)	LH_2	60.8 (55.3)	41 CYCLES TO FAILURE
			TERMINATION	(UNDEFINED)		–	1131 (164.0)	1446 (209.7)	0.782	–	–	–	–	20 (-423)	LH_2	–	
5T-6A-9	0.259 (0.102)	3.045 (1.199)	INITIATION	0.069 (0.027)	0.295 (0.116)	0.233	1131 (164.0)	1446 (209.7)	0.782	1.286	0.053 (0.021)	0.265	1.040	20 (-423)	LH_2	53.0 (48.2)	CYCLED FOR 90 CYCLES
			TERMINATION	0.102 (0.040)	0.302 (0.119)	0.338	1131 (164.0)	1446 (209.7)	0.782	1.600	0.064 (0.025)	0.393	1.076	20 (-423)	LH_2	59.2 (53.9)	
			FAILURE	0.137 (0.054)	0.328 (0.129)	0.419	832 (120.6)	763 [1] (110.7)	>1.0	1.862	0.074 (0.029)	0.529	1.116	295 (72)	AIR	48.9 (44.5)	
5T-6A-10	0.262 (0.103)	3.040 (1.197)	INITIATION	0.048 (0.019)	0.208 (0.082)	0.232	1131 (164.0)	1446 (209.7)	0.782	1.267	0.038 (0.015)	0.185	1.016	20 (-423)	LH_2	43.4 (39.5)	CYCLED FOR 350 CYCLES
			TERMINATION	0.076 (0.030)	0.233 (0.088)	0.341	1131 (164.0)	1446 (209.7)	0.782	1.667	0.046 (0.018)	0.293	1.034	20 (-423)	LH_2	49.0 (44.6)	
			FAILURE	0.117 (0.046)	0.287 (0.113)	0.407	783 (113.5)	763 [1] (110.7)	>1.0	1.840	0.064 (0.025)	0.447	1.082	295 (72)	AIR	31.8 (38.0)	

[1] ASSUMED σ_{YS} FROM REFERENCE 2 (NASA CR-54837)

Table 32: 3.3 mHz (0.2 CPM) Combined Cyclic/Sustained Load Flaw Growth Tests of 5Al-2.5 Sn (ELI) Titanium in Liquid Hydrogen at 20°K (−423°F)

SPECIMEN NUMBER	THICKNESS, t cm (INCH)	WIDTH, W cm (INCH)	SPECIMEN LOADING SEQUENCE	FLAW DEPTH, a cm (INCH)	FLAW LENGTH, 2c cm (INCH)	a / 2c	STRESS, σ MN/m^2 (KSI)	YIELD STRENGTH, σ_{ys} MN/m^2 (KSI)	σ / σ_{ys}	SHAPE PARAMETER, Q	FLAW SIZE, a/Q cm (INCH)	a / t	MAGNIFICATION FACTOR, M_K	TEST TEMPERATURE, T °K (°F)	ENVIRONMENT	STRESS INTENSITY, K_I $MN/m^{3/2}$ $(KSI\sqrt{IN})$	REMARKS
5T-6A-13	0.257 (0.101)	3.045 (1.199)	INITIATION	0.071 (0.028)	0.290 (0.114)	0.246	1131 (164.0)	1446 (209.7)	0.782	1.333	0.053 (0.021)	0.277	1.043	20 (-423)	LH_2	53.3 (48.5)	CYCLED FOR 90 CYCLES
			TERMINATION	0.093 (0.037)	0.305 (0.120)	0.308	1131 (164.0)	1446 (209.7)	0.782	1.540	0.061 (0.024)	0.366	1.071	20 (-423)	LH_2	58.7 (53.3)	
			FAILURE	(DURING	MARKING)	–	–	–	–	–	–	–	–	295 (72)	AIR	–	
5T-6A-14	0.264 (0.104)	3.048 (1.200)	INITIATION	0.051 (0.020)	0.211 (0.083)	0.241	1131 (164.0)	1446 (209.7)	0.782	1.333	0.038 (0.015)	0.192	1.015	20 (-423)	LH_2	44.1 (40.1)	CYCLED FOR 360 CYCLES
			TERMINATION	0.079 (0.031)	0.229 (0.090)	0.344	1131 (164.0)	1446 (209.7)	0.782	1.632	0.048 (0.019)	0.298	1.035	20 (-423)	LH_2	49.7 (45.2)	
			FAILURE	0.132 (0.052)	0.287 (0.113)	0.460	790 (114.6)	763 (110.7)	>1.0	2.080	0.064 (0.025)	0.500	1.048	295 (72)	AIR	40.9 (37.2)	
5T-6A-12	0.257 (0.101)	3.040 (1.197)	INITIATION	0.089 (0.035)	0.363 (0.143)	0.245	1131 (164.0)	1446 (209.7)	0.782	1.296	0.069 (0.027)	0.345	1.078	20 (-423)	LH_2	61.7 (56.1)	36 CYCLES TO FAILURE
			TERMINATION	(UNDE	FINED)	–	1131 (164.0)	1446 (209.7)	0.782	–	–	–	–	20 (-423)	LH_2	–	

Table 33: Load/Unload Tests of 6Al-4V (ELI) STA Titanium

SPECIMEN NUMBER	THICKNESS, t cm (INCH)	WIDTH, W cm (INCH)	SPECIMEN LOADING SEQUENCE	FLAW DEPTH, a cm (INCH)	FLAW LENGTH, 2c cm (INCH)	a / 2c	STRESS, σ MN/m^2 (KSI)	YIELD STRENGTH, σ_{ys} MN/m^2 (KSI)	σ / σ_{ys}	SHAPE PARAMETER, Q	FLAW SIZE, a/Q cm (INCH)	a / t	MAGNIFICATION FACTOR, M_K	TEST TEMPERATURE, T ^oK (^oF)	ENVIRONMENT	STRESS INTENSITY, K_I MN/m$^{3/2}$ (KSI$\sqrt{IN}$)	REMARKS
6T-8A-6	0.645 (0.254)	6.350 (2.500)	INITIATION	0.188 (0.074)	0.851 (0.335)	0.221	848 (123.0)	974 (141.3)	0.870	1.213	0.156 (0.061)	0.291	1.052	295 (72)	GHe	68.4 (62.2)	Δa = 0.008 cm (0.003 IN.)
			TERMINATION	0.196 (0.077)	0.851 (0.335)	0.230	848 (123.0)	974 (141.3)	0.870	1.241	0.157 (0.062)	0.303	1.055	295 (72)	GHe	69.1 (62.9)	
			FAILURE	0.432 (0.170)	1.118 (0.440)	0.386	694 (100.7)	974 (141.3)	0.712	1.847	0.234 (0.092)	0.669	1.085	295 (72)	AIR	72.0 (64.6)	
6T-8A-10	0.638 (0.251)	6.350 (2.499)	INITIATION	0.135 (0.053)	0.640 (0.252)	0.210	848 (123.0)	974 (141.3)	0.870	1.177	0.114 (0.045)	0.211	1.024	295 (72)	AIR	56.9 (51.8)	Δa = 0.006 cm (0.002 IN.)
			TERMINATION	0.140 (0.055)	0.640 (0.252)	0.218	848 (123.0)	974 (141.3)	0.870	1.222	0.114 (0.045)	0.219	1.026	295 (72)	AIR	57.6 (52.4)	
			FAILURE	0.287 (0.113)	0.714 (0.281)	0.402	918 (133.2)	974 (141.3)	0.944	1.822	0.157 (0.062)	0.450	1.024	295 (72)	AIR	72.6 (66.1)	
6T-8A-11	0.635 (0.250)	6.350 (2.499)	INITIATION	0.213 (0.084)	0.965 (0.380)	0.221	772 (112.0)	974 (141.3)	0.794	1.253	0.170 (0.067)	0.336	1.063	295 (72)	AIR	66.2 (60.2)	Δa = 0.008 cm (0.003 IN.)
			TERMINATION	0.221 (0.087)	0.965 (0.380)	0.229	772 (112.0)	974 (141.3)	0.794	1.279	0.173 (0.068)	0.348	1.063	295 (72)	AIR	66.7 (60.7)	
			FAILURE	0.478 (0.188)	0.130 (0.511)	0.368	795 (115.3)	974 (141.3)	0.816	1.740	0.274 (0.108)	0.752	1.144	295 (72)	AIR	93.0 (84.6)	

Table 34: Sustained Load Flaw Growth Tests of 6Al-4V (ELI) STA Titanium in Gaseous Helium at 295°K (72°F)

SPECIMEN NUMBER	THICKNESS, t cm (INCH)	WIDTH, W cm (INCH)	SPECIMEN LOADING SEQUENCE	FLAW DEPTH, a cm (INCH)	FLAW LENGTH, 2c cm (INCH)	a / 2c	STRESS, σ MN/m^2 (KSI)	YIELD STRENGTH, σ_{ys} MN/m^2 (KSI)	σ / σ_{ys}	SHAPE PARAMETER, Q	FLAW SIZE, a/Q cm (INCH)	a / t	MAGNIFICATION FACTOR, M_K	TEST TEMPERATURE, T °K (°F)	ENVIRONMENT	STRESS INTENSITY, K_I MN/m$^{3/2}$ (KSI$\sqrt{IN}$)	REMARKS
6T-8A-2	0.645 (0.254)	6.347 (2.499)	INITIATION	0.211 (0.083)	0.833 (0.328)	0.253	848 (123.0)	974 (141.3)	0.870	1.317	0.160 (0.063)	0.327	1.053	295 (72)	GHe	69.8 (63.5)	FAILED IN APPROX. 1 MIN.
			TERMINATION	(UNDEFINED)		—	848 (123.0)	974 (141.3)	0.870	—	—	—	—	295 (72)	GHe	—	
6T-8A-5	0.632 (0.249)	6.358 (2.503)	INITIATION	0.157 (0.062)	0.652 (0.257)	0.241	848 (123.0)	974 (141.3)	0.870	1.291	0.121 (0.048)	0.249	1.034	295 (72)	GHe	60.0 (54.6)	LOADED FOR 10 HOURS Δa = 0.007 cm (0.003 IN.)
			TERMINATION	0.165 (0.065)	0.652 (0.257)	0.253	848 (123.0)	974 (141.3)	0.870	1.326	0.124 (0.049)	0.261	1.037	295 (72)	GHe	60.8 (55.3)	
			FAILURE	0.304 (0.120)	0.759 (0.299)	0.401	925 (134.2)	974 (141.3)	0.950	1.818	0.167 (0.066)	0.482	1.028	295 (72)	AIR	75.8 (69.0)	
6T-8A-12	0.658 (0.250)	6.347 (2.499)	INITIATION	0.180 (0.071)	0.726 (0.286)	0.248	848 (123.0)	974 (141.3)	0.870	1.290	0.139 (0.055)	0.284	1.045	295 (72)	GHe	64.4 (58.6)	LOADED FOR 10 HOURS Δa = 0.007 cm (0.003 IN.)
			TERMINATION	0.187 (0.074)	0.726 (0.286)	0.259	848 (123.0)	974 (141.3)	0.870	1.321	0.142 (0.056)	0.296	1.047	295 (72)	GHe	65.1 (59.2)	
			FAILURE	0.388 (0.153)	1.000 (0.394)	0.388	790 (114.6)	974 (141.3)	0.810	1.821	0.213 (0.084)	0.612	1.063	295 (72)	AIR	75.7 (68.9)	
6T-8A-16	0.638 (0.251)	6.345 (2.498)	INITIATION	0.121 (0.048)	0.525 (0.207)	0.232	848 (123.0)	974 (141.3)	0.870	1.263	0.096 (0.038)	0.191	1.018	295 (72)	GHe	52.5 (47.8)	LOADED FOR 10 HOURS Δa = 0.005 cm (0.002 IN.)
			TERMINATION	0.127 (0.050)	0.525 (0.207)	0.242	848 (123.0)	974 (141.3)	0.870	1.282	0.099 (0.039)	0.199	1.018	295 (72)	GHe	53.1 (48.3)	
			FAILURE	0.302 (0.119)	0.723 (0.285)	0.418	972 (141.0)	974 (141.3)	0.998	1.888	0.160 (0.063)	0.474	1.023	295 (72)	AIR	77.8 (70.8)	
6T-8A-1	0.650 (0.256)	6.299 (2.480)	INITIATION	0.233 (0.092)	0.977 (0.385)	0.239	772 (112.0)	974 (141.3)	0.794	1.295	0.180 (0.071)	0.359	1.062	295 (72)	GHe	67.8 (61.7)	LOADED FOR 10 HOURS Δa = 0.007 cm (0.003 IN.)
			TERMINATION	0.241 (0.095)	0.977 (0.385)	0.247	772 (112.0)	974 (141.3)	0.794	1.319	0.182 (0.072)	0.371	1.061	295 (72)	GHe	68.2 (62.1)	
			FAILURE	0.368 (0.145)	1.071 (0.422)	0.344	775 (112.5)	974 (141.3)	0.796	1.647	0.233 (0.088)	0.566	1.083	295 (72)	AIR	77.4 (70.4)	
6T-8A-13	0.638 (0.251)	6.347 (2.499)	INITIATION	0.238 (0.094)	1.099 (0.433)	0.217	772 (112.0)	974 (141.3)	0.794	1.236	0.193 (0.076)	0.375	1.072	295 (72)	GHe	70.9 (64.5)	LOADED FOR 10 HOURS Δa = 0.005 cm (0.002 IN.)
			TERMINATION	0.243 (0.096)	1.099 (0.433)	0.222	772 (112.0)	974 (141.3)	0.794	1.246	0.195 (0.077)	0.382	1.072	295 (72)	GHe	71.3 (64.9)	
			FAILURE	0.393 (0.155)	1.219 (0.480)	0.323	760 (110.2)	974 (141.3)	0.780	1.581	0.248 (0.098)	0.618	1.122	295 (72)	AIR	83.0 (75.5)	

Table 35: Sustained Load Flaw Growth Tests of 6Al-4V (ELI) STA Titanium in Methanol at 295°K (72°F)

SPECIMEN NUMBER	THICKNESS, t cm (INCH)	WIDTH, W cm (INCH)	SPECIMEN LOADING SEQUENCE	FLAW DEPTH, a cm (INCH)	FLAW LENGTH, 2c cm (INCH)	a/2c	STRESS, σ MN/m^2 (KSI)	YIELD STRENGTH, σ_{ys} MN/m^2 (KSI)	σ / σ_{ys}	SHAPE PARAMETER, Q	FLAW SIZE, a/Q cm (INCH)	a/t	MAGNIFICATION FACTOR, M_K	TEST TEMPERATURE, T °K (°F)	ENVIRONMENT	STRESS INTENSITY, K_I $MN/m^{3/2}$ (KSI$\sqrt{IN}$)	REMARKS
6T-8A-17	0.640 (0.252)	6.347 (2.499)	INITIATION	0.142 (0.056)	0.538 (0.212)	0.264	848 (123.0)	974 (141.3)	0.870	1.365	0.104 (0.041)	0.222	1.024	295 (72)	METH.	55.0 (50.0)	LOADED FOR 10 HOURS Δa = 0.160 cm (0.063 IN.)
			TERMINATION	0.302 (0.119)	0.965 (0.380)	0.313	848 (123.0)	974 (141.3)	0.870	1.506	0.200 (0.079)	0.472	1.065	295 (72)	METH.	78.7 (71.6)	
			FAILURE	0.538 (0.212)	1.379 (0.543)	0.390	734 (106.5)	974 (141.3)	0.754	1.843	0.292 (0.115)	0.841	1.167	295 (72)	AIR	90.2 (82.1)	
6T-8A-3	0.650 (0.256)	6.352 (2.501)	INITIATION	0.210 (0.083)	0.927 (0.365)	0.227	648 (94.0)	974 (141.3)	0.665	1.296	0.162 (0.064)	0.324	1.059	295 (72)	METH.	53.7 (48.9)	LOADED FOR 10 HOURS Δa = 0.003 cm (0.001 IN.)
			TERMINATION	0.213 (0.084)	0.927 (0.365)	0.230	648 (94.0)	974 (141.3)	0.665	1.312	0.162 (0.064)	0.328	1.059	295 (72)	METH.	54.0 (49.1)	
			FAILURE	0.365 (0.144)	1.059 (0.417)	0.345	772 (112.0)	974 (141.3)	0.793	1.655	0.220 (0.087)	0.563	1.080	295 (72)	AIR	76.4 (69.5)	
6T-8A-9	0.635 (0.250)	6.342 (2.497)	INITIATION	0.271 (0.107)	1.239 (0.488)	0.219	648 (94.0)	974 (141.3)	0.655	1.289	0.210 (0.083)	0.428	1.091	295 (72)	METH.	63.5 (57.8)	LOADED FOR 10 HOURS Δa = 0.058 cm (0.023 IN.)
			TERMINATION	0.330 (0.130)	1.270 (0.500)	0.260	648 (94.0)	974 (141.3)	0.665	1.397	0.236 (0.093)	0.520	1.117	295 (72)	METH.	68.5 (62.3)	
			FAILURE	0.406 (0.160)	1.336 (0.526)	0.304	727 (105.5)	974 (141.3)	0.747	1.523	0.266 (0.105)	0.640	1.152	295 (72)	AIR	84.3 (76.7)	
6T-8A-14	0.637 (0.251)	6.350 (2.500)	INITIATION	0.223 (0.088)	0.975 (0.384)	0.229	648 (94.0)	974 (141.3)	0.665	1.313	0.170 (0.067)	0.351	1.063	295 (72)	METH.	55.5 (50.5)	LOADED FOR 10 HOURS Δa = 0.025 cm (0.010 IN.)
			TERMINATION	0.248 (0.098)	0.975 (0.384)	0.255	648 (94.0)	974 (141.3)	0.665	1.380	0.180 (0.071)	0.390	1.061	295 (72)	METH.	56.8 (51.7)	
			FAILURE	0.482 (0.190)	1.323 (0.521)	0.365	612 (88.8)	974 (141.3)	0.628	1.775	0.271 (0.107)	0.757	1.151	295 (72	AIR	71.5 (65.7)	

Table 36: 333 mHz (20 CPM) Cyclic Load Flaw Growth Tests of 6Al-4V (ELI) STA Titanium in Gaseous Helium at 295°K (72°F)

SPECIMEN NUMBER	THICKNESS, t cm (INCH)	WIDTH, W cm (INCH)	SPECIMEN LOADING SEQUENCE	FLAW DEPTH, a cm (INCH)	FLAW LENGTH, 2c cm (INCH)	a / 2c	STRESS, σ MN/m^2 (KSI)	YIELD STRENGTH, σ_{ys} MN/m^2 (KSI)	σ / σ_{ys}	SHAPE PARAMETER, Q	FLAW SIZE, a/Q cm (INCH)	a / t	MAGNIFICATION FACTOR, M_K	TEST TEMPERATURE, T °K (°F)	ENVIRONMENT	STRESS INTENSITY, K_I $MN/m^{3/2}$ (KSI$\sqrt{IN}$)	REMARKS
6T-8A-7	0.629 (0.248)	6.360 (2.504)	INITIATION	0.123 (0.048)	0.528 (0.208)	0.231	848 (123.0)	974 (141.3)	0.870	1.263	0.096 (0.038)	0.184	1.018	295 (72)	GHe	52.8 (47.9)	CYCLED FOR 1500 CYCLES– UNLOADED JUST PRIOR TO FAILURE
			TERMINATION	0.525 (0.207)	1.361 [1] (0.536)	0.386	848 (123.0)	974 (141.3)	0.870	1.800	0.292 (0.115)	0.835	1.169	295 (72)	GHe	104.6 (95.2)	
			FAILURE	0.629 (0.248)	1.676 [1] (0.660)	0.376	683 (99.0)	974 (141.3)	0.701	1.810	0.348 (0.137)	>0.900	–	295 (72)	AIR	–	
6T-8A-8	0.637 (0.251)	6.352 (2.501)	INITIATION	0.119 (0.047)	0.523 (0.206)	0.228	848 (123.0)	974 (141.3)	0.870	1.236	0.096 (0.038)	0.187	1.017	295 (72)	GHe	52.2 (47.5)	CYCLED FOR 700 CYCLES
			TERMINATION	0.241 (0.095)	0.650 (0.256)	0.371	848 (123.0)	974 (141.3)	0.870	1.727	0.139 (0.055)	0.378	1.027	295 (72)	GHe	63.4 (57.7)	
			FAILURE	0.447 (0.176)	1.003 (0.395)	0.446	742 (107.6)	974 (141.3)	0.761	2.095	0.213 (0.084)	0.701	1.053	295 (72)	AIR	70.6 (64.2)	
6T-8A-18	0.640 (0.252)	6.350 (2.500)	INITIATION	0.185 (0.073)	0.807 (0.318)	0.230	848 (123.0)	974 (141.3)	0.870	1.237	0.149 (0.059)	0.290	1.050	295 (72)	GHe	67.0 (61.0)	CYCLED FOR 303 CYCLES – UNLOADED PRIOR TO FAILURE
			TERMINATION	0.345 (0.136)	0.982 (0.387)	0.351	848 (123.0)	974 (141.3)	0.870	1.658	0.208 (0.082)	0.540	1.068	295 (72)	GHe	80.7 (73.4)	
			FAILURE	0.353 (0.193)	1.303 (0.513)	0.376	685 (99.4)	974 (141.3)	0.703	1.803	0.272 (0.107)	0.766	1.141	295 (72)	AIR	79.5 (72.3)	
6T-8A-19	0.637 (0.251)	6.344 (2.498)	INITIATION	0.091 (0.036)	0.355 (0.140)	0.257	848 (123.0)	974 (141.3)	0.870	1.333	0.068 (0.027)	0.143	1.012	295 (72)	GHe	44.0 (40.0)	CYCLED FOR 1300 CYCLES
			TERMINATION	0.200 (0.079)	0.505 (0.199)	0.397	848 (123.0)	974 (141.3)	0.870	1.837	0.109 (0.043)	0.315	1.021	295 (72)	GHe	55.8 (50.8)	
			FAILURE	0.320 (0.126)	0.741 (0.272)	0.463	924 (134.0)	974 (141.3)	0.948	2.100	0.152 (0.060)	0.502	1.011	295 (72)	AIR	71.1 (64.7)	
6T-9A-1	0.911 (0.359)	7.622 (3.001)	INITIATION	0.279 (0.110)	1.203 (0.474)	0.232	427 (62.0)	974 (141.3)	0.439	1.375	0.203 (0.080)	0.306	1.055	295 (72)	GHe	39.7 (36.1)	CYCLED FOR 900 CYCLES
			TERMINATION	0.342 (0.135)	1.224 (0.482)	0.280	427 (62.0)	974 (141.3)	0.439	1.516	0.226 (0.089)	0.376	1.051	295 (72)	GHe	41.7 (37.9)	
			FAILURE	0.728 (0.287)	1.910 (0.752)	0.382	618 (89.6)	974 (141.3)	0.635	1.851	0.394 (0.155)	0.799	1.152	295 (72)	AIR	87.2 (79.3)	

[1] 2c DIMENSION – FLAW GREW PARALLEL TO LOAD

Table 37: 8.3 mHz (0.5 CPM) Combined Cyclic/Sustained Load Flaw Growth Tests of 6Al-4V (ELI) STA Titanium in Gaseous Helium at 295°K (72°F)

SPECIMEN NUMBER	THICKNESS, t cm (INCH)	WIDTH, W cm (INCH)	SPECIMEN LOADING SEQUENCE	FLAW DEPTH, a cm (INCH)	FLAW LENGTH, 2c cm (INCH)	a / 2c	STRESS, σ MN/m^2 (KSI)	YIELD STRENGTH, σ_{ys} MN/m^2 (KSI)	σ / σ_{ys}	SHAPE PARAMETER, Q	FLAW SIZE, a/Q cm (INCH)	a / t	MAGNIFICATION FACTOR, M_K	TEST TEMPERATURE, T °K (°F)	ENVIRONMENT	STRESS INTENSITY, K_I $MN/m^{3/2}$ (KSI$\sqrt{IN}$)	REMARKS
6T-8A-23	0.629 (0.248)	6.357 (2.503)	INITIATION	0.116 (0.046)	0.495 (0.195)	0.236	848 (123.0)	974 (141.3)	0.870	1.277	0.091 (0.036)	0.185	1.017	295 (72)	GHe	51.1 (46.5)	CYCLED FOR 700 CYCLES
			TERMINATION	0.190 (0.075)	0.574 (0.226)	0.332	848 (123.0)	974 (141.3)	0.870	1.595	0.119 (0.047)	0.302	1.034	295 (72)	GHe	59.3 (54.0)	
			FAILURE	0.309 (0.122)	0.695 (0.274)	0.445	965 (140.0)	974 (141.3)	0.991	2.000	0.154 (0.061)	0.492	1.016	295 (72)	AIR	75.3 (68.5)	
6T-8A-26	0.635 (0.250)	6.360 (2.504)	INITIATION	0.071 (0.028)	0.350 (0.138)	0.203	848 (123.0)	974 (141.3)	0.870	1.167	0.060 (0.024)	0.112	1.011	295 (72)	GHe	41.2 (37.5)	CYCLED FOR 1000 CYCLES
			TERMINATION	0.312 (0.123)	0.762 (0.300)	0.410	848 (123.0)	974 (141.3)	0.870	1.893	0.165 (0.065)	0.492	1.026	295 (72)	GHe	69.0 (62.8)	
			FAILURE	0.365 (0.144)	0.863 (0.340)	0.424	942 (136.6)	974 (141.3)	0.967	1.920	0.190 (0.075)	0.576	1.036	295 (72)	AIR	83.1 (75.7)	
6T-8A-27	0.632 (0.249)	6.347 (2.499)	INITIATION	0.170 (0.067)	0.782 (0.308)	0.218	848 (123.0)	974 (141.3)	0.870	1.218	0.139 (0.055)	0.269	1.045	295 (72)	GHe	64.8 (59.0)	CYCLED FOR 109 CYCLES
			TERMINATION	0.231 (0.091)	0.805 (0.317)	0.287	848 (123.0)	974 (141.3)	0.870	1.421	0.162 (0.064)	0.365	1.048	295 (72)	GHe	69.8 (63.5)	
			FAILURE	(MARKED THROUGH-THE-THICKNESS)						–	–	–	–	295 (72)	AIR	–	
6T-8A-33	0.640 (0.252)	6.342 (2.497)	INITIATION	0.215 (0.085)	0.934 (0.368)	0.231	848 (123.0)	974 (141.3)	0.870	1.250	0.172 (0.068)	0.337	1.060	295 (72)	GHe	73.0 (66.4)	CYCLED FOR 103 CYCLES
			TERMINATION	0.325 (0.128)	0.980 (0.386)	0.332	848 (123.0)	974 (141.3)	0.870	1.580	0.205 (0.081)	0.508	1.067	295 (72)	GHe	80.1 (72.9)	
			FAILURE	0.416 (0.164)	1.092 (0.430)	0.381	840 (121.8)	974 (141.3)	0.861	1.783	0.233 (0.092)	0.651	1.083	295 (72)	AIR	85.9 (78.2)	

Table 38: 3.3 mHz (0.2 CPM) Combined Cyclic/Sustained Load Flaw Growth Tests of 6Al-4V (ELI) STA Titanium in Gaseous Helium at 295°K (72°F)

SPECIMEN NUMBER	THICKNESS, t cm (INCH)	WIDTH, W cm (INCH)	SPECIMEN LOADING SEQUENCE	FLAW DEPTH, a cm (INCH)	FLAW LENGTH, 2c cm (INCH)	a / 2c	STRESS, σ MN/m^2 (KSI)	YIELD STRENGTH, σ_{ys} MN/m^2 (KSI)	σ / σ_{ys}	SHAPE PARAMETER, Q	FLAW SIZE, a/Q cm (INCH)	a / t	MAGNIFICATION FACTOR, M_K	TEST TEMPERATURE, T °K (°F)	ENVIRONMENT	STRESS INTENSITY, K_I MN/m$^{3/2}$ (KSI$\sqrt{IN}$)	REMARKS
6T-8A-24	0.635 (0.250)	6.35 (2.503)	INITIATION	0.130 (0.051)	0.508 (0.200)	0.255	848 (123.0)	974 (141.3)	0.870	1.308	0.099 (0.039)	0.204	1.018	295 (72)	GHe	52.8 (48.0)	CYCLED FOR 695 CYCLES
			TERMINATION	0.193 (0.076)	0.579 (0.228)	0.333	848 (123.0)	974 (141.3)	0.870	1.583	0.122 (0.048)	0.304	1.034	295 (72)	GHe	59.6 (54.2)	
			FAILURE	0.295 (0.116)	0.704 (0.277)	0.419	971 (140.8)	974 (141.3)	0.996	1.871	0.158 (0.062)	0.464	1.021	295 (72)	AIR	76.6 (69.7)	
6T-8A-25	0.645 (0.254)	6.35 (2.502)	INITIATION	0.071 (0.028)	0.338 (0.133)	0.211	848 (123.0)	974 (141.3)	0.870	1.166	0.061 (0.024)	0.110	1.011	295 (72)	GHe	40.9 (37.2)	CYCLED FOR 1034 CYCLES
			TERMINATION	0.142 (0.056)	0.394 (0.155)	0.361	848 (123.0)	974 (141.3)	0.870	1.697	0.084 (0.033)	0.220	1.013	295 (72)	GHe	48.6 (44.2)	
			FAILURE	0.153 (0.060)	0.406 (0.160)	0.375	1118 (162.0)	974 (141.3)	1.146	1.714	0.089 (0.035)	0.236	1.014	295 (72)	AIR	66.2 (60.2)	
6T-8A-32	0.645 (0.254)	6.35 (2.499)	INITIATION	0.173 (0.068)	0.783 (0.308)	0.221	848 (123.0)	974 (141.3)	0.870	1.214	0.142 (0.056)	0.268	1.044	295 (72)	GHe	65.0 (59.1)	CYCLED FOR 109 CYCLES
			TERMINATION	0.204 (0.080)	0.788 (0.310)	0.258	848 (123.0)	974 (141.3)	0.870	1.333	0.152 (0.060)	0.315	1.050	295 (72)	GHe	68.0 (61.8)	
			FAILURE	0.229 (0.090)	0.792 (0.312)	0.288	983 (142.5)	974 (141.3)	1.008	1.385	0.165 (0.065)	0.354	1.047	295 (72)	AIR	81.7 (74.3)	
6T-8A-34	0.643 (0.253)	6.35 (2.503)	INITIATION	0.216 (0.085)	0.938 (0.369)	0.230	848 (123.0)	974 (141.3)	0.870	1.247	0.173 (0.068)	0.336	1.060	295 (72)	GHe	73.0 (66.4)	FAILED ON 133 CYCLE
			TERMINATION	0.389 (0.153)	1.054 (0.415)	0.369	848 (123.0)	974 (141.3)	0.870	1.720	0.226 (0.089)	0.605	1.077	295 (72)	GHe	84.6 (77.0)	

Table 39: 333 mHz (20 CPM) Cyclic Load Flaw Growth Tests of 6Al-4V (ELI) STA Titanium in Methanol at 295°K (72°F)

SPECIMEN NUMBER	THICKNESS, t cm (INCH)	WIDTH, W cm (INCH)	SPECIMEN LOADING SEQUENCE	FLAW DEPTH, a cm (INCH)	FLAW LENGTH, 2c cm (INCH)	a / 2c	STRESS, σ MN/m² (KSI)	YIELD STRENGTH, σ_{ys} MN/m² (KSI)	σ / σ_{ys}	SHAPE PARAMETER, Q	FLAW SIZE, a/Q cm (INCH)	a / t	MAGNIFICATION FACTOR, M_K	TEST TEMPERATURE, T °K (°F)	ENVIRONMENT	STRESS INTENSITY, K_I MN/m$^{3/2}$ (KSI$\sqrt{IN}$)	REMARKS
6T-8A-21	0.637 (0.251)	6.344 (2.498)	INITIATION	0.203 (0.080)	0.873 (0.344)	0.233	648 (94.0)	974 (141.3)	0.665	1.311	0.154 (0.061)	0.319	1.057	295 (72)	METH.	52.4 (47.7)	CYCLED FOR 600 CYCLES
			TERMINATION	0.274 (0.108)	0.937 (0.369)	0.293	648 (94.0)	974 (141.3)	0.665	1.500	0.182 (0.072)	0.430	1.060	295 (72)	METH.	57.0 (51.9)	
			FAILURE	0.414 (0.163)	1.122 (0.442)	0.369	758 (110.0)	974 (141.3)	0.779	1.752	0.236 (0.093)	0.649	1.095	295 (72)	AIR	78.7 (71.6)	
6T-8A-22	0.637 (0.251)	6.347 (2.499)	INITIATION	0.127 (0.050)	0.574 (0.226)	0.221	648 (94.0)	974 (141.3)	0.665	1.282	0.099 (0.039)	0.199	1.019	295 (72)	METH.	40.4 (36.8)	CYCLED FOR 1300 CYCLES
			TERMINATION	0.223 (0.088)	0.665 (0.262)	0.336	648 (94.0)	974 (141.3)	0.665	1.660	0.134 (0.053)	0.351	1.035	295 (72)	METH.	47.9 (43.6)	
			FAILURE	0.335 (0.132)	0.789 (0.311)	0.424	924 (134.0)	974 (141.3)	0.948	1.913	0.175 (0.069)	0.526	1.027	295 (72)	AIR	77.3 (70.3)	
6T-9A-2	0.945 (0.372)	7.627 (3.003)	INITIATION	0.287 (0.113)	1.198 (0.472)	0.239	648 (94.0)	974 (141.3)	0.665	1.345	0.213 (0.084)	0.304	1.053	295 (72)	METH.	61.5 (56.0)	CYCLED FOR 323 CYCLES–UNLOADED JUST PRIOR TO FAILURE
			TERMINATION	0.551 (0.217)	1.595 (0.628)	0.346	648 (94.0)	974 (141.3)	0.665	1.695	0.325 (0.128)	0.583	1.087	295 (72)	METH.	78.2 (71.2)	
			FAILURE	0.680 (0.268)	1.785 (0.703)	0.381	565 (82.0)	974 (141.3)	0.581	1.361	0.365 (0.144)	0.720	1.112	295 (72)	AIR	74.2 (67.5)	
6T-9A-3	0.879 (0.346)	5.722 (2.253)	INITIATION	0.279 (0.110)	1.219 (0.480)	0.229	427 (62.0)	974 (141.3)	0.439	1.358	0.205 (0.081)	0.318	1.057	295 (72)	METH.	39.9 (36.3)	CYCLED FOR 900 CYCLES
			TERMINATION	0.381 (0.150)	1.244 (0.490)	0.306	427 (62.0)	974 (141.3)	0.439	1.613	0.236 (0.093)	0.434	1.056	295 (72)	METH.	42.9 (39.0)	
			FAILURE	0.693 (0.273)	1.828 (0.720)	0.379	680 (98.7)	974 (141.3)	0.699	1.820	0.381 (0.150)	0.789	1.150	295 (72)	AIR	94.2 (85.7)	

Table 40: 8.3 mHz (0.5 CPM) Combined Cyclic/Sustained Load Flaw Growth Tests of 6Al-4V (ELI) STA Titanium in Methanol at 295°K (72°F)

SPECIMEN NUMBER	THICKNESS, t cm (INCH)	WIDTH, W cm (INCH)	SPECIMEN LOADING SEQUENCE	FLAW DEPTH, a cm (INCH)	FLAW LENGTH, 2c cm (INCH)	a / 2c	STRESS, σ MN/m^2 (KSI)	YIELD STRENGTH, σ_{ys} MN/m^2 (KSI)	σ / σ_{ys}	SHAPE PARAMETER, Q	FLAW SIZE, a/Q cm (INCH)	a / t	MAGNIFICATION FACTOR, M_K	TEST TEMPERATURE, T °K (°F)	ENVIRONMENT	STRESS INTENSITY, K_I MN/m$^{3/2}$ (KSI$\sqrt{IN}$)	REMARKS
6T-8A-31	0.636 (0.250)	6.35 (2.498)	INITIATION	0.249 (0.098)	1.127 (0.443)	0.221	648 (94.0)	974 (141.3)	0.665	1.290	0.193 (0.076)	0.392	1.074	295 (72)	METH.	59.7 (54.3)	CYCLED FOR 99 CYCLES
			TERMINATION	0.308 (0.121)	1.260 (0.495)	0.244	648 (94.0)	974 (141.3)	0.665	1.360	0.226 (0.089)	0.484	1.106	295 (72)	METH.	66.6 (60.6)	
			FAILURE	0.340 (0.134)	1.307 (0.514)	0.261	836 (121.2)	974 (141.3)	0.858	1.340	0.254 (0.100)	0.536	1.126	295 (72)	AIR	92.3 (84.0)	
6T-8A-28	0.638 (0.251)	6.36 (2.505)	INITIATION	0.186 (0.073)	0.876 (0.345)	0.212	648 (94.0)	974 (141.3)	0.665	1.258	0.147 (0.058)	0.291	1.054	295 (72)	METH.	51.1 (46.5)	CYCLED FOR 399 CYCLES
			TERMINATION	0.358 (0.141)	1.246 (0.490)	0.288	648 (94.0)	974 (141.3)	0.665	1.500	0.239 (0.094)	0.562	1.120	295 (72)	METH.	69.4 (63.1)	
			FAILURE	0.412 (0.162)	1.298 (0.510)	0.318	674 (97.6)	974 (141.3)	0.691	1.588	0.259 (0.102)	0.645	1.142	295 (72)	AIR	76.3 (69.4)	
6T-8A-30	0.633 (0.249)	6.35 (2.497)	INITIATION	0.117 (0.046)	0.567 (0.223)	0.206	648 (94.0)	974 (141.3)	0.665	1.243	0.094 (0.037)	0.185	1.018	295 (72)	METH.	39.5 (35.9)	CYCLED FOR 699 CYCLES
			TERMINATION	0.402 (0.158)	1.068 (0.420)	0.376	648 (94.0)	974 (141.3)	0.665	1.816	0.221 (0.087)	0.635	1.082	295 (72)	METH.	62.1 (56.5)	
			FAILURE	0.432 (0.170)	1.143 (0.450)	0.378	758 (109.8)	974 (141.3)	0.777	1.790	0.242 (0.095)	0.683	1.099	295 (72)	AIR	79.7 (72.5)	
6T-8A-29	0.638 (0.251)	6.35 (2.501)	INITIATION	0.165 (0.065)	0.737 (0.290)	0.271	648 (94.0)	974 (141.3)	0.665	1.445	0.114 (0.045)	0.259	1.040	295 (72)	METH.	46.9 (42.7)	CYCLED FOR 499 CYCLES
			TERMINATION	0.242 (0.095)	0.826 (0.325)	0.292	648 (94.0)	974 (141.3)	0.665	1.508	0.160 (0.063)	0.378	1.047	295 (72)	METH.	53.0 (48.2)	
			FAILURE	0.260 (0.102)	0.838 (0.330)	0.309	956 (138.7)	974 (141.3)	0.982	1.457	0.178 (0.070)	0.406	1.046	295 (72)	AIR	82.4 (74.9)	

Table 41: 3.3 mHz (0.2 CPM) Combined Cyclic/Sustained Load Flaw Growth Tests of 6Al-4V (ELI) STA Titanium in Methanol at 295°K (72°F)

SPECIMEN NUMBER	THICKNESS, t cm (INCH)	WIDTH, W cm (INCH)	SPECIMEN LOADING SEQUENCE	FLAW DEPTH, a cm (INCH)	FLAW LENGTH, 2c cm (INCH)	a / 2c	STRESS, σ MN/m^2 (KSI)	YIELD STRENGTH, σ_{ys} MN/m^2 (KSI)	σ / σ_{ys}	SHAPE PARAMETER, Q	FLAW SIZE, a/Q cm (INCH)	a / t	MAGNIFICATION FACTOR, M_K	TEST TEMPERATURE, T °K (°F)	ENVIRONMENT	STRESS INTENSITY, K_I $MN/m^{3/2}$ $(KSI\sqrt{IN})$	REMARKS
6T-8A-35	0.648 (0.255)	6.35 (2.502)	INITIATION	0.279 (0.110)	1.270 (0.500)	0.220	648 (94.0)	974 (141.3)	0.665	1.279	0.222 (0.086)	0.431	1.092	295 (72)	METH	64.5 (58.6)	CYCLED FOR 100 CYCLES
			TERMINATION	0.343 (0.135)	1.270 (0.500)	0.270	648 (94.0)	974 (141.3)	0.665	1.436	0.242 (0.094)	0.529	1.115	295 (72)	METH	69.0 (62.7)	
			FAILURE	0.358 (0.141)	1.288 (0.507)	0.278	884 (128.1)	974 (141.3)	0.907	1.382	0.262 (0.102)	0.553	1.123	295 (72)	AIR	98.7 (89.6)	
6T-8A-36	0.648 (0.255)	6.35 (2.500)	INITIATION	0.196 (0.077)	0.902 (0.355)	0.217	648 (94.0)	974 (141.3)	0.665	1.283	0.155 (0.060)	0.302	1.057	295 (72)	METH	52.4 (47.6)	CYCLED FOR 300 CYCLES
			TERMINATION	0.586 (0.231)	1.880 (0.740)	0.312	648 (94.0)	974 (141.3)	0.665	1.582	0.376 (0.146)	>0.900	–	295 (72)	METH	–	
			FAILURE	(MARKED THRU-THE-THICKNESS)						–	–	–	–	295 (72)	AIR	–	
6T-8A-37	0.645 (0.254)	6.35 (2.498)	INITIATION	0.158 (0.062)	0.736 (0.290)	0.214	648 (94.0)	974 (141.3)	0.665	1.265	0.126 (0.049)	0.244	1.036	295 (72)	METH	46.2 (42.0)	CYCLED FOR 300 CYCLES
			TERMINATION	0.229 (0.090)	0.851 (0.335)	0.269	648 (94.0)	974 (141.3)	0.665	1.429	0.162 (0.063)	0.354	1.052	295 (72)	METH	53.3 (48.4)	
			FAILURE	0.272 (0.107)	0.881 (0.347)	0.308	100.2 (145.2)	974 (141.3)	>1.0	1.446	0.190 (0.074)	0.421	1.051	295 (72)	AIR	89.0 (80.9)	
6T-8A-38	0.643 (0.253)	6.35 (2.500)	INITIATION	0.135 (0.053)	0.622 (0.245)	0.216	648 (94.0)	974 (141.3)	0.665	1.262	0.108 (0.042)	0.209	1.023	295 (72)	METH	42.1 (38.2)	CYCLED FOR 300 CYCLES
			TERMINATION	0.246 (0.097)	0.965 (0.380)	0.346	648 (94.0)	974 (141.3)	0.665	1.702	0.147 (0.057)	0.383	1.033	295 (72)	METH	49.7 (45.2)	
			FAILURE	0.284 (0.112)	1.030 (0.400)	0.280	1004 (145.6)	974 (141.3)	>1.0	1.349	0.214 (0.083)	0.443	1.070	295 (72)	AIR	96.3 (87.5)	
6T-8A-39	0.638 (0.251)	6.35 (2.503)	INITIATION	0.122 (0.048)	0.618 (0.240)	0.200	648 (94.0)	974 (141.3)	0.665	1.231	0.100 (0.039)	0.191	1.019	295 (72)	METH	40.6 (36.9)	CYCLED FOR 299 CYCLES
			TERMINATION	0.269 (0.106)	0.654 (0.254)	0.417	648 (94.0)	974 (141.3)	0.665	2.000	0.136 (0.053)	0.422	1.018	295 (72)	METH	47.4 (43.1)	
			FAILURE	0.322 (0.127)	0.738 (0.287)	0.443	921 (133.4)	974 (141.3)	0.944	2.016	0.162 (0.063)	0.506	1.018	295 (72)	AIR	73.3 (66.6)	

Table A-1: *Calculations of Flaw Growth Rates for Specimen A3A-23*

FLAW DEPTH, a cm (INCH)	FLAW PARAMETER, $a/\sqrt{Q}$ cm (INCH)	CONSTANT, C $p\frac{m^2}{N}\left(\mu\frac{IN^2}{LB}\right)$	FLAW OPENING δ μcm (μ INCH)	CYCLES, N	FATIGUE CRACK GROWTH RATES, da/dN μcm/CYCLE (μ INCH/CYCLE)	STRESS INTENSITY, (K_I) AVG. $MN/m^{3/2}$ ($KSI\sqrt{IN}$)
0.2311 (0.0910)	0.2367 (0.0932)	75.3 (0.519)	6147 (2420)	1	254.8 (100.3)	34.8 (31.7)
0.2416 (0.0951)	0.2464 (0.0970)	75.8 (0.523)	6439 (2535)	41	306.8 (120.8)	35.7 (32.5)
0.2548 (0.1003)	0.2586 (0.1018)	76.6 (0.528)	6822 (2686)	85	330.7 (130.2)	36.7 (33.4)
0.2692 (0.1060)	0.2715 (0.1069)	77.3 (0.533)	7234 (2848)	128	363.9 (143.3)	37.8 (34.4)
0.2860 (0.1126)	0.2865 (0.1128)	78.2 (0.539)	7719 (3039)	175	450.0 (177.2)	39.9 (35.5)
0.3089 (0.1216)	0.3063 (0.1206)	79.3 (0.547)	8377 (3298)	226	655.8 (258.2)	40.6 (36.9)
0.3445 (0.1357)	0.3360 (0.1323)	81.2 (0.560)	9413 (3706)	280	785.1 (309.1)	41.9 (38.1)
0.3630 (0.1429)	0.3510 (0.1382)	82.2 (0.567)	9947 (3916)	303	1069.3 (421.0)	43.0 (39.1)
0.3891 (0.1532)	0.3720 (0.1465)	83.5 (0.576)	10719 (4220)	328	1490.9 (587.0)	44.3 (40.3)
0.4232 (0.1666)	0.3988 (0.1570)	85.3 (0.588)	11730 (4618)	351	1927.9 (759.0)	46.3 (42.1)
0.4681 (0.1843)	0.4328 (0.1704)	87.7 (0.605)	13081 (5150)	374	4350.8 (1712.9)	49.6 (45.1)
0.5639 (0.2220)	0.5009 (0.1972)	92.7 (0.639)	16002 (6300)	396		

DISTRIBUTION LIST FOR FINAL REPORT NASA CR-120834

CONTRACT NAS 3-12044

SUBCRITICAL CRACK GROWTH OF SELECTED AEROSPACE PRESSURE VESSEL MATERIALS

THE BOEING COMPANY

Seattle, Washington

RECIPIENT (R)	DESIGNEE (D)	COPIES TO R	COPIES TO D
NASA-Lewis Research Center			
Attn: Contracting Officer, MS 500-313		1	
Rocket Technology Branch, MS 500-203		1	
Technical Report Control Office, MS 5-5		1	
Technology Utilization Office, MS 3-16		1	
AFSC Liaison Office, MS 501-3		1	
Library, MS 60-3		1	
Office of Reliability & Quality Assurance, MS 500-111		1	
R. H. Johns, MS 49-3		1	
G. T. Smith, Project Manager, MS 49-3		18	
R. H. Kemp, MS 49-3		1	
W. F. Brown, Jr., MS 105-1		1	
21000 Brookpark Road			
Cleveland, Ohio 44135			
National Aeronautics & Space Administration			
Attn: RPX/Chief, Liquid Experimental Engineering		1	
KT/Technology Utilization Office		1	
RW/G. C. Deutsch		1	
MTG/J. G. Malament		1	
MHE/N. G. Peil		1	
RWM/J. J. Gangler		1	
RWS/D. A. Gilstead		1	
Library		1	
Washington, D.C. 20546			
National Technical Information Service		30	
Springfield, Va. 22151			
Attn: NASA Representative, Box 333, College Park, Md. 20740		2	

RECIPIENT (R)	DESIGNEE (D)	COPIES TO R	D
NASA-Marshall Space Flight Center			
Attn: S&E-ASTN-AA/C. Lifer		1	
S&E-ASTN-ASR/C. Crockett		1	
S&E-ASTN-AS/H. Coldwater		1	
Library		1	
Marshall Space Flight Center, Ala. 35812			
NASA-Ames Research Center			
Attn: Library		1	
Moffett Field, Ca. 94035			
NASA-Flight Research Center		1	
Attn: Library			
P.O. Box 273			
Edwards, Ca. 93523			
NASA Scientific and Technical Information Facility		2	
Box 33			
College Park, Md. 20740			
NASA-Goddard Space Flight Center	Merland L. Moseson	1	
Attn: Library	Code 620		
Greenbelt, Md. 20771			
NASA-John F. Kennedy Space Center	R. Sannecandro	1	
Attn: Library			
Kennedy Space Center, Fl. 32931			
NASA-Langley Research Center	R. W. Leonard	1	1
Attn: Library	H. Hardrath		1
Hampton, Va. 23365			
NASA-Manned Spacecraft Center	R. E. Johnson	1	
Attn: Library	L. St. Leger		
Houston, Tx 77001			
Jet Propulsion Laboratory	Joe Lewis	1	1
Attn: Library			
4800 Oak Grove Drive			
Pasadena, Ca 91103			
Commanding Officer		1	
U.S. Army Research Office (Durham)			
Attn: Library			
Box CM, Duke Station			
Durham, N.C. 27706			

RECIPIENT (R)	DESIGNEE (D)	COPIES TO R	D
U.S. Army Missile Command Attn: Document Section Redstone Scientific Information Center Redstone Aresenal, Al 35808	Dr. W. Wharton	1	
Arnold Engineering Development Center Attn: Library Air Force Systems Command Tellahona, Tn 37389	R. H. K. Doetsch	1	
Aeronautical System Division Air Force Systems Command Attn: Library Wright-Patterson Air Force Base, Ohio 45433	C. F. Tiffany Code ENF	1	1
Air Force Systems Command Andrews Air Force Base Attn: Library Washington, D.C. 20332	Capt. S. W. Bowen SCLT	1	
Air Force Rocket Propulsion Laboratory (RPM) Attn: Library Edwards, Ca 93523		1	
Air Force Office of Scientific Research Attn: Library Washington, D.C. 20333	Dr. J. F. Masi SREP	1	
Director (Code 6180) U.S. Naval Research Laboratory Attn: Library Washington, D.C. 20390	H. W. Carhart J. M. Krafft	1	
Aerojet Liquid Rocket Company Attn: Technical Library 2484-2015A P.O. Box 15847 Sacramento, Ca 95813	R. Stiff	1	
Aerospace Corporation Attn: Library-Documents 2400 E. El Segundo Blvd. Los Angeles, Ca 90045	J. G. Wilder	1	

RECIPIENT (R)	DESIGNEE (D)	COPIES TO R	COPIES TO D
Bell Aerosystems, Inc. Attn: Library Box 1 Buffalo, NY 14240	T. Reinhardt W. M. Smith	1	
Chrysler Corporation Missile Division Attn: Library P.O. Box 2628 Detroit, MI	John Gates	1	
Chrysler Corporation Space Division Attn: Library P.O. Box 29200 New Orleans, LA 70129		1	
University of Denver Denver Research Institute Attn: Security Office P.O. Box 10127 Denver, CO 80210		1	
Republic Aviation Attn: Library Fairchild Hiller Corporation Farmington, Long Island, NY		1	
General Dynamics/Convair Aerospace Attn: Library P.O. Box 1128 San Diego, CA 92112	Jack Jensen W. Witzel	1	1 1
Missiles and Space Systems Center General Electric Company Valley Forge Space Technology Center Attn: Library P.O. Box 8555 Philadelphia, PA 19101	A. Cohen F. Schultz	1	
Grumman Aircraft Engineering Corporation Attn: Library Bethpage, Long Island, NY	Joseph Gavin W. Lundwig	1	 1

RECIPIENT (R)	DESIGNEE (D)	COPIES TO R	COPIES TO D
IIT Research Institute Technology Center Attn: Library Chicago, IL 60616	C. K. Hersh	1	
Ling-Temco-Vought Corporation Attn: Library P.O. Box 5907 Dallas, TX 75222		1	
Lockheed Missiles and Space Company Attn: Library P.O. Box 504 Sunnyvale, CA 94087	R. E. Lewis	1	1
Stanford Research Institute Attn: Library 3333 Ravenswood Avenue Menlo Park, CA 94025	Dr. Gerald Marksman	1	
TRW Systems Inc. Attn: Tech. Lib. Doc. Acquisitions One Space Park Redondo Beach, CA 90278		1	
TRW TAPCO Division 23555 Euclid Avenue Cleveland, OH 44117	P. T. Angell E. A. Stigerwald	1	 1
United Aircraft Corporation Corporate Library Attn: Library 400 Main Street East Hartford, CT 06108	Dr. David Rix Erle Martin Frank Owen Wm. E. Taylor	1	
United Aircraft Corporation Pratt & Whitney Division Florida Research & Development Center Attn: Library P.O. Box 2691 West Palm Beach, FL 33402	R. J. Coar Dr. Schmitke	1	

RECIPIENT (R)	DESIGNEE (D)	COPIES TO R	COPIES TO D
Western Division McDonnell Douglas Astronautics Attn: Library 5301 Bolsa Avenue Huntington Beach, CA 92647	H. Babel R. Rawe	1	1
McDonnell Douglas Aircraft Corporation Attn: Library P.O. Box 516 Lambert Field, MO 63166	Goren	1	
Rocketdyne Division North American Rockwell Inc. Attn: Library, Department 596-306 6633 Canoga Avenue Canoga Park, CA 91304	Robt. P. Jewett O 589 AC 29	1	1
Space & Information Systems Division North American Rockwell Inc. Attn: Library 12214 Lakewood Blvd. Downey, CA	J. Colipriest	1	1
Northrop Space Laboratories Attn: Library 3401 West Broadway Hawthorne, CA	Dr. William Howard	1	
Purdue University Attn: Library, (Technical) Lafayette, IN 47907	Dr. Bruce Reese	1	
Wright-Patterson Air Force Base Attn: AFFML Wright-Patterson Air Force Base, OH 45433	P. Packman	1	
Wright-Patterson Air Force Base Attn: AFFDL Wright-Patterson Air Force Base, OH 45433	H. A. Wood	1	1
Department of the Army U.S. Army Material Command Attn: AMCRD-RC Washington, D.C. 20315		1	

RECIPIENT (R)	DESIGNEE (D)	COPIES TO R	COPIES TO D
Bureau of Naval Weapons Department of the Navy Attn: RRRE-6 Washington, D.C. 20360		1	
Commander U.S. Naval Ordnance Laboratory Attn: Library White Oak Silver Springs, MD 20910		1	
Thiokol Chemical Corporation Wasatch Division Attn: Library Section P.O. Box 524 Brigham City, UT 84302		1	
Carnegie Institute of Technology Department of Civil Engineering Attn: Library Pittsburgh, PA 15213		1	
Westinghouse Research Laboratories Attn: Library Beulah Road, Churchill Borough Pittsburgh, PA 15235	W. K. Wilson G. T. Wessel	1	 1
Frankford Arsenal Attn: 1320, Library Philadelphia, PA 19137	Carl Carman	1	1
Cornell University Department of Materials Science & Engineering Attn: Library Ithaca, NY 14850	H. H. Johnson	1	1
General Dynamics Attn: Library P.O. Box 748 Fort Worth, TX 76101	C. D. Little	1	1
Brunswick Corporation Defense Products Division Attn: Library P.O. Box 4594 43000 Industrial Avenue Lincoln, NE	J. Carter	1	

RECIPIENT (R)	DESIGNEE (D)	COPIES TO R	D
Brown University Attn: Technical Library Providence, RI	Dr. J. R. Rice	1	1
Case Western Reserve University Attn: Technical Library 10090 Euclid Avenue Cleveland, OH 44115		1	
Pennsylvania State University Attn: Library State College, PA		1	
California Institute of Technology Attn: Library (Technical) Pasadena, CA	V. F. Zackay	1	
Massachusetts Institute of Technology Attn: Library Cambridge, MA		1	
Atomic Energy Commission Division of Reactor Development & Technology Washington, D.C. 20767	N. Grossman	1	
Battelle Memorial Institute Attn: Library 505 King Avenue Columbus, OH 43201	Dr. E. Hulbert Dr. G. Hahn C. Federson	1	 1
National Science Foundation Engineering Division Attn: Library 1800 G. Street, N.W. Washington, D.C. 20540		1	